Journal of Photochemistry and Photobiology C: Photochemistry Reviews 40 (2019) 117–149

Contents lists available at ScienceDirect

Journal of Photochemistry and Photobiology C: Photochemistry Reviews

journal homepage: www.elsevier.com/locate/jphotochemrev

Catalysts in electro-, photo- and photoelectrocatalytic CO_2 reduction reactions

Yawen Wang[a,*,1], Da He[b,1], Hongyu Chen[a], Dunwei Wang[b,*]

[a] Institute of Advanced Synthesis and School of Chemistry and Molecular Engineering, Jiangsu National Synergetic Innovation Center for Advanced Materials, Nanjing Tech University, Nanjing 211816, Jiangsu, PR China
[b] Department of Chemistry, Merkert Chemistry Center, Boston College, Chestnut Hill, MA 02467, United States

ARTICLE INFO

Article history:
Received 25 September 2018
Received in revised form 26 February 2019
Accepted 28 February 2019
Available online 2 March 2019

Keywords:
CO_2 reduction
Catalyst
Electrocatalysis
Photocatalysis
Photoelectrocatalysis

ABSTRACT

Carbon dioxide (CO_2) is regarded as a main contributor to the greenhouse effect. As a potential strategy to mitigate its negative impacts, the reduction of CO_2 is environmentally critical, economically meaningful and scientifically challenging. Being both thermodynamically and kinetically unfavored, CO_2 reduction requires catalysts as a crucial component irrespective of the reaction modes, be it electrocatalytic, photoelectrocatalytic or photocatalytic. In an effort to systematically review the types of catalysts that have been studied for CO_2 reduction, we categorize them into two major groups: those being activated by external sources and those being photoexcited and activated themselves. Attention is focused on the detailed mechanisms for each group by which the reduction of CO_2 proceeds, yielding a summary of the guiding principles for catalyst designs. This review highlights the importance of mechanistic studies, which permits us to discuss our perspectives on potential directions of catalyst investigation for future catalytic CO_2 reduction research.

Contents

* Corresponding authors.
E-mail addresses: ias_ywwang@njtech.edu.cn (Y. Wang), dunwei.wang@bc.edu (D. Wang).
[1] Y. Wang and D. He contributed equally.

https://doi.org/10.1016/j.jphotochemrev.2019.02.002
1389-5567/

Yawen Wang is currently a professor in Nanjing Tech University. She obtained her B. Sc. (2010) and Ph. D. (2015) degree from the Division of Chemistry & Biological Chemistry at Nanyang Technological University in Singapore, and worked as a postdoctoral fellow from 2015 to 2016. She joined Nanjing Tech University in 2016. Her research interest includes controlled synthesis of nanostructures and nanocomposites, and their applications in catalysis.

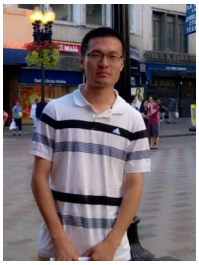

Da He is a doctoral student at Boston College. He graduated from the Univ. Sci. & Tech. of China in 2014 with a bachelor of science in chemistry and has since been working with Prof. Dunwei Wang on photoelectrochemistry.

Hongyu Chen obtained his BSc from the University of Science and Technology of China (USTC) in 1998. In 2004, He obtained his PhD at Yale University. In the same year, he worked as a postdoctoral fellow at Cornell University. From 2006 to 2016, he worked as an Associate Professor in the Division of Chemistry and Biological Chemistry at Nanyang Technological University in Singapore. In 2016, he joined the Institute of Advanced Synthesis at Nanjing Tech University in china as an Executive Dean and Professor. His main research interest is Nanostructure Synthesis, Mechanism Research and Nanomaterial Application.

Dunwei Wang is Professor of Chemistry at Boston College. He holds a bachelor of science degree from Univ. Sci. & Tech. of China (2000) and doctoral degree from Stanford University (2005). Before joining Boston College in 2007, he was a postdoctoral researcher at California Institute of Technology. A former NSF CAREER award, Sloan Fellowship and JSPS Fellowship recipient, Wang directs a research team which studies energy conversation and storage by chemical reactions.

1. Introduction

As the most stable product of fossil fuel utilizations, carbon dioxide (CO_2) is considered a main contributor to the greenhouse effect that rapidly changes the environment in a negative fashion. Prior to the industrial revolution, the carbon cycle had run in such a way that the natural flow of carbon remained balanced. The balance was disrupted by the rapid industrialization and fast growing population, leading to an alarmingly fast consumption of fossil fuels and, hence, the rapid increase of CO_2 emissions since the industrial revolution. The strong correlation between the increase of CO_2 concentration and the change of average global temperatures has compelled scientists to conclude that CO_2 emission is responsible for many of the global-warming related environmental issues [1]. One way to counteract the adverse effect is to reduce CO_2 in the atmosphere.

CO_2 may be removed from the atmosphere via either CO_2 capture and sequestration (CCS) [2] or chemical reduction. The former provides a short-term solution, which stores the captured CO_2 in the Earth's crust or deep ocean. But it poses threats to underground water through contamination and may leak at the storage site. By comparison, CO_2 reductive conversion aims to chemically convert CO_2 into various low-valent carbonaceous molecules. In this way, a new route of carbon cycle may be built to offset CO_2 emitted in the atmosphere due to industrial consumption of fossil fuels. Economically, direct conversion from CO_2 to carbonaceous compounds offers additional benefits. The products may serve as alternative fuel sources and/or raw materials for industrial processes that traditionally rely on fossil fuels or photosynthesis products. Moreover, the thermodynamically uphill nature of CO_2 reduction dictates that this process is also an effective method of energy storage. For instance, electrochemical reduction of CO_2 stores electricity in the form of reduced carbonaceous compounds, and photocatalytic/photoelectrocatalytic reduction of CO_2 may be regarded as artificial photosynthesis in that it can directly utilize solar energy. Taken as a whole, CO_2 reduction not only helps to mitigate environmental issues caused by fossil fuel consumption, but also provides new routes for energy storage, while supplying ready products as industrial precursors.

In itself, CO_2 reduction is an interesting scientific challenge. Carbon-based chemistry is so complex that it is the basis for the sub-discipline of organic chemistry, not mentioning all known live forms are carbon-based. The richness of carbon-based chemistry, however, presents one of the most critical challenges when it comes to reducing CO_2. Just from a simplistic view of the oxidation states of carbon, we see that it could be reduced from 4^+ (in CO_2) all the way to 4^- (in, e.g., CH_4), stopping anywhere in between. In most cases, the electron transfer is coupled with protons, further complicating the situation. How to manage the complex processes is both fundamentally and practically important.

1.1. General introduction of CO_2 reduction

Chemically, CO_2 is the final oxidation product of carbon and a thermodynamically stable compound. It consists of two C=O bond, each of which has a bond dissociation energy (750 kJ mol^{-1}) much higher than that of the C—C (336 kJ mol^{-1}), C—O (327 kJ mol^{-1}) or C—H (441 kJ mol^{-1}) bond. This means that not only is the reduction of CO_2 non-spontaneous, it is also relatively more difficult in comparison with the reduction of many other organic molecules. Several commercial CO_2 reforming processes have already been developed, e.g., to convert CO_2 to methanol via syngas, with CH_4 as the reductant. [3] For instance, the dry reforming involves the reduction of CO_2 with CH_4 to produce CO and H_2 (the syngas), at high temperatures of 800–1000 °C and with the assistant of Ni/MgO [4] or Ni/$MgAl_2O_4$ catalysts [5]. In addition, processes like the methanation reaction or reverse water gas shift are other strate-

gies to reduce CO_2, by which H_2 is applied as a reductant [6]. Alas, these industrial processes usually require considerable amount of thermal energy input, high-pressure environments and involves the oxidation of high energy-density species like H_2 or CH_4. Another important consideration is that capturing and concentrating CO_2 consume significant energy itself [7]. Therefore, these processes can only be considered as green or carbon-efficient if the energy spent are generated by renewable energy sources.

A more economical approach is the electro/photoelectrochemical reduction of CO_2. By reducing CO_2 in an electrolysis process, electric energy can be directly converted to chemical energy. Studies of electrochemical reduction of CO_2 dated back to 1860s while the development of the photochemical reduction of CO_2 was first studied by Honda and Fujishima et al. in the late 1970s, [8] and attracted more attention in recent years. Numerous reviews have been published to discuss the electrochemical reduction of CO_2, covering the basic principles, various aspects of the reaction and state-of-art catalytic systems [9–19]. Generally speaking, upon the application of a bias, CO_2 is reduced at the cathode, with another species (ideally H_2O) oxidized at the anode. The electrochemical reduction of CO_2 usually requires the presence of a catalyst due to the otherwise large activation barriers.

Direct conversion of solar energy into chemical energy via CO_2 reduction represents another area of significant research interest. Indeed, nature carries out this process via the photosynthesis reactions. Fossil fuels are also indirect products of this process. Nevertheless, the biochemical processes tend to be not sufficiently efficient to meet modern industrial needs. Scientists, therefore, are keen to develop artificial photosynthetic processes, such as photocatalytic and/or photoeletrochemical reduction of CO_2, to enable the transformation more efficiently [20–33]. The systems that have been studied may be discussed in two groups, based on how solar energy is harvested and transferred. The first one consists of a sensitizer and a catalyst. The sensitizer absorbs light and generates electron-hole pairs. The excited electrons migrate to the catalyst where the reduction takes place. Therefore, the light-harvesting system may be regarded as an energy source. The benefit of this system is the ability to tailor and optimize the different components (light absorber and catalyst) separately. In the second case, the excited species themselves participate in the CO_2 reduction reaction and directly interact with CO_2. This system could enable reactions that are not accessible by other means of energy supply by, for example, taking advantage of the photoexcited species or intermediates [34,35].

1.2. Challenges in CO_2 reduction

CO_2 reduction reaction is not only a thermodynamically uphill process, but faces great kinetic challenges. The reactions feature highly reactive intermediates, requiring high activation energies. In particular, the formation of the immediate by one electron-reduction ($CO_2^{\bullet -}$) is a well-known thermodynamically unfavorable process, and the redox potential of $CO_2/CO_2^{\bullet -}$ is as negative as −1.9 V (vs RHE at pH 7). Hence, the utility of catalysts in CO_2 reduction becomes critically important. Another important reason for the need of catalysts is the product selectivity, which is one of the key challenges for electrochemical reduction of CO_2 since direct reduction of CO_2 could result in one or more of a myriad of products. In other words, the reaction could proceed through multiple steps following different routes; which direction it actually takes is highly sensitive to factors such as the pH, the overpotential and the temperature [36–41]. In order to achieve desired selectivity and efficiency, various branches of the reactions need to be understood and, ultimately, controlled by the application of different catalysts. To further complicate the situation, we must also consider competing reactions such as hydrogen evolution reactions (HER) [42]. HER is important because it is kinetically favored over CO_2 reduction in the presence of H_2O. We need to carry out the reactions in H_2O as it is the ultimate source of electrons for CO_2 reduction for large scale implementations. Strategies such as choosing an electrode with less HER activity or altering the pH have been shown to suppress HER during CO_2 catalytic reduction process.

1.3. General mechanisms of CO_2 catalytic reduction

Mechanistic studies of the catalytic processes, especially the heterogeneous catalytic reduction of CO_2, can benefit tremendously from insights at the molecular level. For this purpose, we can take advantage of developments in computational chemistry and advanced characterization techniques. From the limited information available to us, we learned that the detailed mechanisms of catalytic CO_2 reduction vary greatly, and some of the proposed reaction pathways are still under debate. Importantly, while the properties of the catalysts themselves are critical in defining the pathways, the environmental factors have been found equally crucial as the electrolyte are intimately involved in the reactions, as well [43,44].

Almost all catalytic CO_2 reduction reactions begin with the activation of the CO_2 by its coordination with a metal center within the catalyst. For homogeneous catalysts, especially organometallic complexes, the binding center is rather easy to identify. On the other hand, on heterogeneous catalysts there could be multiple active sites on the surface, and the chemical environment of the active sites can be different even on a single catalyst species, making it difficult to study the reactions with molecular level details. Irrespective, this initial activation usually leads to the formation of a metal−CO_2 adduct, and a proton-transfer process takes place subsequently to yield a metal-bound *COOH intermediate. It is noted that this one-electron activation is only a general case, sometimes two-electron activation or other form of activation is required for successive interactions with CO_2. [45] The complexity of the CO_2 catalytic reduction appears even at this stage. For instance, there are still debates on whether CO_2 activation takes place as a concerted proton-coupled electron transfer (PCET) process [46] or simply a substrate-assisted electron transfer process followed by the protonation [47]. While PCET has been more accepted in recent years, the debates on the activation process are not settled: The adsorbed COOH could have different orientations; the hydrogenation may occur on either C or O. When the CO_2 molecule coordinates with the metal site via an O atom, C would be protonated, leading to the formation of HCOOH (the formate pathway). If the CO_2 molecule is absorbed via a metal-C bond, one of the two oxygen atoms would be protonated to yield primarily CO as the product (the CO pathway; Scheme 1).

After the dissociation of the primary products, the catalyst would be regenerated/reduced by either sacrificial reagents or an electric bias. The following steps after the initial activation could be more complex, as more possibilities of the reaction pathways would emerge (more detailed discussions in the following sessions). Generally speaking, the different reaction pathways depend on the sequence of the electron transfer, protonation and dehydration processes. Moreover, when C—C coupling is also taken into account, there would be a significant number of possible intermediates and products [48]. Active research is pursued to understand what the intermediates are and how the various C_2 and C_3 products evolve during the reactions.

1.4. Scope of this review

This review focuses on catalytic reduction of CO_2 in aqueous solutions, which may be realized by electrocatalytic (EC), pho-

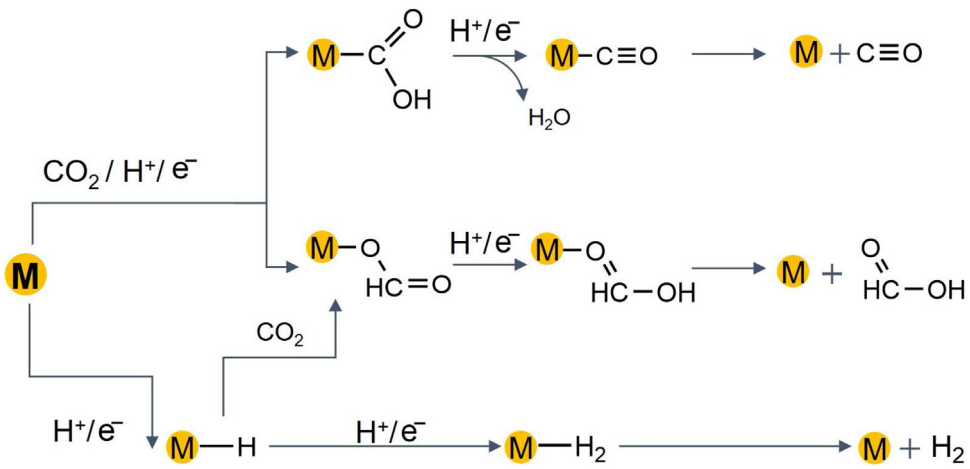

Scheme 1. Schematics illustrating the two branches during the initial CO_2 activation on catalysts and the competing H activation, which would lead to HER.

toelectrocatalytic (PEC) or the photocatalytic (PC) processes. The former two (EC and PEC) involve external biases, and the latter two (PEC and PC) require illumination. Either way, CO_2 is converted to reduced carbonaceous species, and electric and/or solar energy is stored as chemical energy. In each of the three approaches, there exists an enormous body of published works aimed at developing systems with better efficiencies and selectivity. Consequently, a good number of reviews have been published to discuss on the various aspects (e.g., on specific groups of catalysts or on specific steps of the reactions). Our goal of composing this review is to avoid repeating these prior efforts. Instead, we classify the CO_2 reduction systems into two categories: (i) bias-catalyst system and (ii) photo-induced system. The basis of this categorization comes from the insight that, despite the apparent differences in researches focused on the different processes, they share more in common. For instance, the electrocatalysts used in the EC processes are not fundamentally different from the co-catalysts used by many PEC and PC processes. As such, we are provided with a common thread to organize the materials for this present review.

In the first group (bias-catalyst system, Section 2), the actual CO_2 reduction takes place on an individual catalyst such as a metal-complex molecule, a metal or a semiconductor (Scheme 2). In the case of EC, such catalyst would be loaded or connected to the electrodes, and an external bias is used to drive the reaction. A PEC process is similar, except that the catalyst is loaded onto a photoelectrode, and the external bias needed on the photoelectrodes are usually less than what is required for the reduction of the CO_2, as the photovoltage generated by the photoelectrode when the light is on would partially compensate it. In terms of PC, the driving force for CO_2 reduction would be entirely provided by the photocatalysts, which absorb light and usually generate electron-hole pairs. The electrons and holes are then separated and transferred to the surface catalysts to participate in reduction and oxidation half reactions. It is noted that, the phrase "catalyst" here specifically refers to the species that actually interact with CO_2; in the field of photochemistry, the photoelectrodes or the light-absorbing species are normally referred as "catalysts" or "photocatalysts", whereas the reaction site is often referred as the "co-catalysts". In addition, although the co-catalyst in PC/PEC share great similarity with EC catalysts, issues such as interaction with the photosensitizers or photoelectrodes must be considered. Efforts on optimizing interactions between light absorber and catalysts are non-trivial. So it is worth setting a separate session (Section 2.4) for applying those catalysts in PEC/PC system for further discussion.

The second system (photo-induced, Section 3) represents another important family of reactions, where the light plays an important role from a chemistry perspective (Scheme 3). Light, as a quantized energy source, can induce charge excitation. Intermediates different from thermal excitation may be observed in photochemical processes. Therefore, the routes for these photo-induced reactions could be very different from the normal thermal or electrochemical ones. New possibilities for CO_2 reduction become possible. On a fundamental level, the ability to directly use optical energy to power thermodynamically uphill reactions such as CO_2 reduction is extremely appealing. In comparison to EC or PEC, where the electricity comes from solar cell modules, PC represents the most direct utilization of solar energy and, hence, holds the promise for low-cost applications.

2. (Co-)catalysts in EC, PEC and PC CO_2 reduction reactions

Traditionally, catalysts for CO_2 reduction could be divided into the two categories of homogeneous and heterogeneous. Of them, homogeneous catalysts normally refer to molecular complexes, and heterogeneous ones are solids. In recent years, new materials such as metal-organic frameworks or nanostructure materials are also investigated as CO_2 catalysts with record-setting performance (Section 2.2.1) [49–51].

2.1. Homogeneous catalysts

Homogeneous catalysts normally refer to molecular complexes that are mixed with reagents in solutions homogeneously. There is no clear phase segregation between catalysts and reactants. Homogeneous catalysts are usually well-defined in their structures thanks to decades of research on molecular systems. As such, when used for CO_2 reduction, the reaction pathways are well-defined, as well, promising high selectivity. There have been several comprehensive reviews about the homogeneous catalysts, [18,45,52,53] to which interested readers are referred. It suffices to note here that common homogeneous catalysts for CO_2 reduction include metal-complexes, small organic molecules such as pyridinium ion and enzymatic CO_2 reduction catalysts. As research progresses, however, the boundaries between the traditional definitions are being blurred. Increasing efforts attempt to take advantage of the detailed knowledge on molecular catalysts and apply it to heterogeneous systems for extremely high turn-over numbers (TONs). Similar TONs would be inaccessible by conventional homogeneous catalysis systems. One of such approaches is to integrate molecular catalysts with an (photo)electrode. Furthermore, the latest advancements of material synthesis make it possible to synthesize catalysts of atomically dispersed catalytic sites. Although such

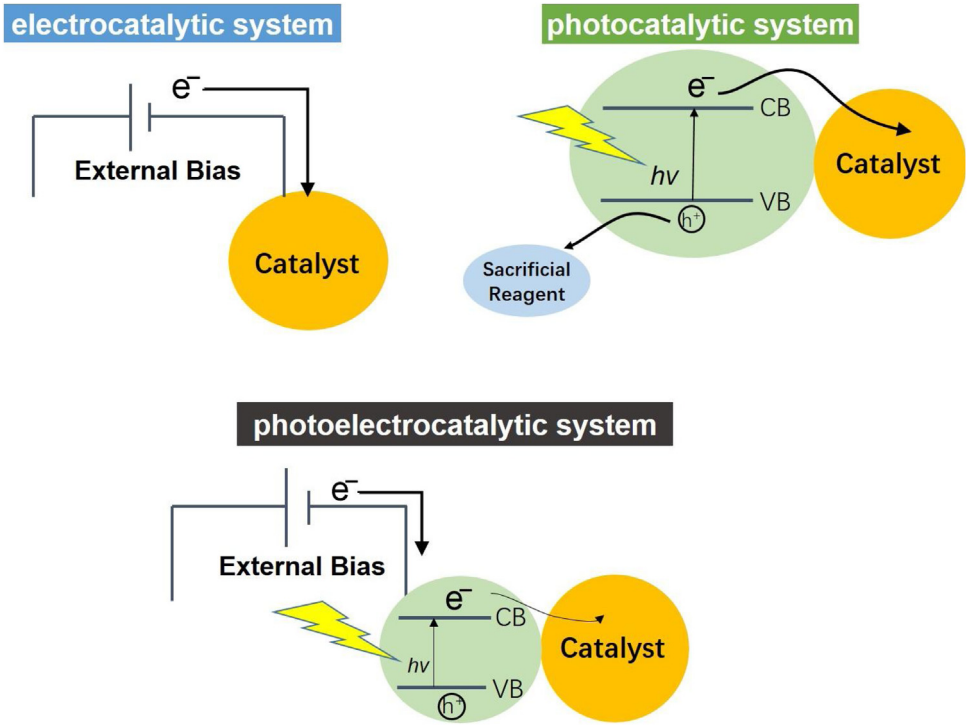

Scheme 2. Schematics illustrating the electron sources and catalysts in the electrocatalytic, photocatalytic and photoelectrocatalytic systems.

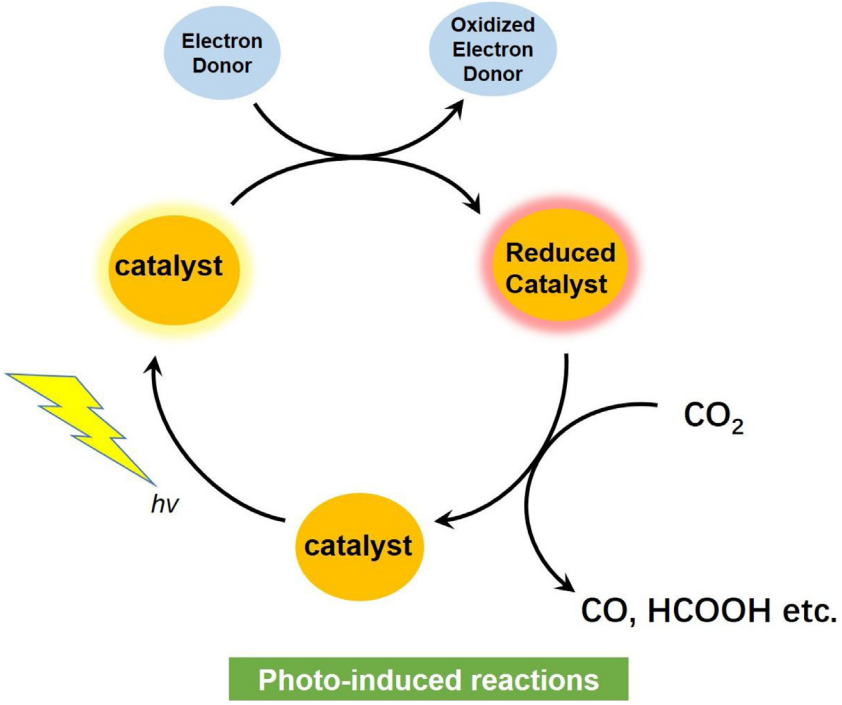

Scheme 3. Schematic illustration of the excitation and reaction of photo-induced processes.

catalysts are not "dissolved" in the solution during reactions, their catalytic center is well-defined, making it possible to understand the reaction mechanisms at the molecular level. These systems are difficult to categorize by the conventional ways, either.

2.1.1. Molecular organometallic complexes

The earliest and mostly discussed family of homogeneous catalysts are molecular organometallic complexes (Scheme 4a). With a typical catalyst molecule, the active center is a transition metal atom, whose oxidation states can vary, making it attractive to hold charges for the desired redox reactions. The ligands help not only to stabilize the metal center in different redox states, but to guide the binding of reacting substrates so as to help define reaction selectivity. Specifically, for CO_2 reduction, CO_2 binds to the metal center directly, and a subsequent inner sphere electron transfer activates the bound molecule, forming a bent structure for further reduc-

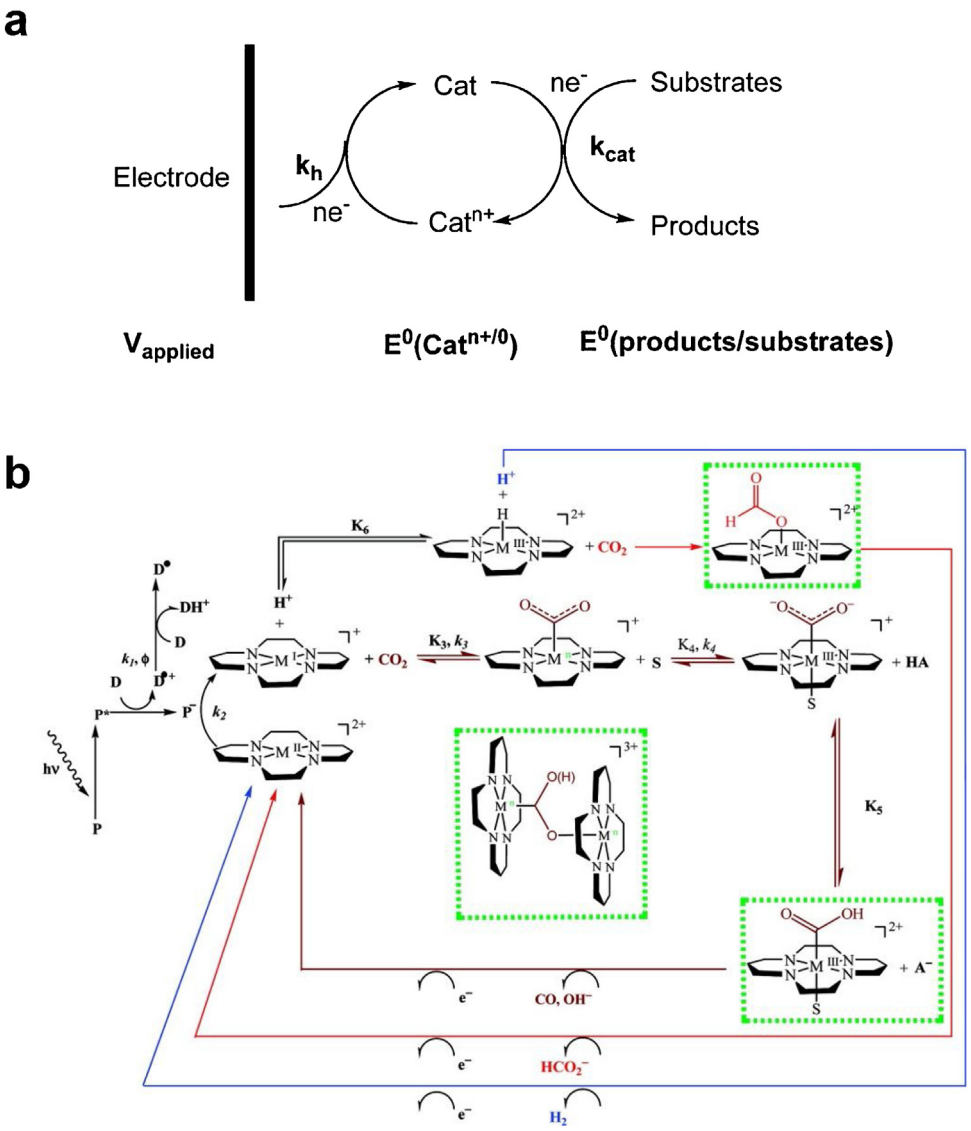

Scheme 4. a) Schematics illustrating the electrocatalytic reduction process with homogeneous catalyst. (Figure reproduced from ref. 53, copyright 2009, Royal Society of Chemistry); b) Proposed CO_2 and HER photoreduction mechanisms on metal-cyclam complex catalysts. (Figure reproduced from ref. 60, copyright 2012, Royal Society of Chemistry).

tion. The metal centers include late transition metals such as Co, Ni, Re, Fe, Cu and Ru [54,55]. Some prior papers also classify the metal complex catalysts with the ligand families, including carbonyl, TPA (tris(2-pyridylmethyl)amine), macrocycles, bipyridines, porphyrines and phosphines. Some of the well-known catalysts include Re-based $Re(bpy)(CO)_3X$ (the Lehn's catalyst) [56], Co or Ni-based tetraazomacrocyclic complexes (by Eisenberg et al.) [57], Fe porphyrins [58] and Pd phosphines [59], just to name a few. Among them, the Re carbonyl catalyst is reported as the most active and selective for converting CO_2 to CO.

Importantly, homogeneous catalysts for CO_2 reduction are usually studied in non-aqueous solutions because of their sensitivity to hydrolysis. Such a configuration mitigates an important concern of potential competition by HER during CO_2 reduction. We next use metal-cyclam (1,4,8,11-tetraazacyclotetradecane) complex as an example to discuss the detailed mechanisms by which CO_2 reduction is carried out [60,61]. As shown in Scheme 4b, the complex first receives an electron, reducing the metal center. Then, the reduced metal center binds to either CO_2 or proton (H^+). In the first case, with a PCET from metal center to CO_2, carboxylate group forms and binds with the metal center. In the meanwhile, the metal center is re-oxidized to the original oxidation state. Further electron transfer and OH desorption lead to the formation of CO that turns over the catalyst. In the second case, after the binding of metal center with proton, CO_2 gets inserted into the M—H bond, resulting in formate formation. A second electron transfer leads to the production of formic acid.

Guided by the mechanisms understood so far, great efforts have been made to adjust 1) the electronic properties of the reaction center and 2) the steric environment near the activity center to improve electrochemical/photochemical CO_2 reduction by homogeneous catalysts. Accordingly, researches on catalyst designs mostly focused on the choices of metal centers and the modification of the ligands [62–65]. For example, in a recent publication, Nippe et al. designed an imidazolium-functionalized Lehn's catalyst and achieved an increase in the reaction rate and selectivity of CO formation [66]. The authors demonstrated that the intramolecular imidazolium group forms a second coordination sphere (C_2-H···Cl-, C_2-H···CO^{2-}, and C_2-H··· OH_2) and attributed the improvement of the performance to the resulting faster dissociation of Cl- after comparing catalysts with similar ligand structures (Fig. 1a).

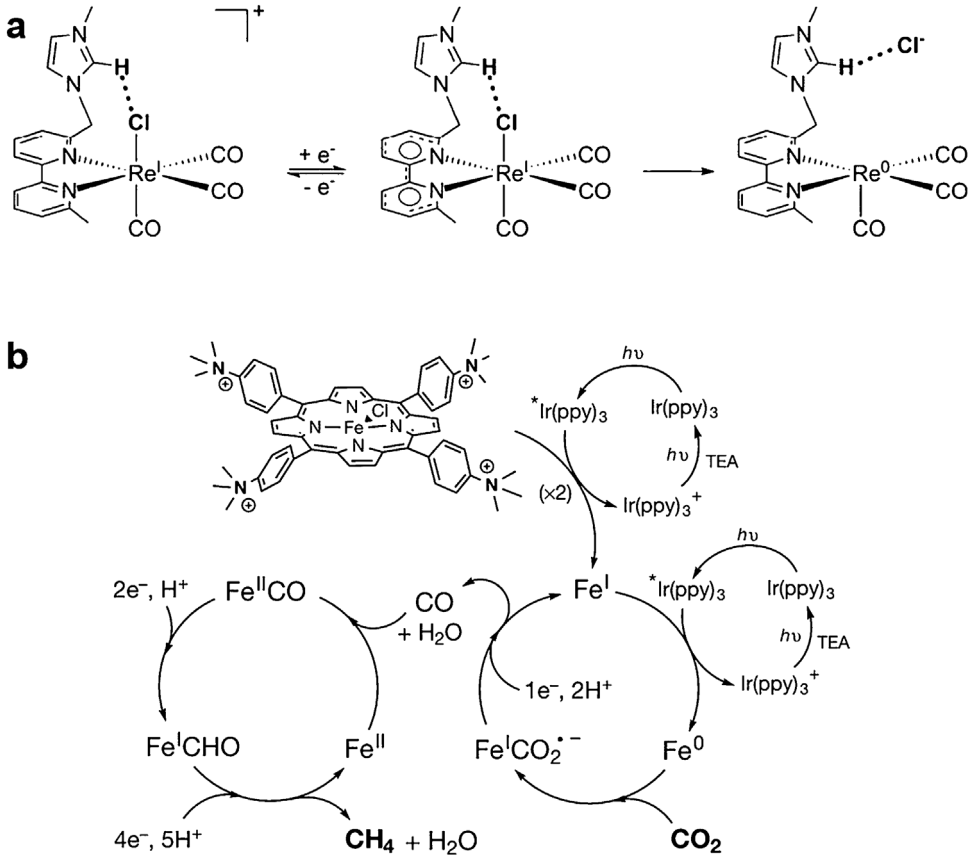

Fig. 1. a) Proposed Cl^- dissociation process during the 1 e- reduction on an imidazolium-functionalized Re catalyst. The nearby imidazolium group promoted the dissociation via intramolecular coordination. (Figure modified from ref. 66, copyright 2017, American Chemical Society); b) Proposed mechanism for CO_2 reduction to CH_4 by the iron n-tetraphenylporphyrin complex functionalized with trimethylammonio groups. (Figure reproduced from ref. 76, copyright 2017, Nature Publishing Group).

The so-called early transition metal complexes are also introduced in this area for CO_2 reduction in recent years. [67] Whereas late transition metal complexes usually yield formate and CO as a result of the $2e^-$ transfer nature, in some cases early transition metal complexes can be more reactive toward products such as methanol and methane. [67] For instance, methanol is the main product in some of the reactions catalyzed by Zr and Ti complexes [68,69]. On the other hand, varieties of Mn-based metal complexes are developed to replace the more precious Re or Ru-based metal complex catalysts [70–72].

Most metal complex catalysts produce $2e^-$ reduction products such as HCOOH or CO. They rarely exhibit selectivity toward reduction products such as methanol, methane or other hydrocarbons, with an exception of a handful of successful examples whose mechanisms are unclear beyond CO formatio. [73–75]. The phenomenon could be simplistically explained by the fact that most of these metal complexes feature a single binding site which would lose the reduction ability after transferring e^- to CO_2. Moreover, in most cases, the reduction potential of the complex is not low enough for further reduction of the CO or HCOOH. In a recent work, Rao et al. reported the production of CH_4 with a molecular Fe catalyst, iron tetraphenylporphyrins, in a photochemical system driven by visible light [76]. Previously Fe complexes with 4 para-phenyl trimethylammonio substitution groups had been shown the most efficient for electrochemical conversion of CO_2 to CO, with the catalyst reduced from the Fe^{III} to Fe°. In this work, the oxidation state of Fe shifts between 0 and 1 with $Ir(ppy)_3$ as the photosensitizer (Fig. 1b). It is hypothesized that the co-existence of redox pairs Fe^{II}/Fe^{I} and Fe^{I}/Fe° makes it possible to drive the reduction beyond CO formation. More specifically, the catalyst further forms a $Fe^{II}CO$ intermediate to start another catalytic cycle to convert CO to methane. The authors emphasized the importance of the redox potentials of the specific catalysts and the functional groups that could stabilize the intermediates to the observed reactivity. Changing the substitution group to —OH at the ortho and ortho' positions would lower the standard redox potential by 75 mV, and CH_4 production decreased. The metal complex without substitution groups on the phenyl has the highest standard redox potential of $E^{\circ}(Fe^{I}/Fe^{\circ})=-1.67$ V vs. SCE in DMF, and it could not produce CH_4 at all. The photosensitizer is also of great importance for driving the reduction beyond the two e^- processes. The redox potential of the photoexcited species must be more negative than all three redox couples of the Fe complexes. Metal complex catalysts usually participate in the electrocatalytic reduction of CO_2 in a homogeneous manner; alternatively, they can be grafted onto the electrode to work in a heterogeneous fashion [77]. To this end, Brudvig and Wang et al. recently reported a Cu-porphyrin complex as a heterogenized molecular catalyst [78], which was able to convert CO_2 to hydrocarbon at a potential of -0.976 V vs. RHE with a Faradaic efficiency of 44% at a mass loading of 0.25 mg cm^{-2}. The catalyst was directly deposited on a polytetrafluoroethylene-treated carbon fiber paper with a porous carbon coating layer. The porous carbon layer was made of carbon nanoparticles and acted as the support for catalysts. These heterogenized molecular catalysts exhibited the advantage of readily tuned catalysis efficiency and selectivity, as the molecular structure of the catalysis active site could be designed and tailored.

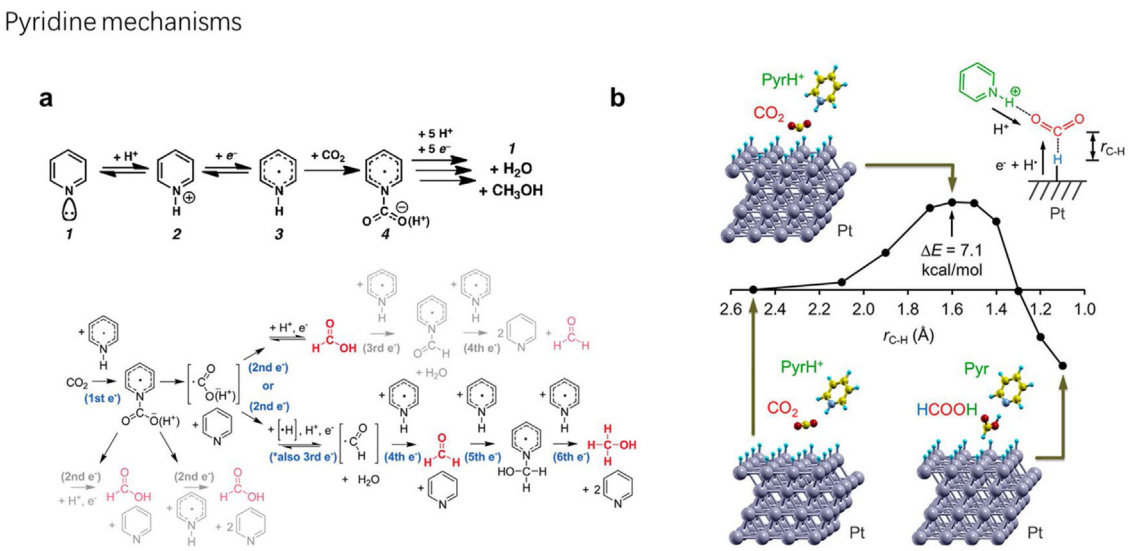

Fig. 2. a) Proposed pyridine protonation and pyridinium-catalyzed reduction of CO_2 to formic acid, formaldehyde, and methanol by Bocarsly et al. (Figure reproduced from ref. 80, copyright 2010, American Chemical Society); b) pyridine-H^+ promoted proton-coupled hydride transfer on the Pt(111) surface. (Figure reproduced from ref. 81, copyright 2013, American Chemical Society).

2.1.2. Pyridinium system

Pyridine has been identified as a non-metal molecular catalyst for electrocatalytic reduction of CO_2 for over two decades. In 1994, Bocarsly et al. reported the use of pyridine as a homogeneous catalyst for CO_2 reduction to CH_3OH at overpotentials <1 V on the Pd electrode. [79] The same group also demonstrated using p-type GaP with pyridine for photoelectrochemical CO_2 reduction to CH_3OH. Since then, pyridine has been applied to a variety of electrochemical, photoelectrochemical and photochemical systems for the production of CH_3OH and formic acid. Despite the experimental successes, however, the exact mechanisms by which pyridine-catalyzed CO_2 reduction proceeds remains under debates.

Bocarsly and coworkers proposed that the one-electron reduced pyridinyl radical from the protonated form of pyridinium would bind to CO_2 to form a carbamate radical adduct, activating CO_2 (Fig. 2a). [80] Since pyridine is rarely used alone but usually coupled with Pt or p-GaP etc., Araujo and Batista et al. proposed a pyridinium-assisted activation of CO_2. A proton-couple hydride transfer takes place when the protons of the pyridinium interact with CO_2, together with surface-bound hydride, causing the CO_2 molecule to bend and get activated (Fig. 2b). [81] In a different view, Carter et al. calculated the thermodynamic energies of various pyridine-derived intermediates and concluded that a surface-bound dihydropyridine (DHP) species, instead of the pyridinyl radical, is the actual catalyst in the reaction (Fig. 3a). [82–85] The surface-bound DHP facilitates efficient hydride transfer in both homogenous solutions and on a photoelectrode surface, making it a general mechanism.85] Musgrave et al. also carried out similar calculations to investigate the effect of pyridine in the p-GaP system. Their results suggested a solvent-assisted PCET process in the homogeneous phase through the formation of the pyridine carbamate radical adduct, while the electrode surface only acts as a site for the regeneration of the pyridinyl radical.

There are also other proposed mechanisms. For instance, MacDonnell et al. designed a photochemical system for CO_2 reduction with a ruthenium (III) trisphenanthroline as the chromophore, ascorbic acid as a sacrificial reductant and pyridine as the catalyst [86].The system operated by visible light excitation and produced CH_3OH and formate with quantum yields of 0.025 and 1.1×10^{-4}, respectively. Another key feature in this system is that addition of Pt would cause no effects for CH_3OH production, in stark contrast to most pyridine-based electrocatalytic systems. In a more recent work, Xu and Yan et al. studied pyridine-mediated CO_2 reduction on Pt surfaces using in situ Infrared spectroscopy and proposed that pyridinium promoted the formation of formate only as a proton donor in the second PCET process (Fig. 3b). [87]

2.1.3. Enzyme

The naturally occurring catalytic reduction of CO_2 to CO takes place on carbon monoxide dehydrogenase (CODH). The CODHs found in aerobic bacteria feature a Mo-and Fe-containing active site, and those found in anaerobic bacteria have a Ni- and Fe-containing active site. Both groups of enzymes are capable to catalyze this reaction reversibly, efficiently, and as their names indicate, selectively. The latter (Ni- and Fe-containing one) is also capable to catalyze the synthesis of acetyl-CoA, which is most studied in the literature. The CODH isolated from *Moorella thermoacetica* has a $\alpha_2\beta_2$ quaternary structure, consisting of 4 clusters. The C-cluster, which is a Ni-Fe-S cluster with cubane connections, is found responsible for the CO_2/CO redox reaction. The reversible redox reaction involves the coordination of CO_2 with Ni and forming a Ni-C-O-Fe bridge. [88] The CODH can be applied in vitro for both electrochemical reduction and photocatalytical reduction of CO_2. In order to participate in the electrocatalysis reaction, the enzyme could be applied directly as a homogeneous catalyst or attached to electrodes, namely the protein film electrochemistry (PFE). In the first case, since the enzyme does not directly accept electrons from an electrode, Shin et al. employed an electron-transfer mediator (methyl viologen) (Fig. 4a) [89]. Later, Armstrong et al. studied the reversible conversion of CO and CO_2 of the CODH I purified from the anaerobic thermophile *Carboxydothermus hydrogenoformans* (*Ch*) on an electrode [90].

Other families of enzymes have been shown to promote CO_2 reduction, as well [91,92]. For instance, CO_2 could be converted to formate by formate dehydrogenase (FDH) [92] or carbon dioxide (CO_2) reductase [93]. Hirst et al. reported the conversion of CO_2 to formate with W-containing FDH1 adsorbed on an electrode. [94]. The thermodynamically reversible reaction requires only small overpotentials and produces formate as the sole product. In another demonstration, the same group reported reversible reduction of CO_2 with a Mo-containing FDH H purified from *Escherichia coli* [95]. The catalyst contained one Mo-selenocystein residue, two molyb-

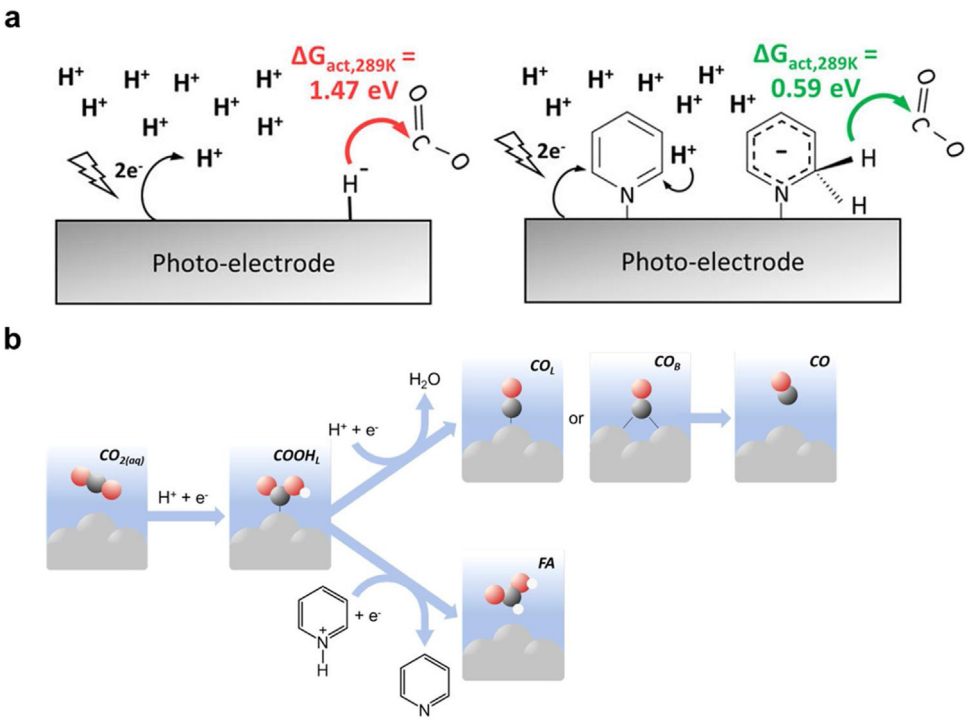

Fig. 3. a) Normal and 2-PyH^{-*} intermediate promoted hydride transfer on GaP(111) for photoreduction of CO_2. (Figure reproduced from ref. 85, copyright 2017, American Chemical Society); b) Pyridine catalyzed–CO_2 reduction mechanism on Pt electrodes proposed by Xu's group based on the reactivity and spectroscopic results. (Figure reproduced from ref. 87, copyright 2017, American Chemical Society).

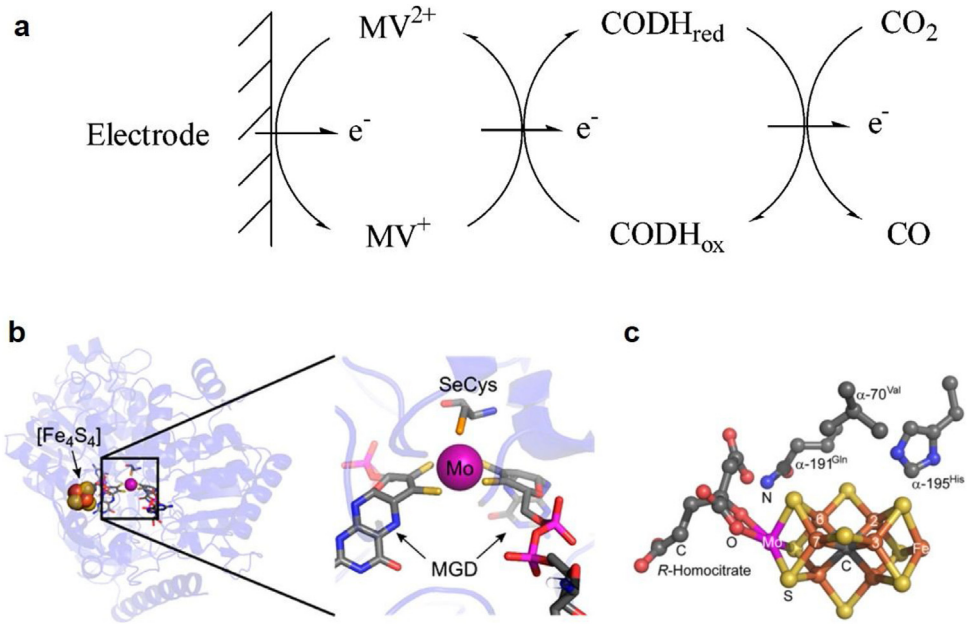

Fig. 4. a) Schematics illustrating the electrocatalytic reduction of CO_2 with CODH as homogeneous catalyst. (Figure reproduced from ref. 89, copyright 2003, American Chemical Society); b) the active site of the EcFDH-H consisting of Mo coordinated by a SeCys residue and two molybdopterin guanine dinucleotides. A nearby [4Fe-4S] cluster transports electrons to the active site. (Figure reproduced from ref. 95, copyright 2014, American Chemical Society); c) the active site of the Nitrogenase containing the FeMo cofactor with surrounding key amino acid residues. (Figure reproduced from ref. 96, copyright 2012, National Academy of Sciences).

dopterin guanine dinucleotides, and a 4Fe-4S cluster that transfers electrons to the active center (Fig. 4b). PFE studies showed the catalyst had similar activity with W-containing FDH1, yet their solution-based catalytic activities were different. The turnover frequencies for the FDH H-catalyzed CO_2 reduction with the methyl viologen as the electron transfer reagent was less than 1 s^{-1}, much lower than the reverse reaction, making it thermodynamically unfavorable. The author suggested two possibilities: (1) the inactive purified catalyst state or (2) the single 4Fe-4S cluster was in a high reducing potential and, as such, not ready to accept electrons from methyl viologen. Nitrogenase, whose main function is to catalyze the multi-electron reduction of N_2, could also promote CO_2 reduction to CO. To this end, Seefeldt et al. reported a remodeled nitrogenase for the reduction of CO_2 to CH_4, forming up to 16 nmol (methane) $nmol^{-1}$ (MoFe protein) over a 20 min reaction (Fig. 4c) [96].

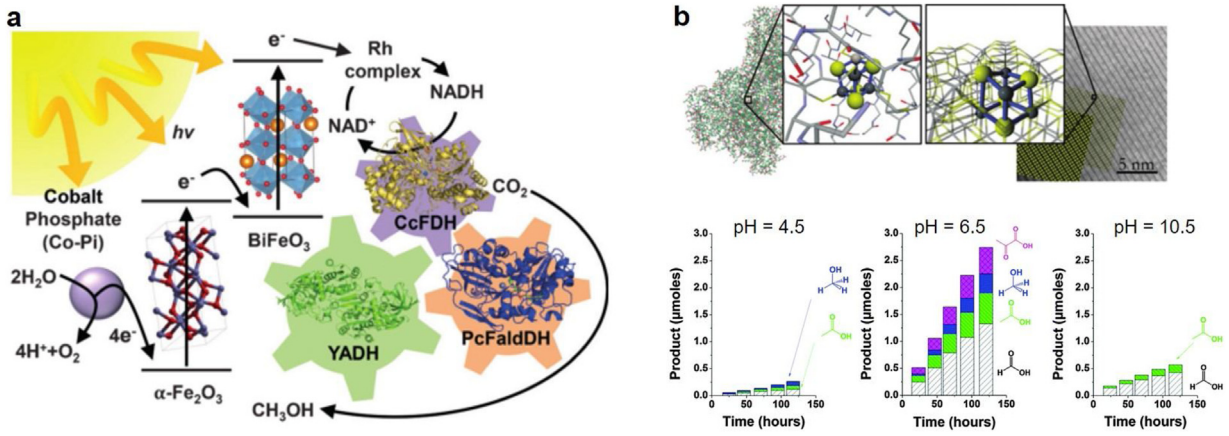

Fig. 5. a) Schematic illustration of the production of methanol through a three-enzyme (CcFDH, PcFaldDH, YADH) tandem cascade. (Figure reproduced from ref. 97, copyright 2017, Wiley·VCH; b) Schematics illustrating the similarity between the ferredoxin center of the CODH enzyme and the greigite surface where the Fe_3S_4 (001) are cubane structure, and the various amount of formic acid, acetic acid, methanol and pyruvic acid produced at different pH with Fe_3S_4 as catalyst. (Figure reproduced from ref. 99, copyright 2015, Royal Society of Chemistry).

When the biocatalysts are employed for CO_2 reduction, a vast pool of enzymes with various functions are available. Such an advantage allows the design of tandem reactions. For instance, FDH can be used to reduce CO_2 to formic acid, and AldDH (aldehyde dehydrogenase) and ADH (Alcohol dehydrogenase) can then be used to further reduce the formic acid to methanol [91]. Lee and Park recently reported a hybrid PEC system that integrated a complex enzyme-cascade system together with a Z-scheme system with a Co-Pi/α-Fe_2O_3 photoanode and a $BiFeO_3$ photocathode (Fig. 5a) [97]. Water oxidation occurred on the photoanode, and electrons generated on the electrode were first transferred to a Re-complex and NAD^+. The NAD^+ was then reduced to NADH. Next, a CcFDH-PcFaldDH-YADH enzyme cascade was used to produce CH_3OH from NADH, in which the PcFaldDH was discovered with superior formate-reduction ability. The tandem PEC system could generate NADH from NAD^+ without external bias and using water as the electron donor; when a 0.8 V bias was applied, an 80% yield of NADH regeneration rate was obtained. When both photoelectrodes were illuminated, a spontaneous photocurrent of 38.3 μA cm^{-2} and an open circuit potential of 909.2 mV were measured.

A common feature of enzymes active for CO_2 reduction is that their active center contains a metal cluster. More specifically, a Fe-S cluster is present in all cases, with another metal ion of Ni, Mo or W. This common component has attracted significant research interests. Nørskov et al. carried out a computational study on the Ni-Fe-S cubane for CO_2 reduction. [98] The binding energies of the reduction intermediates, such as COOH*, on the cubanes with various Ni were calculated, and it was found that the presence of Ni improved the catalytic selectivity of CO formation. The cubane containing 1 or 4 Ni was concluded to be theoretically as active as noble metal surfaces for the reduction to CO, and only those contains 1 or 0 Ni are stable. In another work, de Leeuw et al. found similar cluster structure in the iron sulfite mineral greigite (Fe_3S_4) and performed CO_2 reduction on greigite surface to obtain soluble organic molecules including formic, acetic, pyruvic acid and methanol (Fig. 5b). [99] Importantly, the surface of greigite (001) resembles the [4Fe-4S] clusters in the CODH enzymes.

The lessons learned on enzymes can be transferred for catalyst designs of metal complexes. The co-existence of the multiple metal centers within an enzyme could be the origin of their high selectivity. Mankad et al. demonstrated the utility of this knowledge by designing a series of Cu-Fe, Cu-W, Cu-Mo and Cu-only N-hetercyclic carbine-ligated catalysts [100]. The heterobimetallic effect allowed the control of products from HCOOH to CO. Similarly, an iron porphyrin dimer with co-facial orientation and suitable separation of the Fe centers has been shown to promote CO_2 reduction activity, selectivity and stability [101]. The co-facial orientation offered a special site where the two Fe centers provided a local push-pull mechanism for the coordinated CO_2.

2.2. Heterogenized homogeneous catalysts

While homogeneous catalysts hold the advantages of high activity and selectivity, it is often difficult to separate the catalysts from the reaction mixture and, hence, a challenge to reuse the catalyst. Moreover, the activity of the catalyst tends to be sensitive to the structural integrity, making it difficult to achieve TONs. One emerging approach to address this challenge is to combine homogeneous catalysts with metal-organic frameworks (MOFs), [50,51,102,103] covalent-organic frameworks (COFs) and carbon-based nanomaterials. From a practical application perspective, the resulting catalysts may be considered as “heterogenized” homogeneous catalysts because they have the potential to feature advantages of both homogeneous and heterogeneous catalysts.

2.2.1. MOFs and COFs

MOFs are formed with metal ion nodes and organic connections. The metal nodes are usually secondary building units that are made of metal complexes. The properties of the MOFs can be highly diverse depending on the choice of the metal ion and the organic ligands, as well as the way they are connected. Fine tuning of MOF properties such as the porosity is also possible by adjusting the molecular structures of the organic connectors. When applied for CO_2 reduction, MOFs may be used as either a sensitizer for photocatalytic reaction or a catalyst. In addition, they could also be employed as the support for holding other active catalysts to facilitate reactions in a nanoscale reactor.

Since the metal ions in a MOF coordinate with the organic molecules the same as in a molecular metal complex, it may be treated as an assembled homogeneous catalyst for the study of reaction mechanisms, despite their heterogeneous appearance. Such an approach makes it possible to tap into the rich knowledge base of mechanistic studies on molecular catalysis. For instance, Yang and co-workers incorporated a Co-porphyrin unit into the $Al_2(OH)_2$TCPP-H_2 backbone and achieved a CO Faraday efficiency of 76% and 7 h stability for CO_2 reduction (Fig. 6a) [104]. In another work, Hupp and co-workers deposited a thin film of MOF-525 on an FTO electrode and installed a Fe-porphyrin unit as the catalytic site (Fig. 6b). The MOF support enabled a much higher loading of catalysts than simple heterogenized molecular complexes. Con-

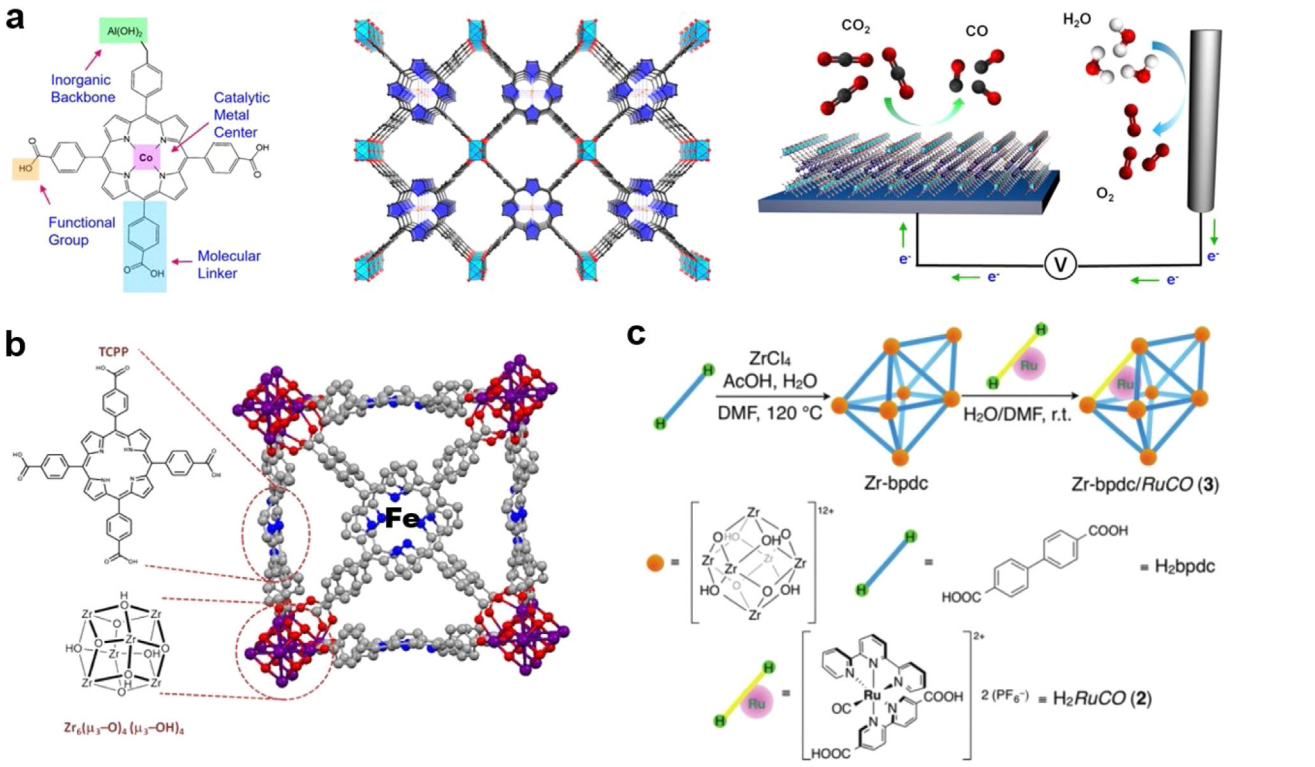

Fig. 6. Schematics illustrating a left: the cobalt-metalated TCPP organic building units; middle: the assembled 3D $Al_2(OH)_2$TCPP-Co MOF, with each carboxylate of the organic building unit bound to the aluminum inorganic backbone; right: The CO_2 electrochemical reduction system constructed by integrating the $Al_2(OH)_2$TCPP-Co MOF with a conductive substrate. (Figure reproduced from ref. 104, copyright 2015, American Chemical Society); b) the structure of Fe_MOF-525, including the chemical structure of the TCPP linker and the Zr_6-based node. (Figure reproduced from ref. 105, copyright 2015, American Chemical Society); c) the integration of the CO_2 catalyst into the Zr-based MOF UiO-67 with a $Ru^{II}(H_2bpydc)(terpy)(CO)](PF_6)$ derivative bearing carboxylic acid substituents. (Figure reproduced from ref. 106, copyright 2016, Wiley·VCH).

sequently, a more efficient catalyst than either the homogeneous form or the simple heterogenized forms was obtained [105].

A unique advantage offered by MOF-based catalysts stems from the porous nature of its structure. The high surface area facilitates better CO_2 adsorption. Kitagawa et al. incorporated photoactive Ru^{II}-CO catalyst into a Zr-based MOF and discovered that the CO_2 adsorption ability by the MOF could promote the reaction (Fig. 6c) [106]. Moreover, the synergetic effect between the MOF backbone and the catalytic unit enabled catalytic activities even at a low CO_2 concentration of 5% CO_2/Ar. One additional benefit of confining catalysts in a nanoscale space is the possibility of accessing unusual reaction selectivity. In a system different from MOF, Sun and co-workers studied the effect of the curvature of Co-porphyrin nanotubes on CO_2 reduction (Fig. 7a). [107] Using DFT calculations, the authors found that the Co-porphyrin could be rolled into nanotubes with different diameters, and their results predicted that these nanotubes would catalyze CO_2 to CH_4 or CO with lower overpotentials than on Cu or Au, respectively.

Similar to MOF, covalent organic frameworks (COFs) have been explored as a catalyst host for CO_2 reduction. Aside from the benefits expected from MOF-based catalysts, COFs present a platform for possible integration of functionally different yet structurally similar molecular catalysts. To this end, Yaghi and Chang et al. designed a COF structure that contained catalytic Co-porphyrin units as well as structural Cu units by linking the catalytic motifs and Cu-porphyrin units with imine bonds (Fig. 7b). They were able to obtain a maximum of 26-fold increase in activities for the reduction of CO_2 to CO in water. [108]

2.2.2. N-doped CNT/graphene

Carbon-based nanostructures are yet another attractive host for the integration with molecular catalysts. For instance, carbon nanotubes (CNT) have been popularly studied for this purpose. One added benefit of using CNT is the inherent catalytic activity, which may be exploited for important reactions such as oxygen reduction reactions (ORR). In particular, N-doped carbon nanomaterials have been identified active for CO_2 reduction. Guo et al. performed first principle calculations to study N-doped graphene and CNTs for electrochemical CO_2 reduction. [109] The doped N can be classified as graphitic N (gN), pyridinic N (pN), or pyridinum (pNH); the local configuration may be perfect or contain the defect or zigzag edge. They revealed that gN doped edge sites are the most effective for CO_2 reduction. pN doped Stone-Wales defect and pN doped edges are also active but with higher activation barriers. Moreover, the authors also suggested that the selectivity and limiting potentials for given products of CO_2 reduction could be tuned by the curvature effect. One conclusion drawn was that graphene would be favorable for CO and HCOOH formation, whereas CNTs would feature sites for the formation of HCHO and CH_3OH.

On the experimental efforts, Kumar et al. demonstrated the superior performance of the N-doped carbon nanofibers prepared by pyrolysis of the polyacrylnitrile, and attributed the enhancement to the reduced carbon rather than N (Fig. 8a). [110] Ajayan et al. synthesized N-doped CNTs by a liquid chemical vapor deposition method from acetonitrile and dicyandiamide. The obtained bamboo-shaped multiwall N-doped CNTs were highly efficient and stable toward CO formation. They featured lower overpotentials in comparison to noble metals like Au and Ag, and a FE of 80% was obtained at −0.26 V vs. RHE. The activity and selectivity of the N-doped CNT was attributed to the existence of pyridinic N and pyrrolic N. These structural motifs remind us of the activities of pyridine for CO_2 reduction. Calculations showed that the binding energies of COOH intermediates on pyridinic N was negative and similar to those on Ni or Pt, while the binding energies of CO inter-

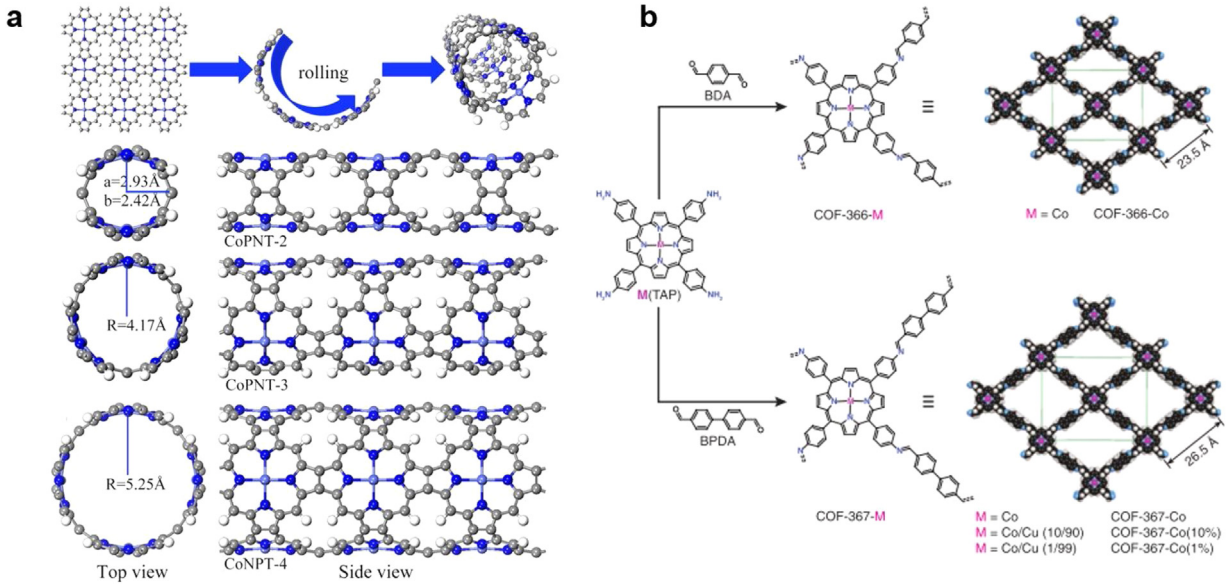

Fig. 7. a) Schematics illustrating the rolling of 2D CoPor sheet and the obtained CoPorNT-2, CoPorNT-3, CoPorNT-4 formed by confining different number of CoPor Monomers. (Figure reproduced from ref. 107, copyright 2016, American Chemical Society); b) 2D covalent organic frameworks COF-366-M and COF-367-M derived from different metalloporphyrin monomers. (Figure reproduced from ref. 108, copyright 2015, AAAS).

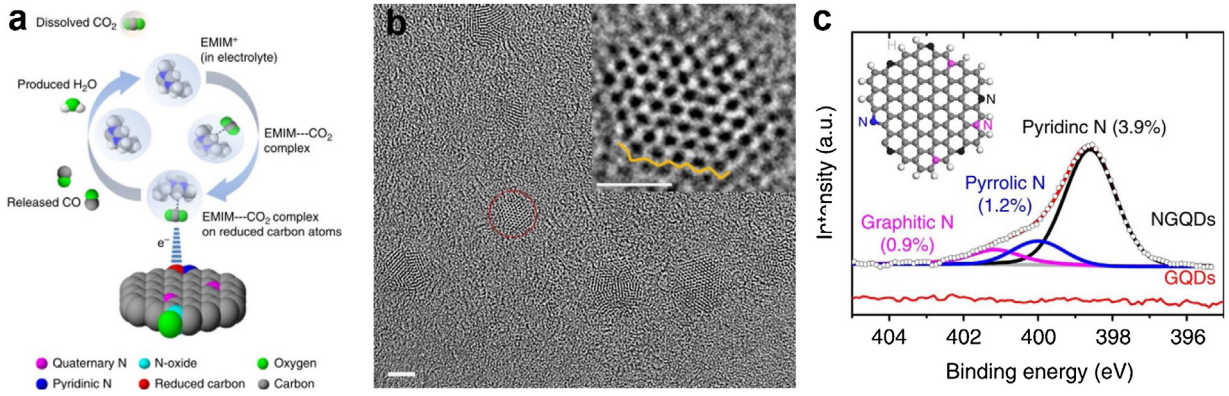

Fig. 8. a) Schematics illustrating the reduction of CO_2 on a polyacrylonitrile-based heteroatomic carbon nanofiber. (Figure reproduced from ref. 110, copyright 2013, Nature Publishing Group); b) High-magnification TEM image of N-doped graphene quantum dots (NGQDs). The enlarged image shows zigzag edges of the NGQDs. c) High-resolution N 1 s XPS spectrum for NGQDs, which is deconvoluted into three sub-peaks representing pyridinic, pyrrolic and graphitic N. The inset demonstrates the N-bonding configuration with respect to pyridinic (black), pyrrolic (blue) and graphitic (pink) N. (Figures reproduced from ref. 111, copyright 2015, Nature Publishing Group).

mediates were close to those on Au or Ag. The net result was that CO_2 was easily activated on these catalysts with ready desorption of CO as the preferred product.

N-doped graphene quantum dots (NGQDs) have been shown by Ajayan et al. as effective catalyst for the reduction of CO_2 to multi-carbon hydrocarbons. [111] The total FE reached up to 90%. The NGQDs were synthesized from exfoliated graphene oxides, using DMF solvents to achieve in situ N-doping during the synthesis. The catalysts were ca. 1–3 nm in diameters, ca. 1–3 atomic layers in thickness (Fig. 8b). At low overpotentials of −0.26 V vs. RHE, CO and HCOOH were produced; at high overpotentials (e.g., −0.61 V vs. RHE), deep reduction products such as methane, ethane, and multi-carbon oxygenates like ethanol, acetate and n-propanol were predominant. The authors compared the activity of NGQDs with pristine graphene quantum dots and N-doped reduced graphene oxide and concluded that CO_2 reduction on NGQDs was much faster. They suggested it was due to the high density of pyridinic N formation at the edge site (Fig. 8c).

2.2.3. Single-atom catalysts

As an intensely studied class of catalysts, single atom catalysts (SACs) refer to materials with active metal centers that are atomically dispersed on a support. Graphene is one of the most widely used support materials for SACs. In a way, SACs should be regarded as heterogeneous catalysts as they are not dissolved in the media during reactions. A critical advantage of this type of catalysts is the easy separation from the reactants/products for ready reuse. In the meanwhile, they also feature unique characteristics that are not available to typical heterogeneous catalysts. That is, the active sites are well-defined in structures, making it possible to study the reaction mechanisms at molecular levels. Despite the intense efforts, research on SACs is in its infancy stage, especially for CO_2 reduction. A recent calculation study assessed various SACs for the applications of CO_2 reduction. [112]. The authors found that many M@sv-Gr or M@dv-Gr, which referred to catalysts with a single transition metal (Ag, Au, Co, Cu, Fe, Ir, Ni, Os, Pd, Pt, Rh or Ru) atoms anchored on defective graphene with single or dou-

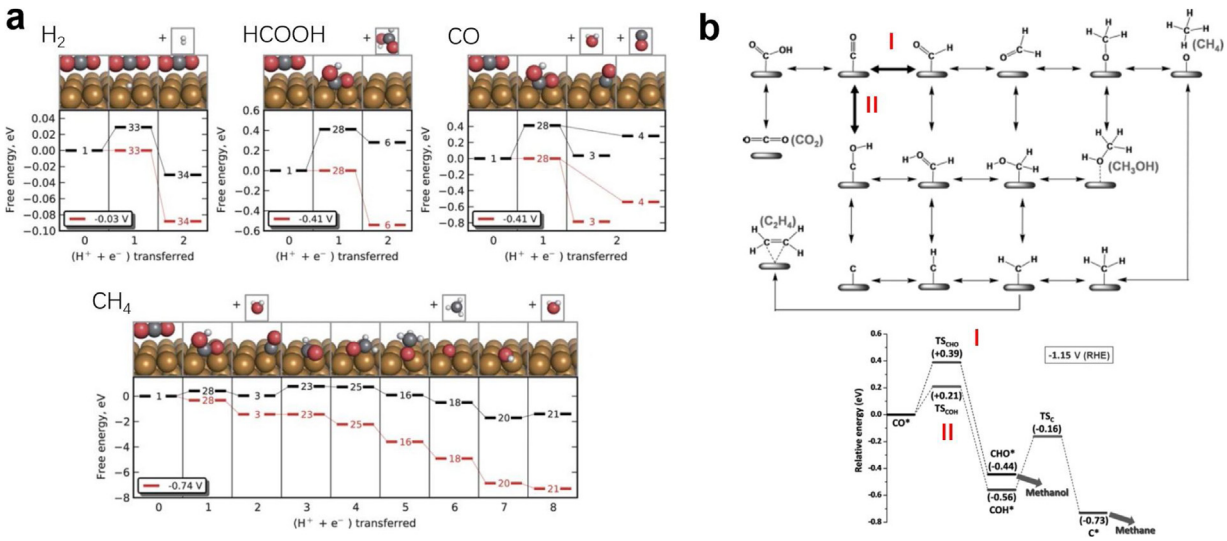

Scheme 5. a) Calculated free energy diagrams showing the lowest energy pathway to H_2, HCOOH, CO and CH_4 on Cu surface. (Scheme reproduced from ref. 122, copyright 2010, Royal Society of Chemistry); b) Proposed CO_2 reduction pathway to various products on Cu (111) surface and the calculated energy diagram showing the selectivity between the two main pathways. (Scheme reproduced from ref. 124, copyright 2013, Wiley·VCH).

ble vacancies, respectively, were selective toward CO_2 reduction. Among them, Pt@dv-Gr showed better selectivity toward CH_3OH production because of its single atom state. In another work, the authors investigated the performance of SACs on TiC and TiN and predicted that Ir@d-TiC would be the one with an extraordinarily low overpotentials (-0.09 V vs. RHE) for CH_4 production [113]. Experimentally, low valent Ni(I) SACs were recently prepared on defective N-doped graphene and exhibited enhanced CO_2 reduction to CO (97% FE) [114]. At a moderate overpotential of 0.61 V, the catalyst achieved a high specific current density of 350 A g^{-1} and a turnover frequency of 14,800 h^{-1}. Wang et al. also dispersed the single atom Ni on the graphene nanosheets and obtained comparable performance. [115] At a low overpotential of 0.55 V, the CO selectivity reached 95%.

2.3. Heterogeneous catalysts

Compared with homogeneous catalysts, heterogeneous ones offer advantages of low toxicity, low cost and simple post-preparation. The simplest heterogeneous catalyst would be a flat metal substrate. Research on using metal electrodes for electrochemical reduction of CO_2 started in the early 1980s. A number of metals have been found active for CO_2 reduction, including Hg, Au, Pb, Zn, Cd, In and Ru. These early studies usually focused on the liquid phase products, e.g., formate or methanol. In 1985, Hori and Suzuki reported CH_4 gaseous products on Cu [116]. They also studied a series of other metals and divided them into several groups. For instance, Cd, In, Sn and Pb produced mainly formate, with small amounts of CO and CH_4; Ag and Au yielded predominantly CO with slight amounts of formate; Cu was more favorable for CH_4 formation; Ni, Fe were more active to H_2 production. It is important to note that nearly all metal electrodes faced the problem of significant HER when CO_2 reduction was carried out in H_2O. Hori et al. again summarized and reviewed published works of CO_2 reduction on metal substrates in 2008 [117]. In recent years, similar research has been broadened to other materials, including metal oxides [118], metal chalcogenides [119], metal alloys [120] and, as discussed above, MOF materials. Also, with the emergence of nanoscience and nanotechnology, a number of new heterogeneous catalysts have been also developed with improved catalytic efficiency and selectivity [121].

Compared to homogeneous catalysts, the active centers of heterogeneous ones are often less well defined. Consequently, there lacks mechanistic understandings at the molecular level. Notwithstanding, important progresses have been made concerning the reactions as evidenced by improved selectivity and efficiency. Generally speaking, in the activation step of a heterogeneous CO_2 reduction reaction, two pathways are possible. In the first one, CO_2 is first reduced to carboxylate via PCET, which binds to the catalyst surface through metal-carbon bonds. Then with another PCET process, the hydroxide group from *COOH desorbs, leaving adsorbed CO on the surface, which is either further reduced to more reduced products or desorbs from the catalyst surface to yield gaseous CO. This process is similar to what happens on metal-based homogeneous catalysts during CO_2 reduction. It is believed to be the favorable pathway for reactions taking place on metal catalysts such as Pt, Au and Cu. CO is the major product for most metal catalysts except Cu, which could facilitate further reduction of CO. By comparison, a competing activation pathway does not involve the metal-carbon bond formation. Instead, an intermediate species *OCOH with the oxygen binding to the metal catalyst forms via either a direct activation of CO_2 by PCET or surface hydride mediation. Often, formic acid is the final product of this process. Metals with high oxygen affinities, such as Pd, Hg, and Pb, favor this activation pathway. Typically, a PCET process precedes the CO_2 activation step, forming adsorbed H (H^*) on the catalyst surfaces. The newly formed metal-hydrogen bond is highly active, which is a critical intermediate for the hydrogenation reactions. Subsequent CO_2 adsorption inserts in the metal-hydrogen bond, leading to the formation of a formate intermediate with oxygen binding to the surface. Further PCET processes help protonate the oxygen of the metal-oxygen bond to release formic acid and turn over the reactive site. This simplified summary helps us see that CO is an important intermediate for more reduced products. Formic acid, on the other hand, tends to be a terminal product that is more difficult to further reduce in an electrocatalytic system. As such, great efforts have been undertaken to investigate the reaction pathways from CO and onwards, and the goals are often to achieve valuable products, including CH_4, CH_3OH, C_2H_4 and CH_3CH_2OH.

The understanding as outlined above is supported by computational studies by Peterson et al. (Scheme 5a). [122] The authors showed that after the formation of CO, each step is associated with a PCET process to form thermodynamically favorable reaction inter-

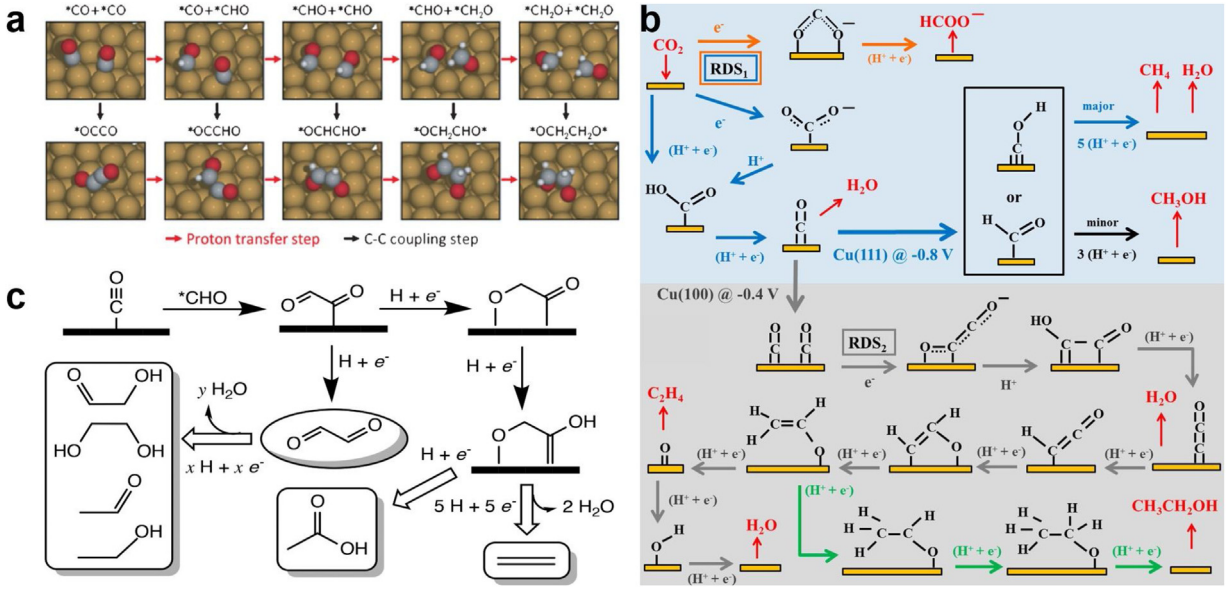

Scheme 6. a) Proposed C–C coupling pathways for CO and hydrogenated CO and the calculated free energy diagram for these processes. The activation barrier decreases after hydrogenation. (Figure reproduced from ref. 145, copyright 2013, Wiley·VCH); b) Proposed CO_2 reduction pathway to various products, with the C–C coupling proceeds via CO dimerization. (Figure reproduced from ref. 10, copyright 2013, American Chemical Society); c) Proposed C–C coupling by CO and CHO and the following evolution to various C_2 products. (Figure reproduced from ref. 127, copyright 2018, American Chemical Society).

mediates. Importantly, the second C–O bond breaking was shown to take place at a later stage. The adsorbed CO would be first reduced to *CHO, which was considered the rate-determining step (RDS). Another subsequent PCET process would yield adsorbed formaldehyde. Critical to our discussions, we see in Scheme 5a that the surface anchoring group is switched from C—M to O—M during this step. The newly formed formaldehyde could be further reduced to methoxy group, which would be either converted to methanol or transformed to CH_4.

However, it is important to note that competing arguments have been presented concerning how C_1 products form on metal catalyst surfaces. For instance, the mechanisms involving formaldehyde and methoxy group could not explain the fact that formaldehyde can only be reduced to methanol but not further reduction products such as CH_4 [123]. Nie et al. have demonstrated an alternative pathway by considering not only thermodynamic but also kinetic factors. In their proposed mechanism, the second C—O bond breaking takes place at a relatively early stage (Scheme 5b) [124]. Rather than *CHO, protonation takes place on oxygen atom from CO and forms *C–OH. A further PCET process on the OH group would lead to surface carbon (C^*) formation with the release of water. Finally, the C^* would undergo several PCET processes to yield CH_4. Compared to Peterson's mechanism, Nie et al.'s model does not involve bonding switch between C–M and O—M. Additional research is needed to reconcile the apparent discrepancies.

Different from C_1 products, forming C_2 products requires C—C bond formation. Knowing when and how it forms plays an important role in understanding the reaction mechanisms and contributes to the ultimate goal of tuning the reaction selectivity. Common C_2 products include C_2H_4 (ethylene), C_2H_6 (ethane) and CH_3CH_2OH (ethanol). Let us consider C_2H_4 as an example. Nørskov et al. found that C–C coupling takes place after CO hydrogenation (Scheme 6a), [125] whereas Nie et al., proposed the dimerization of $*CH_2$ based on their proposed CH_4 mechanisms (Scheme 5b). It should be noted that in both mechanisms, the C–C coupling step shares the same reaction intermediates. More importantly, both mechanisms share the same RDS. It is, therefore, reasonable to predict that if these mechanisms hold, the overpotentials of CH_4 and C_2H_4 formation should be comparable. Furthermore, the reactions should exhibit similar dependence on pH. However, these predictions were not supported by some experimental results. For instance, Hori et al., found that the formation of CH_4 from CO showed a different pH dependence from the formation of C_2H_4 [126]. In addition, C_2H_4 formation was observed at less negative potentials without simultaneous formation of CH_4, especially on Cu (100) surfaces. According to these experimental observations, Koper et al. proposed a third reaction mechanism that C–C coupling is enabled by a rate-determining CO dimerization with the help of one electron transfer process (Scheme 6b). [10] This mechanism would explain the less negative potentials for C_2H_4 formation and the different pH dependence (C_2H_4 is more favored in alkali media). In a very recent work, Head-Gordon et al. emphasized the difference of Cu (111) and (100) surface and proposed that the C–C coupling takes place between CO and CHO, producing *COCHO as the key intermediates (Scheme 6c). [127] They also investigated the reaction pathway after the C–C coupling and explained the formation of all 7 C_2 products.

2.3.1. *Catalysts with different compositions*

Over the years, researchers have surveyed nearly all transition metals for their catalytic activity and selectivity toward CO_2 reduction [128]. It is agreed that noble metals such as Ag and Au are more selective to CO production, while other metals such as Pt or Ni would be more favorable for HER. Among them, Cu may be the most studied metal catalyst as it can produce a variety of multi-carbon molecules, including ethane, ethanol and sometimes propane. For example, Jaramillo et al. studied the reactivity of seven transition metals in reducing CO_2 for methanol and methane formation [129]. They discovered that all studied metals were capable of producing either methanol or methane; five of them could produce both but under different overpotentials. The intrinsic surface binding energies of CO were believed to play important roles in the stabilities of the intermediates and therefore the selectivity (Fig. 9a) [130]. A volcano plot was generated by plotting the CO_2 reduction current densities versus the calculated CO binding energies on these metal surfaces (Fig. 9b). Metals with lower binding energies than Au exhibited lower CO_2 reduction current densities, presumably due to poor CO_2 activation. Metals with too high CO binding energies also

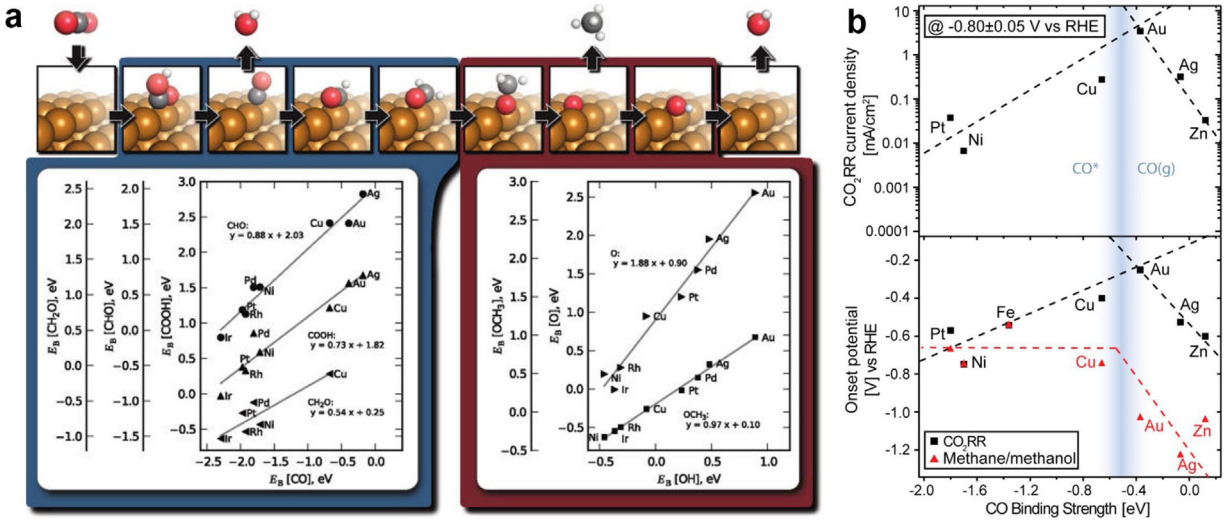

Fig. 9. a) Proposed pathway for reducing CO_2 to CH_4 on copper surfaces, and the calculated adsorption energies of the key reaction intermediates on fcc (211) of different metals. More tightly bound adsorbates correspond to more negative binding energies. (Figure reproduced from ref. 130, copyright 2012, American Chemical Society); b) Volcano plot of CO_2 reduction current density of various metals at $-0.8\,V_{RHE}$ and their distinct onset potentials vs CO binding energy. (Figure reproduced from ref. 129, copyright 2014, American Chemical Society).

featured low current densities because of the slow desorption rate of CO, which is believed to be critical for the subsequent reactions. On the other hand, on metals that bind too weakly to CO, it would quickly desorb and, thus, makes it difficult for further reduction. An increased overpotential would be required.

Post-transition metals represent another important group of CO_2 reduction catalysts. The catalytic activity of the *p*-block metals such as In, Sn and Pb have been extensively studied. For instance, formic acid has been observed as the main CO_2 reduction product on Pb surfaces. One explanation of this selectivity was that Pb surfaces are of low affinities toward various C-species but comparable affinities toward O-species to Ag, Pd and Pt [131]. As a result, during the activation step, CO_2 would be activated to *OCHO species instead of *COOH species. While the *COOH species favor the formation of CO, the *OCHO intermediates prefer the formate route. Moreover, Pb surfaces are considered weak for H adsorption, leading to the suppression of HER.

2.3.1.1. Alloys. Metal alloys have been broadly studied for CO_2 reduction, as well [120]. The surfaces could be more complex, as both the composition and the geometric distribution of each components would affect the surface chemistry. In other words, the surface chemistry of alloy catalysts could be tailored, presenting a new dimension in controlling the reaction selectivity and activity of CO_2 reduction. For instance, Yang et al. demonstrated a bimetallic catalyst by assembling a monolayer of various Au-Cu bimetallic nanoparticles and revealed synergistic electronic and geometric effects on the binding affinities of the various intermediates on the alloy surfaces (Fig. 10) [132]. At the peak of the volcano plot toward CO production sits Au_3Cu. Electronically, the binding strengths of COOH and CO define the activity. Similar reactivity is difficult to achieve on monometallic surfaces. On the Au-Cu alloy surface, an additional bond between oxygen and Cu is believed to further stabilize COOH on the surface. Such local atomic arrangements is an important geometric factor that promotes the catalytic activity toward CO. Bell et al. proposed that the existence of compressive strains on Cu-Ag bimetallic surfaces could help to suppress HER, rendering the reaction more favorable for multi-carbon products than on pure Cu electrode [133]. Upon forming alloys with Ag, the resulting compressive strain would increase the density of states in the valance band, leading to weaker interactions with O and H by Cu. As such, the Cu domain in a Cu-Ag alloy is more selective toward C–C coupling over HER than pure Cu. It was argued that CO_2 would be first reduced to CO on the Ag domains and be segregated onto the Cu domains for further reduction. Alloy catalysts such as Pd-Pt nanoparticles have also been reported. For example, Koper et al. surveyed Pd-Pt/C catalysts with various compositions and found that $Pd_{70}Pt_{30}$/C exhibited the highest FE of 90% for formic acid production [134]. The bimetallic catalysts featured low onset potentials and minimal poisoning effects by CO.

Doping could be yet another potential way to modify the surface properties of metal catalysts for CO_2 reduction. To this end, Cai and Wu et al. synthesized Pd-B/C catalysts and showed that the FE for formate reached 70% over 2 h at -0.5 V vs RHE, which is ca. 12 times higher than that of Pd/C [135]. This improvement was attributed to the changes in the kinetic pathways as a result of B doping. The adsorption energy of $HCOO^*$ became more negative than that of $^*COOH$. Consequently, the formate pathway was more favorable than the CO pathway.

2.3.1.2. Metal oxides. One motivation for developing metal oxides as CO_2 electrochemical reduction catalysts is to replace the expensive noble metals. Some metal oxides were initially used as the precursor for the preparation of complex metal catalysts, and later it was found that they themselves were also active toward CO_2 reduction. Some metal oxides, including RuO_2, TiO_2 and Co_3O_4, with high conductivity have been shown effective for CO_2 reduction for a long time [136,137]. Due to the poor conductivity of most other metal oxides, they were usually applied as thin coatings on current collectors or supported on carbon [138]. Recently, synergistic effects between the support and metal oxides have been reported [139].

When metal oxides are used for electrochemical reduction of CO_2, the cathodic current would reduce the oxides first. Indeed, reductive peaks appeared when a Cu_2O layer was used as a CO_2 reduction catalyst [140]. Similarly, oxide-derived Ag would be first reduced to Ag during the initial stage of CO_2 reduction [141]. However, although the "real" catalyst might be the metal itself with surface features, the oxide-derived catalysts benefit more than the morphologies. To this end, Kanan et al. developed an electrochemical method to prepare an amorphous Au oxide layer with more than 1 μm thickness [142]. The Au oxide layer was reduced to Au° to form Au nanoparticle agglomerates during CO_2 reduction, which exhibited superior activity, selectivity and stability for CO

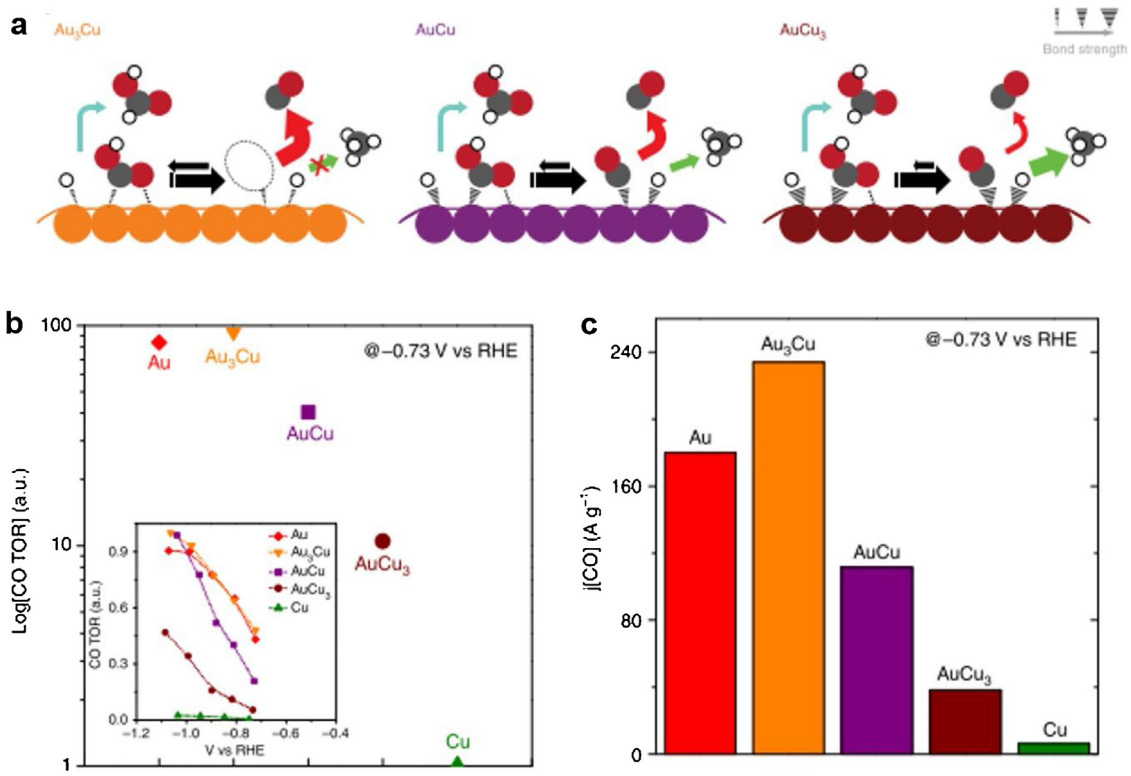

Fig. 10. a) Schematics illustrating the mechanisms for CO_2 reduction on various Au–Cu bimetallic catalysts. b) Comparison of the relative TORs for CO at -0.73 V vs RHE. The TOR of Cu is set to one. Inset: relative CO TORs for various catalysts as a function of potential; c) CO mass activity (total metal) of Au–Cu bimetallic catalysts at -0.73 V vs RHE. (Figures reproduced from ref. 132, copyright 2014, Nature Publishing Group).

production than Au nanocatalysts prepared by other methods. For instance, the catalysts reduced CO_2 to CO at only 140 mV overpotentials and lasted for 8 h. The authors also proved that the improvement of catalytic activity cannot not be solely explained by the nanoparticle nature. It was hypothesized that the oxide-derived Au nanostructures feature metastable surfaces that could stabilize $CO_2^{\bullet -}$ radicals. Kinetic analyses showed that the RDS on the oxide-derived Au was different from that on polycrystalline Au.

The importance of an oxide layer to the CO_2 reduction efficiency on was also observed for Sn. Kanan et al. compared Sn catalysts containing native SnO_x with pre-etched, oxide-free ones. While higher current densities were measured on the pre-etched sample, they were mostly from HER. The authors attributed this change of selectivity to the ability of SnO_x in stabilizing $CO_2^{\bullet -}$ radicals. To further support this conjecture, they prepared Ti electrode decorated with Sn/SnO_x by electrodeposition and observed 7–8 fold higher current densities than on native Sn foils [143].

Even though the exact mechanisms by which oxide-derived Au works so well for CO_2 reduction remains to be uncovered, the partial oxidation (or reduction) strategy has proven effective for other catalysts [144]. For example, Xie et al. studied the origin of the catalytic activity by partially oxidized Co surfaces. They found that the atomically thin layer of oxide surface was inherently more active than bulk metal surfaces, with better selectivity, as well [145]. Later the authors used this model system to further study the effect of oxygen vacancies in CO_2 reduction on metal oxides (Fig. 11) [146]. They proposed that proton transfer is the RDS for CO_2 reduction on Co_3O_4. Oxygen vacancies facilitate the proton transfer step by stabilizing the $HCOO^{-*}$ intermediates and lowering the activation barriers by 0.11 eV.

Recently, Bocarsly et al. carried out ATR-IR spectroelectrochemistry studies on several post-transition metals, including In, Sn, Pb and Bi [147]. They found that surface oxides were critical for the electrocatalytic activity of CO_2 reduction on some of these metal surfaces. In particular, they discovered that a metastable oxide layer would form on In, Sn and Pb surfaces under electrochemical conditions. This oxide layer was crucial for CO_2 reduction on In and Sn by facilitating the formation of metal-carbonate species that would eventually produce formate. However, no oxide formation was found on Bi.

2.3.1.3. Metal chalcogenides. Transition metal chalcogenides represent another group of materials that have been screened for CO_2 reduction. Hara et al. added Na_2S into the electrochemical system and demonstrated that the presence of S^{2-} on transition metal (Fe, Ni, Pd, Cu, Zn, Ag, and Pt) surfaces led to changes of product selectivity [148]. It was hypothesized that the presence of transition metal chalcogenides in black smoker at deep-sea hydrothermal vents may be natural catalysts that enable the reduction of CO_2 in the CO_2-saturated ancient ocean. In addition, the presence of the Fe-Ni-S cluster as well as Fe_3S_4 in enzymes active for CO_2 reduction implies the potential CO_2 reduction activity by this group of materials. DFT calculations support that MoS_2, $MoSe_2$ and Ni-doped MoS_2 are capable of reducing CO_2. Detailed activities of different edges on two dimensional (2D) materials have been calculated. It was revealed that specific sites such as the S edge of Ni-doped MoS_2 and the Mo edge in $MoSe_2$ are active for the reduction of CO_2 to hydrocarbons or alcohols [149]. Experimental results have been obtained with MoS_2 in EMIM-BF_4, with overpotentials as low as 54 mV and current densities higher than Ag nanoparticle catalysts. The FE of CO reached 98% at -0.764 vs. RHE. The metallic character and high d-electron density at the Mo edge of MoS_2 was considered the origin of the superior performance [150]. Later, the same group synthesized WSe_2 nanoflakes as CO_2 reduction catalyst under similar reaction conditions, which showed even higher performance than their previous study.[119] After integrated with PV solar cell and

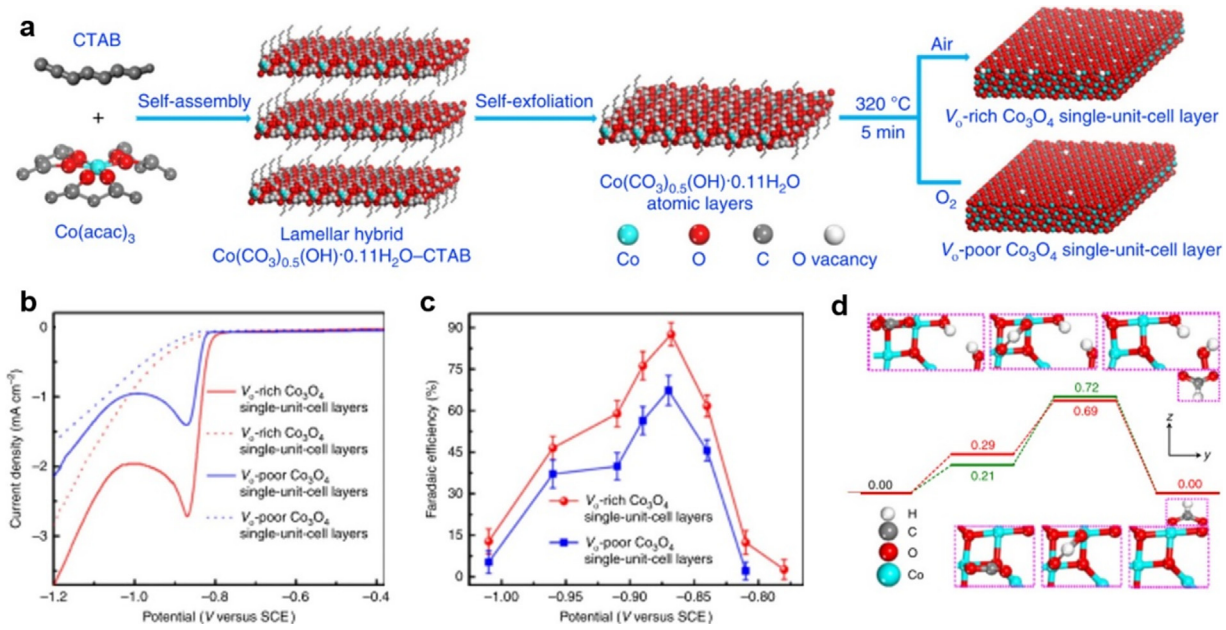

Fig. 11. a) Schematics illustrating the synthesis of $V_{o\text{-}rich}$ and $V_{o\text{-}poor}$ Co_3O_4 single-unit-cell layer; b) LSV scans of the two types of oxides in CO_2 (solid line) and N_2-saturated (dashed line) 0.1 M $KHCO_3$ aqueous solutions; c) FEs of formate at different applied potentials on the two oxides; d) Calculated free energy diagrams for the reduction of CO_2 to formate on the Co_3O_4 single-unit-cell layers with oxygen vacancies (top, red) and the intact Co_3O_4 single-unit-cell layers (bottom, green), respectively; energy unit in eV. (Figures reproduced from ref. 146, copyright 2017, Nature Publishing Group).

cobalt(II) hydroxide as anode material, ~4.6% solar-to-fuel efficiency was obtained.

2.3.1.4. Ligand binding. As in homogeneous catalysts, ligand binding may be used to tune the electronic properties of heterogeneous catalysts. For example, Yang et al. functionalized Au nanoparticles with N-heterocyclic carbenes (NHC) and discovered an increase of the catalytic current densities as well as the FE of CO production. [151] Through strong σ-donation to Au nanoparticles, the NHC ligand facilitated fast electron transfer between Au and CO_2. In addition, the ligand binding was believed to destabilize the Au surface yield more "defects" that are favorable for CO_2 reduction. Similar organometallic surface modifications were also realized on Pd. [152] By chelating Pd surfaces with tridentate NHC, the authors improved both catalytic activity and stability. The selectivity of formate production was observed as opposed to CO production on Pd foils. DFT calculations indicated that the surface energetics after the chelation was more favorable for the production of HCOOH.

2.3.2. Morphology effects

A distinct feature offered by heterogeneous catalysts is that their catalytic properties may be influenced by the morphologies. At the most rudimental level, the size of the catalysts directly define the exposed surface areas – high surface areas would correspond to more active sites when all other factors are fixed. Next comes the shape of the catalyst, which is connected to what facets are exposed. Surface science research has long established that the catalytic activities are highly sensitive to the exposed facets. More recently, there are reports indicating that the catalyst morphologies may exert a profound influence to the mass transport near the catalytically active surfaces, by which the reaction kinetics are altered.

2.3.2.1. Size effect. One initial rationale of employing nanoparticles as catalysts for heterogeneous CO_2 catalytic reduction was to make use of the high surface area. The underpinning thought was that within a given geometric electrode area, more catalyst surface areas would enable more turnovers of the catalytic reactions. To this end, nanoparticles feature surface-to-volume ratios tens of times higher than bulk materials. For instance, Lu and Rosen et al. demonstrated that the electrochemical surface area (ECSA) of Ag nanoparticles derived from dealloying of Ag-Al electrode was ca. 150 times larger than that of polycrystalline Ag [153].The benefit of nanoporous catalysts could be realized in photoelectrocatalytic system as well. For example, Oh et al. prepared nanoporous Au film on Si photoelectrode by electrochemical reduction of anodized Au thin film [154]. The catalytic activity as well as the FE_{CO} were increased. By incorporating the nanoporous film as a mesh on the Si photoelectrode, the current for CO production reached -2.94 mA cm^{-2} at the CO_2/CO equilibrium potential under 1 sun illumination, and FE of CO was over 90%. These promises notwithstanding, one drawback of nanoporous catalysts is that they are usually difficult to study quantitatively. In fact, reproductive synthesis of these porous structures remain a challenge in itself.

It is important to note that while desired reactions (i.e., CO_2 reduction) are enhanced on high surface area catalysts, competing reactions (e.g., HER) may also be enhanced, sometimes disproportionally. As such, one must exercise cautions in scaling the sizes of the catalysts. To this end, Sun and Peterson et al. studied the catalytic activity and selectivity of monodispersed 4, 6, 8 and 10 nm Au nanoparticles (Fig. 12). [155] It was found that the mass activity of Au nanoparticles increased as the nanoparticle sizes decreased owing to the increasing surface-to-volume ratios. However, the Faradaic efficiency of CO production does not follow the same trend. Au nanoparticles of 8 nm nominal sizes exhibited the highest FE of 90% at –0.67 V vs. RHE. In order to explain the decreased selectivity, the authors carried DFT calculations for Au (111) surfaces, Au (211) surfaces and Au_{13} clusters. The results showed that the free energy for activation of CO_2 to $COOH^*$ on Au (211) is significantly lower than on Au (111). Au_{13} clusters featured slightly lower free energy for $COOH^*$ binding, but the free energy for CO^* binding was too low for successful liberation of the products. Furthermore, the free energy of H^* on Au_{13} clusters was lower than that of $COOH^*$, suggesting HER is more favorable on smaller nanoparticles.

Similarly, Strasser and Cuenya et al. synthesized 9 types of Au nanoparticles ranging from 1.1 nm to 7.7 nm using an inverse

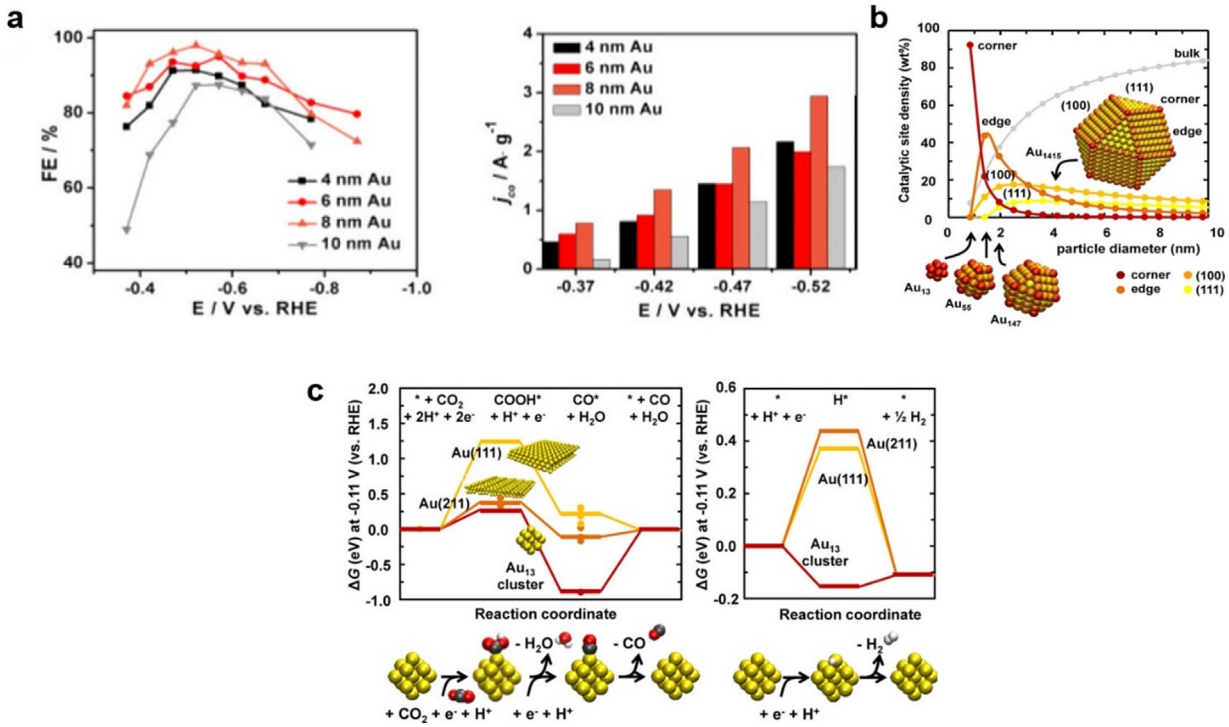

Fig. 12. a) FEs and mass activities of the C-Au-IL on electrocatalytic reduction of CO_2 to CO in the presence of 10 μL IL; b) Density of adsorption sites on (111) facets, (001) facets, edges, or corner sites vs the cluster diameter on closed-shell cuboctahedral Au clusters. c) Free energy diagrams for CO_2 reduction and HER on Au(111) (yellow), Au(211) (orange), or a 13-atom Au cluster (red) at −0.11 V_{RHE}. (Figure reproduced from ref. 155, copyright 2013, American Chemical Society).

micelle encapsulation method [156]. They showed that the reaction activity increased dramatically as the Au nanoparticle sizes decreased. The largest nanoparticles exhibited similar activity as bulk gold, whereas the current density measured on the smallest ones was ca. 100 times that of the largest ones. However, the increased current density was mainly due to HER. The Faradaic efficiency of CO production for 7.7 nm Au nanoparticles was ca. 45%, which was decreased to 9% for 1.1 nm Au nanoparticles. The authors attributed the increase of HER to the increased stability of adsorbed H^* on smaller nanoparticles. DFT calculations indicated that the stabilization energies of $COOH^*$ and H^* decreased monotonically from Au (111) to Au (211) and then to Au_{55} and Au_{38}, but the $COOH^*$ stabilization energy was consistently higher. Therefore, as the nanoparticles sizes decreased, both reaction activity and selectivity toward HER increased. Apparently, such a trend is not desired for CO_2 reduction applications.

Ag nanoparticles exhibited similar trends. Min and Hwang et al. synthesized and investigated Ag nanoparticles of different sizes on carbon with cysteamine as an anchoring agent [157]. They discovered that of 3, 5, and 10 nm Ag nanoparticles, the 5 nm Ag nanoparticles exhibited the best reaction activity for CO_2 to CO conversion. In another work, the same group studied Au nanoparticles as a thin film on a carbon film and found that nanoparticles of 4 nm were the best, whereas H_2 was the main product for the smallest nanoparticles [158].

These efforts on Au and Ag nanoparticles helped us see that while the small sizes favor high reactivity, poorer selectivity of CO_2 reduction against HER would be expected on nanoparticles <4-5 nm in sizes. In these catalysts, the (111), (110) and (100) facets are flat surfaces, and the (211) facet is an edge surface with stepping defects. Calculation showed that these facets exhibited different affinities toward H*, $COOH^*$ and CO^*. For example, Au (100) and Au (211) were calculated to bind H^* more strongly than other Au sites [159]. When the sizes of the nanoparticles decreased, the ratio of the edge facets increased. As a result, HER became more predominant.

Compared to Au and Ag, Cu nanoparticles produced hydrocarbons beyond CO. Nevertheless, a similar trend in terms of size-dependence was observed. For instance, Strasser and Cuenya et al. studied Cu nanoparticles of 2–15 nm and found the overall reduction activity did change significantly when the catalyst sizes decreased from bulk to ca. 5 nm [160]. Below 5 nm, however, a dramatic increases of the reduction current was observed. While bulk catalysts mostly produced methane, the nanoparticles mainly yielded CO and H_2. Different from the results obtained on Au and Ag, the production of CO increased relative to HER when the sizes of the catalysts dropped below 5 nm.

One important but sometimes overlooked issue when evaluating the catalyst activity and selectivity was the catalyst stability during reactions. This issue is especially important for heterogeneous catalysis. Although a catalyst may be defined as “unchanged” during a reaction, they do participate in the primary steps of the reaction. In heterogeneous catalysis, although the chemical composition of the catalyst may not change during the reaction, the morphology and/or monodispersity of the catalyst are likely modified by the reaction. For instance, Au nanoparticles were observed to undergo random diffusion, collision and fusion into dendrimers during a reductive polarization process at room temperature, even in the presence of binders [161]. Crooks et al. addressed the stability issue in their recent work by using stable Au nanoparticles covered with poly(amidoamine) dendrimers [162]. While citrate-stabilized Au nanoparticles increased from 2 nm to 6 nm, the G8-NH_2(Au_{147}) DENs counterparts stayed the same.

2.3.2.2. Facets exposure. A key factor that defines the reactivity and selectivity of CO_2 reduction is the affinities and/or binding energies of the various reactants, intermediates and products to the catalyst surfaces, which in turn are highly sensitive to the nature of the exposed surfaces. [163] This is especially true for nanoscale cata-

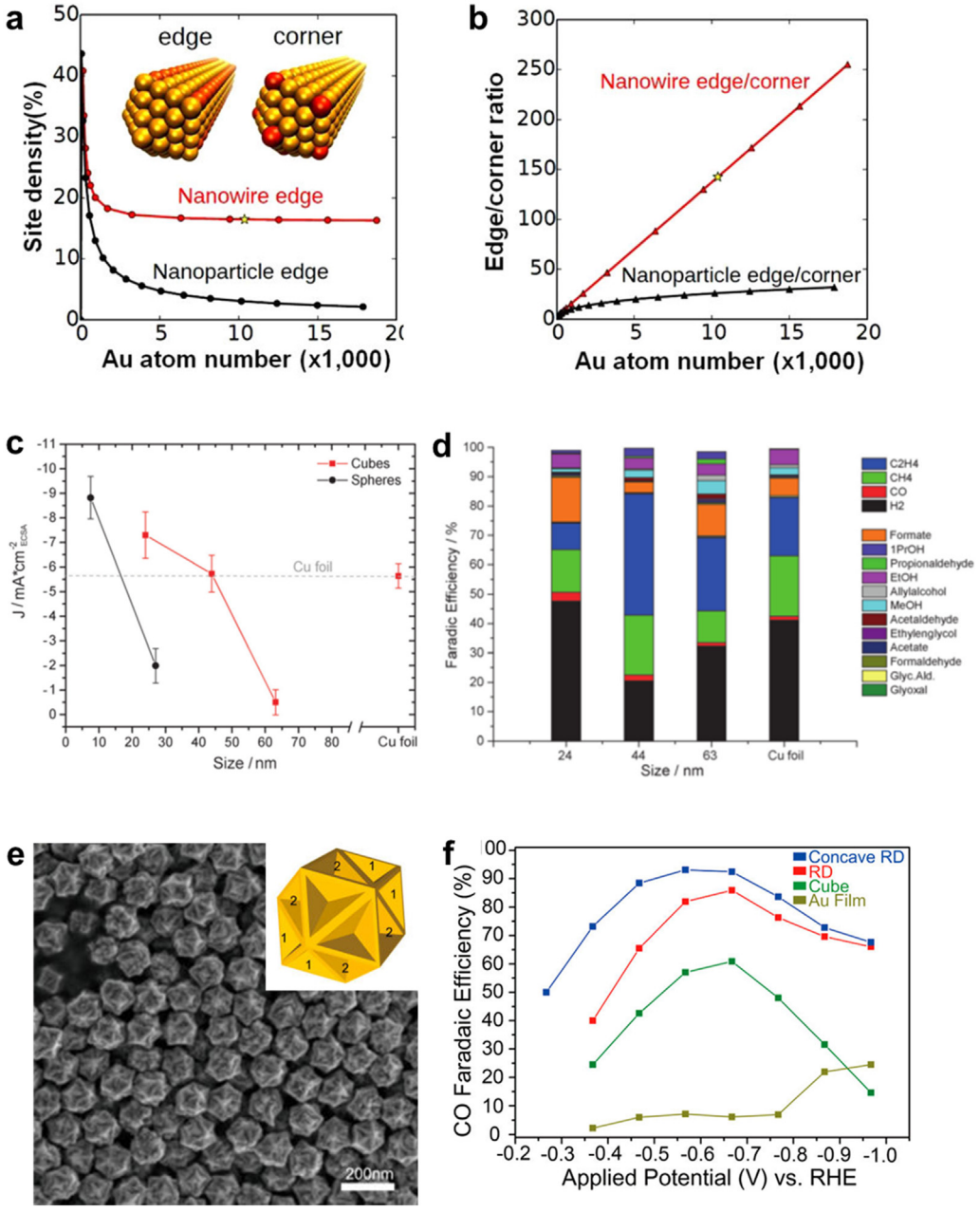

Fig. 13. (a) & (b) Comparison of Au nanowires and nanoparticles (a) Edge site weight percentage in 2 nm Au nanowire and nanoparticle as a function of the number of Au atoms. (b) Calculated optimum edge/corner ratio in Au nanowire and Au nanoparticle. (Figures reproduced from ref. 163, copyright 2014, American Chemical Society); (c) & (d) Performances of different Cu catalysts (c) Current densitis at -1.1 V vs. RHE of Cu nanocubes with different sizes. (d) FEs of each product for Cu nanocubes with different sizes and Cu foil at -1.1 V vs. RHE. (Figures reproduced from ref. 164, copyright 2016, Wiley·VCH); (e) & (f) morphology and performance of concave rhombic dodecahedral Au nanocrystals (e) SEM image of the concave rhombic dodecahedral Au nanocrystals. (f) FE_{CO} of various Au catalysts at different potentials. (Figures reproduced from ref. 165, copyright 2015, American Chemical Society).

lysts with high surface areas. To this end, Sun et al. studied CO_2 eletrocatalysis on ultrathin Au nanowires of 2 nm in diameters and varying lengths (Fig. 13a-b). They discovered that the longer the nanowires, the more active the catalysts would be. [47] The carbon-supported 500 nm-long nanowires enabled a maximum CO FE of 94% and a mass activity of 1.84 A/g at -0.35 V, much better than polycrystalline Au nanoparticles. The binding modes of $COOH^*$ on the nanowires were calculated, together with the binding energies of the intermediates on nanowires, Au_{13} clusters and Au (211) facets. It was concluded that the length dependence was due to the maximized edge-to-corner ratios, which increased with the length of the nanowires.

For systematic studies of the facet effects, cubic metal nanoparticles would be an excellent platform as they are enclosed by 6 equivalent (100) facets. Buonsanti et al. group synthesized Cu nanospheres of 7.5 nm and 27 nm and Cu nanocubes of 24 nm, 44 nm and 63 nm (Fig. 13c-d). [164] They compared the size and facet effects of these catalysts within the context of CO_2 reduction. They found that the cubic morphology is more active than the spherical ones. The catalytic activity increased as the nanoparticle sizes decreased. Of them, the 44 nm Cu nanocubes exhibited the highest selectivity toward carboneous products, with the major product being ethylene. It was concluded that the selectivity was originated from the (100) facets. It also suggested that the edge sited were active for CO_2 reduction to ethylene. Taken as a whole,

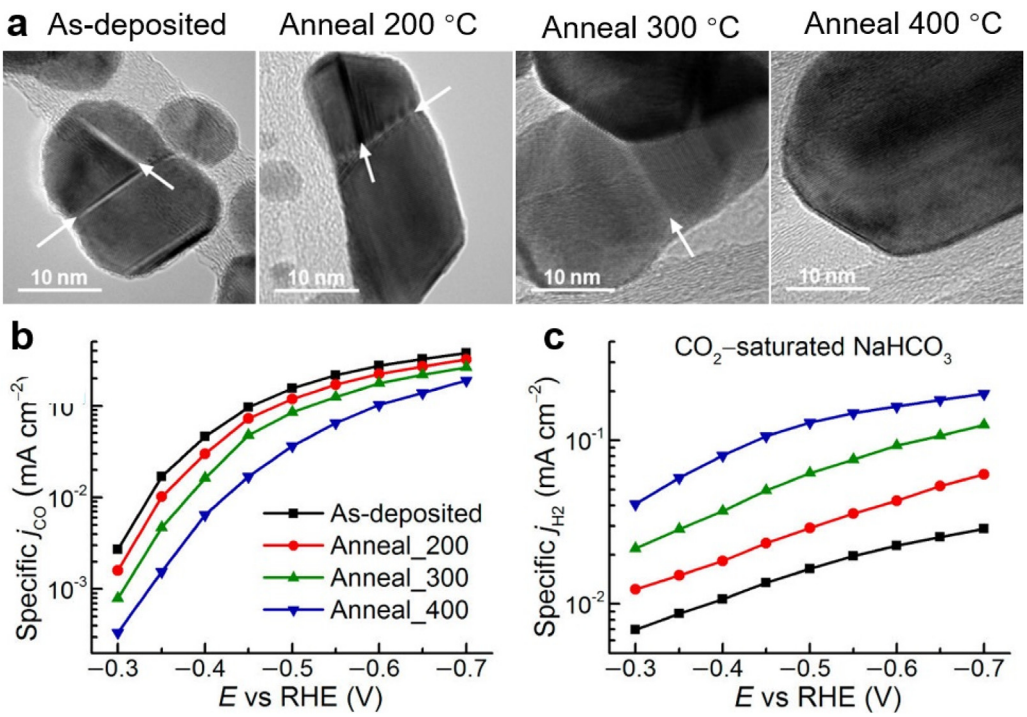

Fig. 14. a) TEM images of the Au nanoparticles in Au/CNT electrodes showing different surface densities of grain-boundary; b) Specific current density for CO production (j_{CO}) vs potential on different Au/CNT electrodes; (b) Correlation between j_{CO} and surface density of grain-boundary at low overpotentials. (Figures reproduced from ref. 167, copyright 2015, American Chemical Society).

the ratios between the (100) facets and the edge sites were critical to the observed reaction and selectivity.

An important limiting factor in studying and further developing the nanoscale catalysts for practical CO_2 reduction applications is the synthesis. To create nanoparticles with high index facets, Nam et al. recently reported Au concave rhombic dodecahedrals with high index facets such as (331), (221) and (553) (Fig. 13e-f). [165] As a demonstration, the authors investigated catalytic properties of these nanoparticles. The concave rhombic dodecahedrals exhibited much higher FE of CO than Au cubes, Au rhombic dodecaherals or Au films. In another work, Yin et al. selectively etched Pd@Cu nanocubes for enriched high energy facets [166]. This new type of nanoparticles showed enhanced CO_2 reduction activity by featuring more high-energy facets.

2.3.2.3. Grain boundaries. Grain boundaries have been used to explain the improved catalytic performance of some nanoparticle catalysts. Kanan et al. established a quantitative correlation between grain boundaries and the catalytic properties using nanoparticles prepared with metal vapor deposition of Au on carbon nanotubes. [167] The obtained Au nanoparticles were 14–22 nm in diameters and contained 0–4 visible grain boundaries. The authors quantified the grain boundaries by measuring their projection lengths on the nanoparticle images, converted them to surface lengths using geometrical models and calculated the fraction of the grain boundaries on Au nanoparticle surfaces. As an important control experiment, the authors annealed as-deposited Au nanoparticles at 200 °C, 300 °C and 400 °C, respectively. Subsequent electrochemical measurements demonstrated a dependence of CO_2 reduction activities on the density of grain boundaries (Fig. 14). A linear relationship was established at low overpotentials of -0.3 to -0.4 V vs. RHE. The results suggested that the grain boundary terminations are highly active sites for catalytic CO_2 reduction.

Kim and Lee et al. emphasized the importance of grain boundaries for CO_2 reduction with calculations. [168] By extensive DFT calculations, they proposed that the metal-to-absorbate π-back bonding ability of Au would be increased near the grain boundaries due to the breaking of local spatial symmetry. As a result, the intermediates of *COOH could be better stabilized at grain boundaries, leading to a decrease of overpotentials for ca. 200 mV.

The grain boundary effect has been observed in other catalysts, as well. For instance, Wang et al. reported different activities and selectivities by two types of Cu nanowires with similar morphologies. [169] The one synthesized with forming gas reduction contained mainly metallic Cu, while the one obtained by electrochemical reduction featured surfaces of small grains as well as small amount of Cu_2O residue domains. The electrochemically-reduced sample exhibited higher catalytic activity and higher selectivity than that by forming gas annealing. The excellent performance of the electrochemical reduced Cu nanowires was believed to be a result of the surface structures, as the small grains would lead to more surface grain boundaries and more low-coordinated surface sites. Recently, Ager et al. proposed that the increased number of grain boundaries after in situ reduction was the reason for the high selectivity of oxide-derived Cu toward C_2 and C_3 products. [170] Using O [18] labeling, they studied the catalysts for CO_2 reduction and found that the oxides were not stable at any given moment. Thus, the high density of grain boundaries would be the more likely origin of the enhanced performance by this type of catalysts.

At high overpotentials (e.g., <-1.2 V vs. RHE), grain boundaries play an even more significant role in defining the selectivity of CO_2 reduction products. In a recent paper, Yang et al. revealed that Cu nanowires with well-defined 5-fold twinned morphologies produced only methane as carboneous products. [171] Nevertheless, the morphology of the nanowire was not stable. During reaction, nanoparticle nucleation happened on the surface of the nanowires, causing degradations of the twinning boundaries. Correspondingly, the product selectivity shifted to gradually favor ethane as the reaction proceeded and the surface structures evolved.

2.3.2.4. Space confinement and local pH. In 2015, Surendranath et al. reported high selectivity of CO_2 reduction by Au inverse opal thin

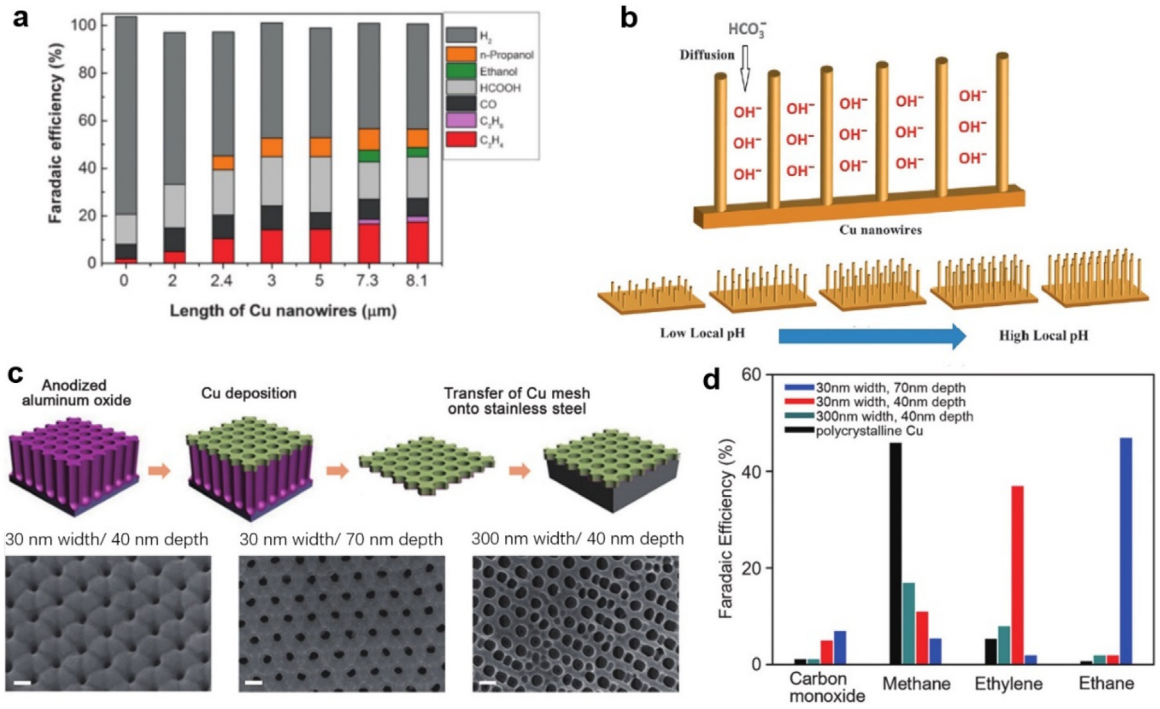

Fig. 15. a) FEs for C_2H_4, C_2H_6, CO, HCOOH, ethanol, n-propanol, and H_2 on Cu nanowire arrays with different lengths at -1.1 V versus RHE in CO_2-saturated 0.1 M $KHCO_3$ electrolytes; b) Schematics illustrating the diffusion of electrolytes into Cu nanowire arrays and the change of local pH by the nanowire array. (Figures reproduced from ref. 174, copyright 2016, Wiley·VCH); c) Schematics illustrating the synthesis process of the Cu mesopore electrodes and the SEM images of the electrode with various width and depth; d) FEs for CO, CH_4, C_2H_4 and C_2H_6 on various Cu mesopore electrodes. (Figures reproduced from ref. 176 copyright Copyright 2016, Wiley·VCH).

films. [172] They found that the selectivity of CO_2 reduction over HER increased by up to 10 times with an increasing thickness of the porous film. They attributed this phenomenon to the mesostructure of the electrode surface, which suppressed HER due to local pH gradients during reactions. Even on a flat electrode surface, HER and CO_2 reduction exhibit different dependence on mass transport requirements, with the HER activity increasing when a rotating electrode is rotated at a higher speed. On the surface of a porous electrode, the diffusion limitation effect is amplified, leading to the increase of selectivity of CO_2 reduction over HER. Later, Surendranath et al. observed similar effects on Ag inverse opal thin films. By tuning the electrode roughness factors, the authors were able to change the specific activity toward H_2 and CO in a near linear fashion. [173]

Another group led by Smith observed similar effects on oxide-derived Ag [141] and Cu nanowire arrays [174]. The dependence of CO formation on the pH near the electrode surface was demonstrated in electrolytes containing different buffers on polycrystalline Ag electrode. Electrolytes without buffers would see high local pH's during the reaction (as OH^- is generated as a HER by-product), which yielded the highest faradaic efficiencies of CO. On oxide-derived Ag, however, the faradaic efficiencies were almost the same in all three electrolytes. This was due to the fact that mass transport would be limited on Ag with porous surfaces; as such, the surface pH would be less sensitive to whether the solution was buffered or not.

The case of Cu was more complex compared to Au and Ag, as the selectivity considerations involved not only CO and H_2, but also various hydrocarbons. Smith et al. made this point in a nice study carried out on Cu nanowire arrays (Fig. 15 a, b). [174] The Cu nanowires were synthesized on Cu foils by first growing $Cu(OH)_2$ nanowires and then annealing at 150 °C to obtain CuO nanowires. The Cu nanowires were generated in situ during CO_2 reduction. This two-step synthesis allowed for the control over the length and density of the resulting Cu nanowires. Electrochemical performance of the Cu nanowires with lengths between 0–8.1 μm were analyzed. All samples exhibited stable currents after the initial reduction of CuO for up to 5 h. The Faradaic efficiencies of competing HER decreased as the nanowires became longer and denser, while the total Faradic efficiencies of CO_2 reduction increased. Among the various products, the faradic efficiencies of C_2H_4 increased with the nanowire lengths, reaching 17.5% on the 8.1 μm samples. Importantly, C_3 products of n-propanol were only detected when the nanowire lengths were longer than 2.4 μm, and C_2H_6 only started to appear when the nanowire lengths reached 7.3 μm. The authors attributed the unique selectivity to the increase of local pH's due to the nanowire array morphology. During electrolysis, OH^- would be generated near the electrode surface. Normally, HCO_3^- could act as a buffer to maintain the local pH. In the nanowire arrays, the diffusion of OH^- and HCO_3^- was limited, hampering the buffering effect and leading to higher local pH's and, hence, suppressed HER. Moreover, the increased FEs of C_2H_4, C_2H_6 and C_3 products could be explained by the high local pH effect, which would favor CO dimerization.

In another work, Broekmann et al. prepared Cu foam with a template-assisted electrodeposition process and demonstrated its superior selectivity towards C_2 products. [175] Furthermore, the authors observed a strong dependence of the FE's of each C_2 product on the pore sizes. They suggested that the Cu foam only provided large surface areas to increase the active sites for CO_2 adsorption and reduction, but its morphology was critical in trapping gaseous carbonaceous intermediates. Such a spatial confinement effect suppressed C_1 pathways and produced more C_2 products. [175] Similarly, Nam et al. demonstrates this morphology effect with Cu mesopore electrodes [176]. The pore size of the Cu electrodes could be well controlled by the AAO templates. Combining with computational results, they demonstrates that the morphology of electrodes alters the local pH and the retention time of the intermediates. As a result, the FEs of methane, and especially the

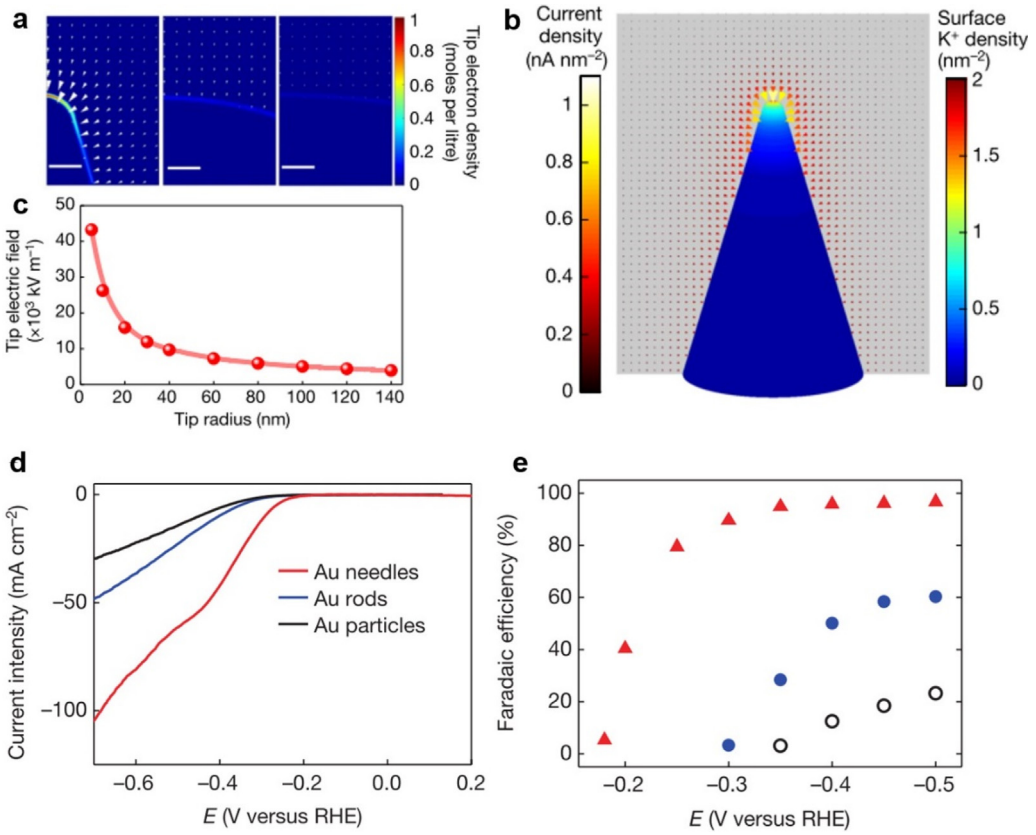

Fig. 16. (a) Color map of the free electron density distribution on the surface of electrodes with 5 nm (left), 60 nm (middle) and 140 nm (right) tip radius. Arrows shows the electrostatic field distribution around the electrode The scale bar is 5 nm; (b) current density distributions and Surface K^+ density on the surface of a 5 nm Au tip; (c) Decrease of the electrostatic field intensity as the tip radius increases. (d) LSV scan of the Au needles, rods and particles at a scan rate of 10 mV·s^{-1} ; (e) FE_{CO}s of the Au needles, rods and particles at various potentials. (Figures reproduced from ref. 177, copyright 2016, Nature Publishing Group).

C_2 product ethane and ethylene could be readily tuned by the pore size of the Cu electrodes (Fig. 15c-d).

2.3.2.5. Field-induced enhancement. One unique effect arising from nanoscale catalysts for CO_2 reduction is that the high local electric field could induce reagents to concentrate on the nanosized tip of Au. In a recent work, Liu and Pan et al. described this phenomenon, even when the applied potential was low (Fig. 16). [177] The high local electric field would concentrate cations, leading to high local concentrations of CO_2 near the active electrode surface. Both simulation and experimental results supported this conjecture. A kinetic model of this tip-enhanced effect was proposed later, which highlighted the importance of reaction kinetics to product selectivity. [178]

2.4. Integrating (co-)catalysts with photosensitizers and photoelectrodes

When (co-)catalysts are combined with (photo)electrode systems for photo(electr-)chemical reactions, new interfaces would be generated. They often lead to new scientific phenomena that deserve additional attention here. For instance, matching the energetics of the catalyst with electrode could be of critical importance for efficient charge transfer. To this end, Yang and Zhao et al. recently reported a metal complex-semiconductor hybrid of $Ru(bpy)_2dppz$-Co_3O_4 that exhibited up to 99.95% selectivity toward formate at -0.60 V vs. RHE condition. [179] The presence of H_2O, however, was shown to significantly compromise the direct injection of photo-induced electrons from the conduction band of the light absorber to the LUMO of the molecular catalyst.

2.4.1. Homogeneous photosensitizers

Traditionally, homogeneous catalysts have been studied in combination with homogeneous photosensitizers for photo-driven reactions, including CO_2 reduction. Upon illumination, the light absorber or photosensitizers would be excited first. The excited species is usually reduced by a sacrificial electron donor. The excited electron is transferred to the catalyst, which is reduced to initiate the catalytic cycle. Common photosensitizers include Ir- and Ru-complexes, such as the aforementioned $Ir(ppy)_3$ and $[Ru(bpy)_3]^{2+}$. Other photosensitizers, especially those made of earth-abundant metals have been studied, as well. For instance, Ishitani et al. have reported a photocatalytic system consisting of a Cu(I) diimine complex photosensitizer and a Fe-complex as the catalyst [180]. In order to start the catalytic cycle, the reduced form of photosensitizer must reduce the catalyst. The redox reaction then driven by the reduced molecular complexes. The situation would be more complicated when biocatalysts are involved because additional electron-transfer systems are usually required. Common electron-transfer mediators include $NADH/NAD^+$, bipyridinium salts (BPs) and Rh complexes. The readers are directed to recent reviews on this topic elsewhere. Unconventional electron-transfer systems have been reported, too. In one demonstration, Armstrong et al. demonstrated efficient photochemical reduction of CO_2 with *Ch* CODH I as the catalyst (Fig. 17a), Ru-containing metal complex $[Ru^{2+}(bpy)_2(4,4'$-$(PO_3H_2)2$-$bpy)]^{2+}$ as the photosensitizer and TiO_2 nanoparticles as the catalyst support [90]. The enzyme was attached to the RuP-modified TiO_2 nanoparticles, where were not only a catalyst support, but also a mediator to facilitate electron transfer from the sensitizer to the enzyme. The authors were able to achieve a turnover rate of $\tilde{5}30\ h^{-1}$ ($0.14\ s^{-1}$) per mole CODH

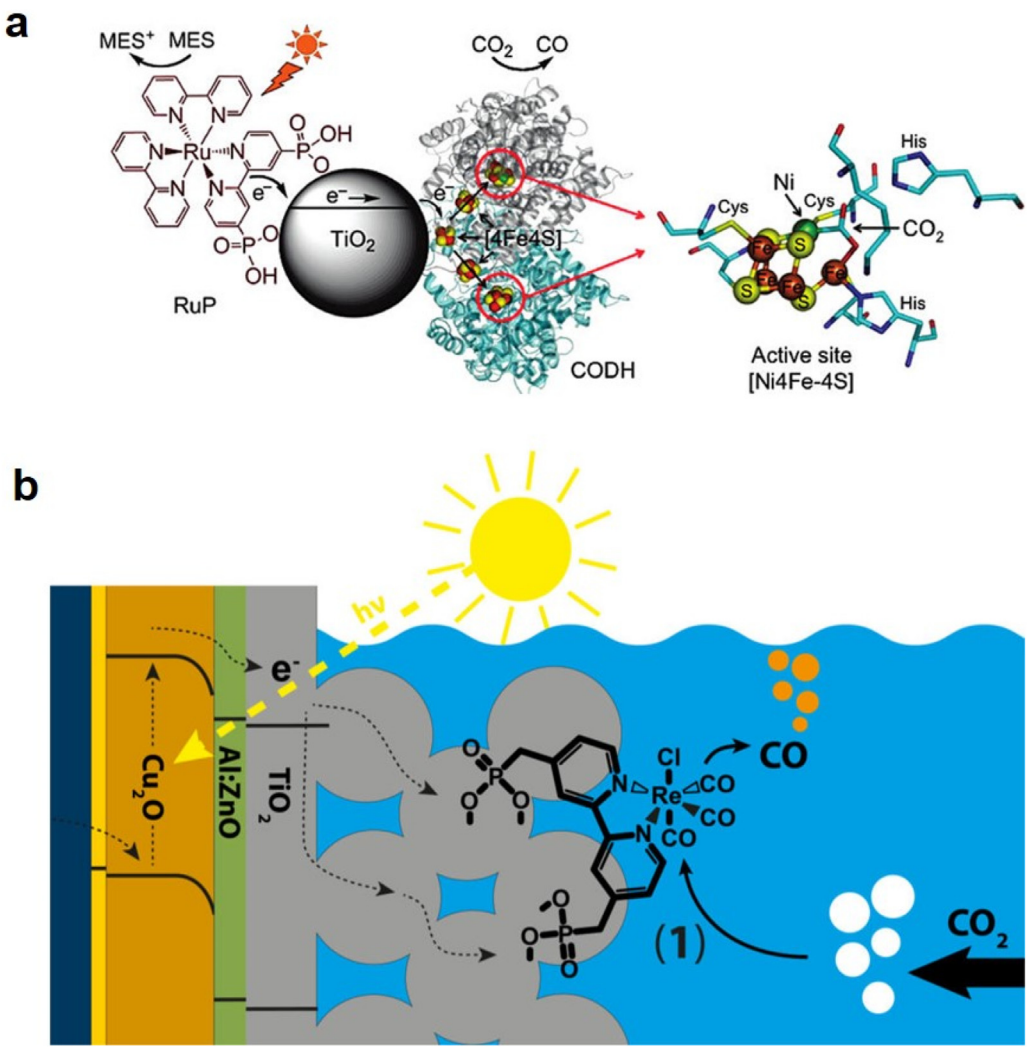

Fig. 17. (a) CO_2 photoreduction system with Ch CODH I as the catalyst and RuP complex-modified TiO2 nanoparticles as the sensitizer. (Figures reproduced from ref. 90, copyright 2010, American Chemical Society); (b) Schematic illustrating the covalently grafted Re-complex catalyst on the TiO_2 support layer. (Figures reproduced from ref. 189, copyright 2015, American Chemical Society).

under artificial illumination and 0.09 s^{-1} under natural lighting. Homogeneous photosensitizers have been used with MOF-based catalysts, [181] as well. In yet another variation, Zhao et al. reported a CoPc (Cobalt(II) phthalocyanine)-loaded TiO_2 catalysts and proposed that electrons were transferred from the CoPc to the TiO_2 conductive band upon illumination. [182]

2.4.2. Heterogeneous light absorbers and photoelectrodes

The most commonly studied heterogeneous photosensitizers are semiconductors. Their utilizations in photoelectrochemical CO_2 reduction may be traced back as early as the late 1970s. Photoelectrocatalytic CO_2 reduction usually employed p-type semiconductors such as Si, III–V, II–VI, and oxides, and the idea was to use the minority carriers (electrons) for the reduction reactions. Simply speaking, to act as a photosensitizer in a photocatalytic system, the conduction band edge needs to be more negative than the CO_2 reduction potential. Moreover, sufficient overpotentials are necessary to provide enough kinetic driving forces in order to carry out the reactions at a meaningful rate. Some semiconductors exhibit inherent catalytic activity, although no universally recognized mechanism has been established. Many believed that the formation of an adsorbed surface species of CO_2 is governed by the chemical constituents, surface microstructure, electronic structure, and crystal phase, among other factors. We will discuss the CO_2 reduction on the semiconductor surface in the next session (Section 3.2).

A more common approach has been to combine heterogeneous photoelectrodes or particles with molecular catalysts. For instance, CO_2 reduction by Ru, Re-based complex catalysts have been demonstrated on photoelectrodes such as p-type Si, [183] InP [184], C_3N_4 [185], CdS [186], TiO_2 [187], Cu_2O [188,189] and Polyoxometalate [190]. Similar to the EC system, here the catalyst can either be dispersed in solution or attached to the photoelectrode. The latter configuration may be achieved by either physical adsorption or via chemical linkers, which are usually anchoring groups such as phosphonate. For instance, Gratzel and Mayer et al. covalently grafted molecular catalysts $Re(bpy)(CO)_3Cl$ on the TiO_2-Cu_2O photoelectrode by modifying the bypyrindine group with a phosphate linker (Fig. 17b) [189]. The phosphate linker was bound to the TiO_2 support layer. It is noted that they also introduced a methylene group between the bipyridine and the phosphate to avoid the change of electronic structure of the catalyst. With a mesoporous TiO_2 support, the loading of the molecular catalyst was greatly increased. The covalently grafted catalytic system exhibited two significant advantages: (1) the quantity of the catalysts required in the system was much smaller than a normal homogeneous system; (2) the covalent bond allowed direct electron transfer from the heterogeneous photoabsorbers to the catalytic active sites. The

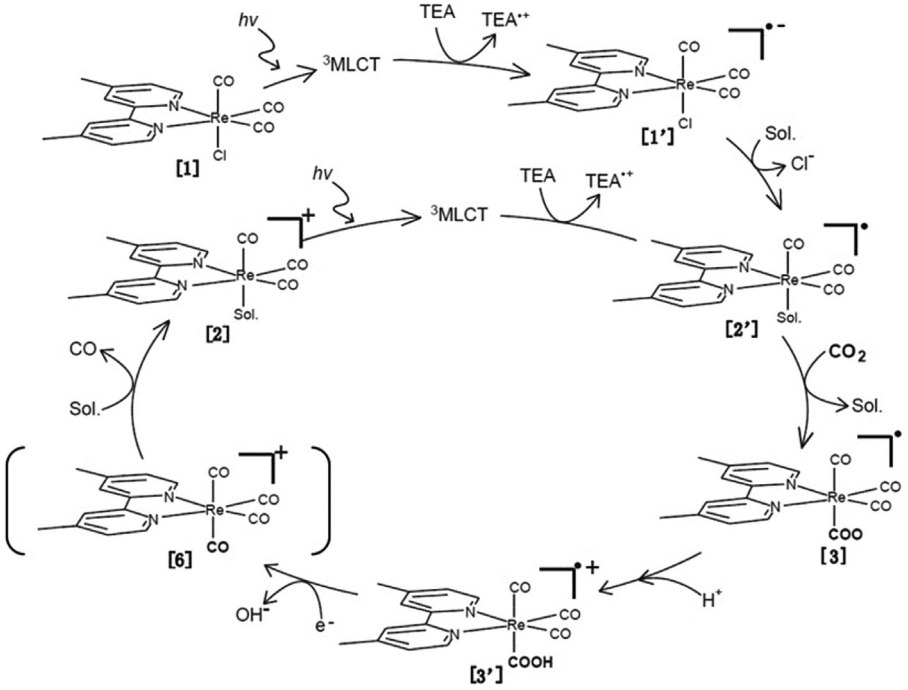

Fig. 18. Proposed photochemical CO_2 reduction cycle with [Re(dmbpy)$(CO)_3$Cl] as the catalyst. (Figures reproduced from ref. 201, copyright 2014, American Chemical Society).

authors previously reported the use of free standing molecular catalyst with Cu_2O and found that the electrostatic repulsion between the polarized photoelectrode and the catalyst would have measurable detrimental effects. [188] To reduce the repulsion effect, they had to use protic solvents for better charge transfer from Cu_2O to the molecular catalyst.

Attaching enzyme to heterogeneous photosensitizers is expected to enable direct electron transfer and has, therefore, been explored. For instance, Armstrong et al. attached CODH to visible-light-harvester CdS nanocrystals. [191] Upon illumination, the electrons in CdS quantum dots were excited and transferred to the enzyme, reducing CO_2 to CO with a turnover frequency of 0.25 s^{-1}. Moreover, a turnover frequency of 1.23 s^{-1} was obtained when the CdS nanorods were used, emphasizing the importance of the photosensitizer morphology.

Loading metal particles on the heterogeneous semiconductor electrodes has long been explored for PEC. Typically, metal particles were photo-reduced onto the semiconductor surface prior to CO_2 reduction, but other methods such as sol-gel methods have also been employed. Besides acting solely as a catalyst, metal particles may functionalize as an electron reservoir to help the separation of photogenerated charges. Several semiconductor materials modified with various metal particles have been shown promising. For example, p-Si photoelectrodes decorated with either Cu, Au, or Ag particles have been shown to produce CO, CH_4 and C_2H_4 in aqueous media [192,193]. These studies demonstrated that obtaining fine control of surface structure of the particles on the surface was critical in decreasing surface recombination and matching the interface energetics between the semiconductor and the solution. The authors predicted that the optimum yield of CO_2 reduction could be obtained with metal particles of 5 nm in sizes.

In photocatalytic CO_2 reduction, modifying photocatalysts such as TiO_2 with metal particles or thin films co-catalysts is a common approach. When TiO_2 and metal particles are in contact, the formation of a Schottky barrier would result in the decrease of electron density in TiO_2, enhancing photocatalysis efficacy. There have been numerous studies involving transition metals as well as carbon in the forms of graphene and nanotubes. The most commonly used metals on TiO_2 were Cu, Ag, and Au. For CO_2 reduction, the metallic co-catalysts yielded almost identical product distributions as with the bulk metal electrodes.

3. Photoactivated catalysts for CO_2 reduction

Plasmonic effect is yet another unique feature offered by nanostructured metal catalysts. It was proposed to promote CO_2 reduction, although direct experimental evidence to support this proposal remains to be seen. [194] In one prototypical study, Garcia et al. examined Au-Cu alloy nanoparticles on TiO_2 for CO_2 reduction. [195] The authors proposed that the plasmonic effect of Au is responsible for the reactivity in the visible range. The plasmonically excited charges transferred from metal (Au) to TiO_2, where CO_2 reduction took place.

More broadly, the ability to directly use light as an energy input to drive thermodynamically uphill reactions such as CO_2 reduction represents a new research area that deserves separate discussions. Most studies focus on the integration of co-catalysts with light absorbers as mentioned in the previous session. However, very few studies pay attention to the photoactivated surfaces/species that participate in the catalysis and influence the product selectivity. In this session, we summarize the efforts toward this end. Specifically, "photocatalysts" mentioned in this session both serve as light absorbers and participate in the catalytic reactions without co-catalysts.

3.1. Homogeneous photocatalysts

Similar to electrocatalytic systems, photocatalysts may be homogeneous molecules. For instance, the Lehn's catalyst (Re(bpy)$(CO)_3$X) and related compounds respond to light stimulations, are, therefore, also photocatalysts. In 1982, Lehn and Ziessel et al. reported that under the irradiation of visible light, $Ru(bpy)_3^{2+}$ and $CoCl_2$ solution would reduce CO_2 to CO in the mixed solution of acetonitrile/water/triethylamine. [196] Later they also demonstrated that Re(bpy)$(CO)_3$Cl could be a photocatalyst in reducing CO_2 with visible-light as an energy input. [197] Two competing

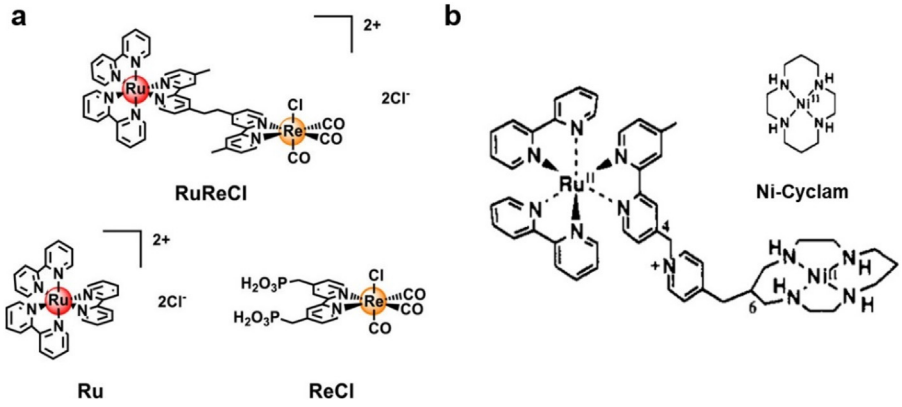

Fig. 19. a) Structures of the model complexes Ru and ReCl and the Ru(II)–Re(I) supramolecular photocatalyst RuReCl. (Figure reproduced from ref. 204, copyright 2015, American Chemical Society); b) Structure of the Ni-cyclam complex and the derived Ru(II)(bpy)2(bpy-py-cyclamNi(II) complex prepared by Kimura et al. (Figure reproduced from ref. 207, copyright 1994, American Chemical Society).

pathways of CO and formate formation were proposed in this work, with the presence of excess Cl^- a key deciding factor for the selectivity [61].

Over the years, various molecular complexes have been studied within the context of photocatalytic CO_2 reduction, the metal centers of which are critical for both light absorption and the catalytic processes. Two well investigated groups of complexes are the metallomacrocycle compounds such as metalloporphyrins and the Re(bpy)$(CO)_3$X-derived complexes. [61] Other ligand systems such as the N-heterocyclic-carbene [198], phosphines [199] and thiolates [200] have also been developed. While the detailed mechanisms of CO_2 reduction on Re(bpy)$(CO)_3$Cl had been proposed for decades, experimental detection and/or isolation of some important reaction intermediates were only achieved recently. Inoue et al. successively detected the solvent-coordinated Re complex Re(dmbpy)$(CO)_3$DMF as well as CO_2 coordianted Re(dmbpy)$(CO)_3$(COOH) using cold-spray ionization spectrometry. [201] The discovery helped to complete the catalytic cycle proposed earlier. Briefly, after photoexcitation, a triplet ^{3}MLCT state is formed, which would be reductively quenched by sacrificed electron donors, e.g., trimethylamine, to form a one-electron-reduced species. Cl^- in the complex then dissociates, resulting in a DMF-coordinated intermediate. CO_2 undergoes an electrophilic attack to the metal center, the product of which would subsequently be protonated to yield a COOH-coordinated Re complex. This CO_2 adduct takes another electron and yields CO. The solvent-coordinated complex is then regenerated and becomes the major species that absorbing light and continue the catalytic cycle (Fig. 18).

For the ease of optimizations of a photocatalyst, a more versatile approach may be to separate the photoharvesting function from the catalytic one so that the light absorption and the catalytic cycle could be tuned separately. Without repeating ourselves, we use discussions on the supramolecular systems (note: the original definition by Lehn of the supramolecular chemistry discusses the super-molecules formed by non-covalent interaction, here the extended definition of Balzani is employed to illustrate the bifunctional nature of the complexes) as a platform to illustrate this point. To this end, Ishitani et al. have developed a series of Ru(II)-Re(I) supramolecular systems based on Re(bpy)$(CO)_3$X complexes (Fig. 19a) [202–205]. Kimura et al. developed another family of Ru(II)-Ni(I) based on Ni cyclam catalysts (Fig. 19b). [206,207] It should be noted that when Ishitani et al. conducted CO_2 reduction using Ru(II)-Re(I) catalysts in aqueous solutions, the main product was formic acid instead of CO as in organic solvents. [203] The authors also found the reaction quantum yield was low. Although a detailed explanation with compelling experimental evidence is still missing, the authors attributed the low yield to back-electron-transfer from the one-electron-reduced species to the oxidized ascorbate. In addition, the photocatalyst underwent photochemical conversion to Ru(II) bisdiimine complex by the ascorbate. One critical feature of these supermolecular systems is the ability to link light absorption units with catalytic ones by molecular linkers, presenting exciting opportunities for chemists to tailor design and synthesize photocatalysts.

3.2. Heterogeneous photocatalysts

Heterogeneous photocatalysts are arguably studied to a greater extent, the most representative ones being semiconductors. As far as CO_2 reduction is concerned, a large portion of such studies focused on engineering the materials for more efficient light absorption and charge separation; efforts have been directed toward understanding and tuning surface adsorption affinities for CO_2 and various intermediates, as well. Below we use the prototypical TiO_2 photocatalyst as an example to discuss the various considerations.

3.2.1. TiO_2

TiO_2 is perhaps the most widely studied photocatalyst for CO_2 reduction and other photocatalytic reactions. [22] Within the context of this Review, many of the considerations are not unique to CO_2 reductions. For instance, with a bandgap of ~3.0 eV, the narrow absorption with respect to the solar spectrum represents a key challenge that has yet to be solved. Different polymorphs of TiO_2 have been shown to exhibit different band gaps and surface facets and, thus, different catalytic efficiency and selectivity toward CO_2 reduction. [208] In practical systems, mixed phases are not uncommon. For instance, the most widely studied TiO_2 mineral (P25) is a mixture of ~70% anatase and ~30% rutile TiO_2. The benefit of having mixed phases may lie in better charge separation. As far as the catalytic processes are concerned, TiO_2 surfaces are believed to participate in the reactions and sometimes play an important role in defining the selectivity and activity. Photocatalytic CO_2 reduction on TiO_2 appears to be sensitive to the media in which the reaction takes place, as well. For instance, gaseous H_2O has been shown to lead to the formation of CO and CH_4 [209], whereas aqueous solutions yielded methanol [210]. Formic acid has only been observed when the reaction was carried out in solutions [211]. Below we mainly focus our discussions on the chemical nature of photocatalytic CO_2 reduction on TiO_2.

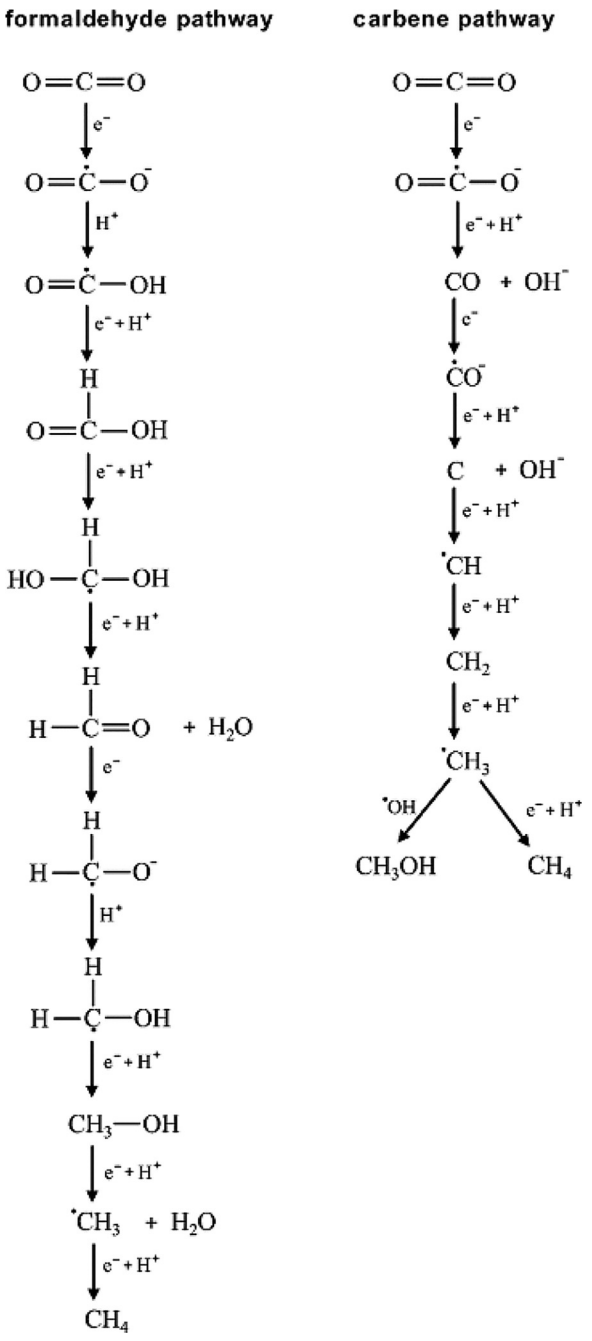

Scheme 7. Proposed formaldehyde and carbene pathway for the reduction of CO_2 to CH_4 on TiO_2. (Scheme reproduced from ref. 22, copyright 2013, Wiley·VCH).

3.2.1.1. Reaction pathways. Generally, two reaction pathways, the formaldehyde pathway and the carbene pathway, have been discussed (Scheme 7). [22]

The initial activation of CO_2 involves a single electron transfer from TiO_2 to CO_2 to form $CO_2^{\bullet-}$ radicals. Afterwards, the intermediates could form formic acid with two oxygen atoms adsorbed on the surface in a bidentate mode. Subsequent proton-coupled electron transfer reduces this species to formaldehyde and methanol. Finally, CH_4 could form with a C—O bond dissociation in methanol. This would be the formaldehyde route. Its key distinguishing character is the anchoring atom to the surface, O. By contrast, the carbene pathway involves CO adsorption to the surface by the C atom after the first C—O bond dissociation. Further reduction by an H radical or a PCET process leads to the formation of C. Afterwards, a sequence of hydrogenation takes place on the carbon atom to form CH_3 radicals. Further hydrogenation or recombination with OH radicals would produce CH_4 or CH_3OH, respectively. It is important to note that neither of the reaction pathways have been experimentally verified explicitly. Koci et al. evaluated the experimental results of CO_2 reduction on TiO_2 to kinetic models of both reaction pathways and concluded that the carbene pathway may be the more plausible one. Besides, Shkrob et al. carried out EPR studies of the reaction intermediates and detected CHO radicals. The authors also found that formaldehyde and methanol are much easier to be oxidized on TiO_2 than being reduced under illumination. They proposed yet another mechanism including the formation of CHO. It should be noted that the reaction pathways may be highly sensitive to the detailed experimental conditions. The accumulation of knowledge is not yet adequate to draw a clearer picture of the reaction mechanisms.

3.2.1.2. Active species on the surface of TiO_2 for CO_2 reduction. When TiO_2 is illuminated, the first event is electron excitation from the valance band (chiefly O 2p orbitals) to the conduction band (chiefly Ti 3d orbitals). As such, it is easy to understand that the formation of Ti^{3+} and $O^{\bullet-}$ is a natural consequence of photoexcitation. The Ti^{3+} centers may serve as active sites where CO_2 binds. Several schemes of CO_2 binding configurations on TiO_2 catalysts surface had been proposed. For instance, Anpo et al. suggested that CO_2 bound to Ti^{3+} with carbon, and one of the two O bound to a hole next to the photogenerated electron. A subsequent charge transfer from Ti^{3+} to C and from O to the hole led to the cleavage of the C—O bond. This process was repeated to yield a C radical on the surface, which was then combined with surface adsorbed O or H to give CH_4 or CH_3OH (Fig. 20a). [212] Modern views of CO_2 adsorption normally involve the binding between C and the Ti^{3+} site, producing a bent $CO_2^{\bullet-}$ [27]. On the other hand, oxygen vacancies in TiO_2 have been demonstrated to be important for specific surface processes. A CO_2 molecule may be bound to the surface by occupying one of the O vacancies by an O in CO_2. In a recent work, Weitz et al. discussed the surface binding configuration of carbonates on TiO_2 nanotubes. [213] By treating pristine TiO_2 nanotubes with O_2 and H_2, Ti^{3+}, $Ti^{(4+\alpha)}$ and $Ti^{(4-\delta)}$ sites were generated. The authors then studied the configurations of CO_2 using in situ FT-IR. They observed the adsorption of bidentate or monodentate carbonates or bicarbonates, as well as carboxylates on TiO_2 surface (Fig. 20b). The exact configuration of each species depended on the Lewis acidity of the binding sites, yielding a vast collection of possible forms. Given the importance of the Ti^{3+} and oxygen vacancy, efforts have been devoted to increase their densities. In a recent work, Yin et al. doped TiO_2 with F. The interaction between Ti^{3+} and F- created an internal electric field to increase the Ti^{3+} density. [214] Li et al. studied the relationship between the different phases of TiO_2 with the different concentrations of defects and they affect CO_2 reduction activity. [208] Through DRIFTs experiments, the authors detected $CO_2^{\bullet-}$ radicals, HCOOH and CO as reaction intermediates. They also found that by helium pretreatment of different TiO_2, only anatase and brookite could form defective surfaces, and rutile remained defect-free. Production of CO and CH_4 from CO_2 photoreduction was significantly improved on defective anatase and brookite TiO_2. In addition, defective brookite TiO_2 was more active than anatase one due to the lower formation energy of O vacancies. In another study by the same group on TiO_2/Cu integrated systems, the authors found that O vacancies could facilitate adsorption of CO_2 and the C—O bond dissociation [215].

It was, therefore, expected that anisotropic TiO_2 crystals would exhibit different reaction efficiency and/or selectivity on different facets, as the density of the various sites would be different on different facets. Although the correlation between facets and specific catalytic route is not fully established yet, some experimental

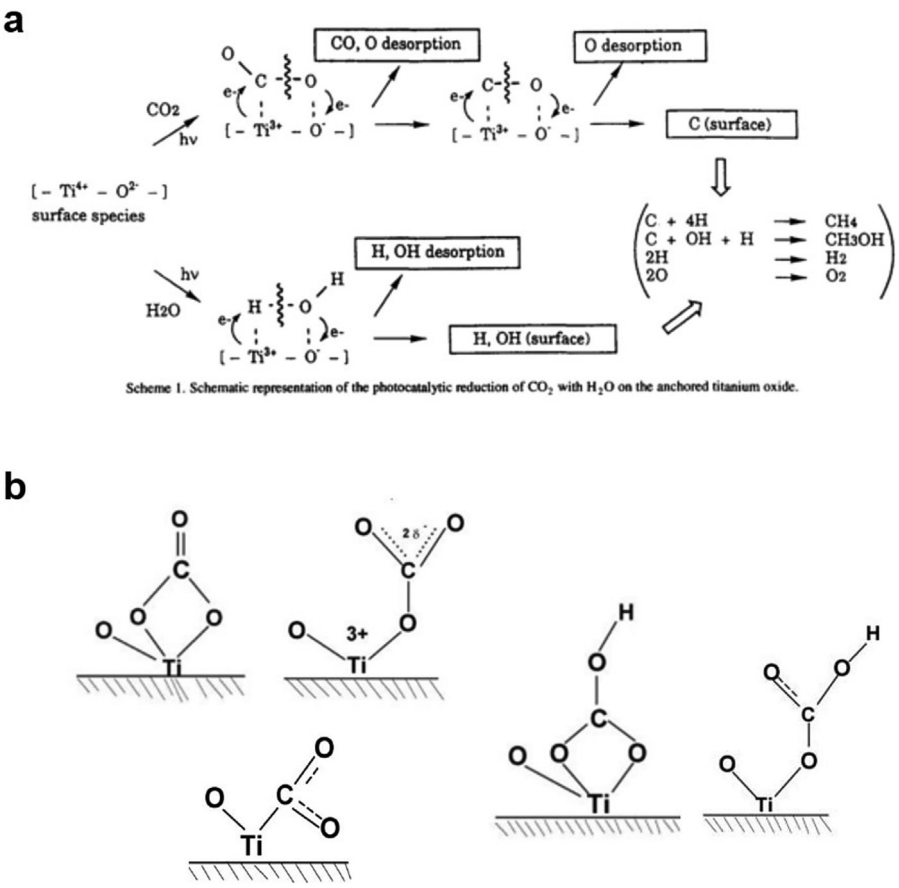

Scheme 1. Schematic representation of the photocatalytic reduction of CO_2 with H_2O on the anchored titanium oxide.

Fig. 20. Schematics illustrating activation of CO_2 on TiO_2. (a) The photocatalytic reduction of CO_2 with H_2O. (Figure reproduced from ref. 212, copyright 1995, Elsevier); (b) Various CO_2 activation configurations on TiO_2 surface. (Schemes reproduced from ref. 213, copyright 2014, American Chemical Society).

results have been obtained. For example, the high concentration of Ti on the (100) surface would lead to the production of only methanol, at low efficiencies though. The (100) facets would be more favorable for CH_4 production. Synergistic effects of different facets are believed to play a role in the activity of CO_2 photoreduction, as well. Yu et al. synthesized TiO_2 nanoparticles with different (100) to (101) ratios [216]. Under their experimental conditions, samples of 1:1 ratio showed the most CH_4 production, indicating that the two facets work together to assist CH_4 formation. With the help of DFT calculations, the authors proposed that a heterojunction was formed between (100) and (101) facets, facilitating charge separation.

TiO_2 is also active toward CO_2 reduction in the absence of light, although relatively few efforts have been directed toward studying the reaction mechanisms and comparing them with photoreduction of CO_2. Recently, Kamat et al. carried out electrocatalytic reduction of CO_2 on nanostructured TiO_2 by depositing a thin film of TiO_2 on glassy carbon [217]. They detected the conversion of Ti^{4+} to Ti^{3+} at -0.95 V vs. RHE, and the reduction of CO_2 to the one-electron-reduced species of $CO_2^{-\bullet}$ in acetonitrile. Without TiO_2, this reduction required a more negative potential of -1.9 V vs. RHE. However, in contrast to photocatalytic processes, multiple proton-coupled electron reduction was not observed here. The authors emphasized the central role of Ti^{3+} as an active site for CO_2 binding and reduction. The following reactions of reduced $CO_2^{\bullet-}$, such as dimerization, or further reduction and protonation were thermodynamically favorable. In this work, methanol was the major product with water as a proton source. The surface Ti–OH group near the binding site was also considered crucial for the production of methanol.

3.2.2. Other semiconductors

Besides TiO_2, a variety of semiconductor metal oxides and metal chalcogenides have been studied as photocatalysts for CO_2 reduction. Typical examples include p-Si, [218] SiC [219], GaP [220] in a photoelectrochemical system, and metal oxides ZnO [221], WO_3 [222], NiO [223], Ga_2O_3 [224], $ZnGa_2O_4$ [225], $BiVO_4$ [226], Bi_2WO_6 [227], BiOCl [228], Cu_2O, [219] sulfides Bi_2S_3 [229], CdS [230], and polyoxometaletes [231]. Summaries of the state-of-art semiconductor photocatalysts systems have been reviewed elsewhere [23–27,31,32]. It is noted that whether the semiconductor functionalized solely as the photoabsorber or as the photocatalyst (as defined in this review) is normally not discussed. Majority of the literature has been focused on band gap engineering to address the light absorption issue for better utilization of the solar spectrum. Sometimes, the importance of oxygen vacancy defects and surface hydroxyl group has been mentioned.

3.3. Metal photocatalysts

Most recently, plasmonic metals have emerged as a new group of catalysts for photochemical transformation. Upon illumination, hot charges may be generated in these metals. These hot charges may undergoes either radiative or non-radiative decay in fast timescales (*fs* to *ps*). While the efficiency may be low, it is possible to utilize these charges for CO_2 reduction. In addition, photons with different energy may lead to the formation of different hot carriers, which further lead to unique selectivity. For instance, Cronin et al. experimentally showed that both plasmonic and interband transition would allow for the utilizations of metal for photocatalytic reduction of CO_2, but with different product selec-

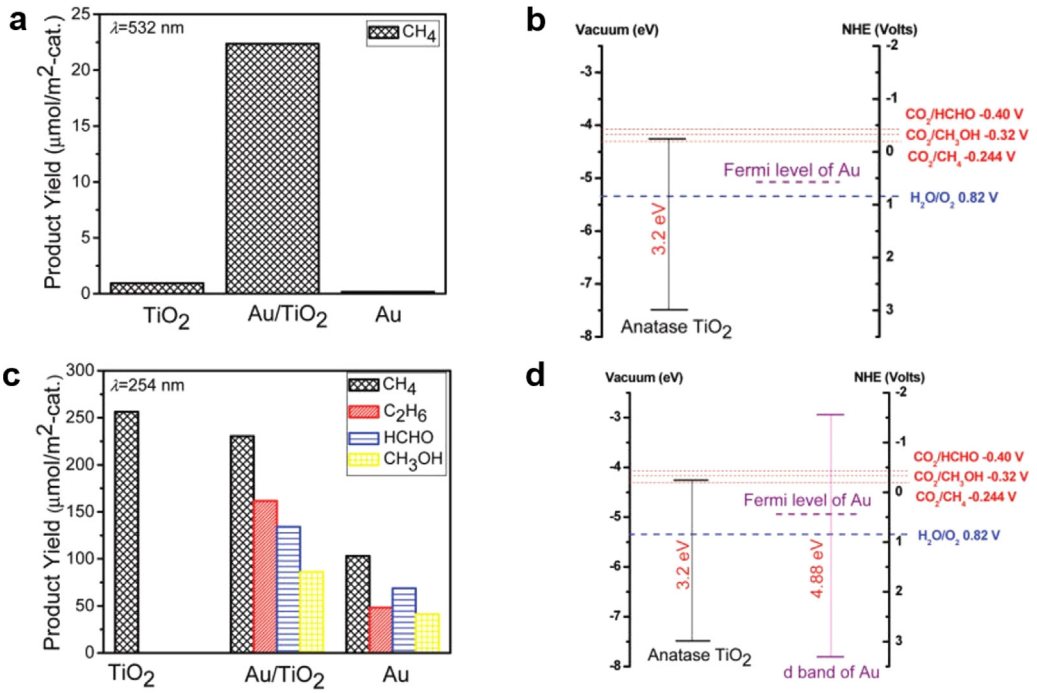

Fig. 21. a) Photocatalytic product yields of TiO_2, Au/TiO_2 and Au after 15 h irradiation of visible light; b) Energy band diagram of the TiO_2 and Au under visible light irradiation; c) Photocatalytic product yields of TiO_2, Au/TiO_2 and Au after 15 h irradiation of 254 nm UV light; d) Energy band diagram of the TiO_2 and Au under UV light irradiation. (Figures reproduced from ref. 232, copyright 2011, American Chemical Society).

tivities (Fig. 21). [232] Au continuous films and nanoparticles have been shown to produce carbonaceous products such as CH_4, C_2H_6, CH_3OH and HCHO with λ = 254 nm UV illumination, while only CH_4 could be obtained under plasmonic wavelength (λ = 532 nm) irradiation. Similar activity was observed in Cu foil and Pt film, as well. Forming a metal-oxide interface was believed to help to increase the life time of hot electrons. Surface adsorbates were employed to extract the hot electrons from the metal. In a recent work, Jain et al. demonstrated that multi-electron excitation and C–C coupling could be achieved on Au nanoparticles. [233] However, as pointed out by the authors, plasmonic-driven photocatalysis for CO_2 reduction remains underdeveloped. [234] One intriguing observation in recent studies by the Cronin group was that the product yields under UV irradiation, including the percentage of C_2 species, were higher on Au and Pt photocatalysts than on Cu. This is in contrast to that observed in the electrochemical system. The difference between electrocatalytic and photocatalytic reactions suggests that light-driven CO_2 reduction possibly proceeds through a different mechanism from that in electrochemical processes. While the selectivity was determined by the binding strength of the species and the catalyst surface during the electrocatalytic process, unique photoexcited states of the metal/adsorbate complex may be involved in the reaction pathways. New opportunities to tune the activity and selectivity may be presented by photocatalysis.

4. Summary and perspectives

The reduction of CO_2 has been a hot research topic for decades. In the case of CO_2 catalytic reduction, a large number of potential catalysts materials have been screened. In the search for catalysts of better performance for this reaction, researchers have benefited from efforts focused on screening known compositions and/or combining components of known functionalities. Moving forward, it has become clear that we need mechanistic understandings of the catalytic details, especially at the molecular level, so as to come up with rational designs for accelerated catalyst discovery. These efforts will depend on the latest development of experimental techniques and computational capabilities.

As far as selectivity is concerned, it has been shown that the relative ease and/or difficulty of the various kinetic pathways is sensitive to the energetics of surface-bound species. Indeed, the adsorption energy has been used as a convenient descriptor to compare various catalysts in different settings. Nevertheless, discussions entirely based on a simple descriptor often fail to capture all details necessary to move the field forward with better catalysts. For instance, in one set of such discussions, we see that the configuration of the initially adsorbed CO_2 helps to define whether the reaction would proceed through the *COOH pathway and yield CO as a product or the*OCOH pathway and produce HCOOH as the first step product. Comparatively, discussions on the selectivity among these and other C_1 products such CH_4 or CH_3OH have received less attention. The formation of more complex, C_2 and C_3 products would require C–C coupling, which demands the adsorption of at least two C_1 species in close vicinity. Appreciation of the complexities alone could help us to see how studies on homogeneous catalysis of CO_2 reduction could affect the binding geometry of CO_2 through controlling the ligands. The intramolecular interactions and/or the steric effects play critical roles in these examples. Similar approaches should be able to be borrowed for heterogeneous catalysis of CO_2 reduction, as well. However, how to achieve similar goals remains an open challenge. Moreover, the electronic properties of the active center of a homogeneous catalyst may be influenced by ligands, too. Even slight variations of substituents have been shown to result in significant changes of the catalyst redox potentials. Controlling how the substrates bind on a heterogeneous catalyst is exceedingly challenging, especially when the molecular structures of the binding sites remain to be clearly identified. These caveats notwithstanding, surface treatments such as doping, alloying, de-alloying, oxidation, sulfurization and ligand adsorption have been widely applied for catalyst optimization. As far as CO_2 reduction is concerned, in most cases, the binding energies of CO_2 and intermediates on both modified and the orig-

inal surfaces have calculated to explain the origin of the catalyst selectivity, but the true reasons behind each demonstration would require further research to be identified.

Apart from the surface properties, how the morphology of the catalyst affects its performance is yet another critical factor to consider. For one, different morphologies often represent a difference in the exposed crystal facets, each of which often features different catalytic characteristics. For another, the different morphologies may lead to different mass transport characteristics to influence the reaction rate and selectivity. In order to further exploit this aspect, precise controls over the size and shape, as well as the distribution, of the catalyst, particularly at the nanometer scale, are of critical importance.

With all the accumulation of knowledge on electrocatalysts, their applications in photo(electro)catalytic systems are expected. Factors important to selectivity and efficiency in the electrocatalytic systems may be important in the photo(electro)catalytic systems, too. Together with the development of new materials as light absorbers, the co-catalyst design will help push the field forward as measured by better overall performance.

Lastly, the potentials of photochemistry for CO_2 reduction has not yet been fully explored. One unique feature of photocatalyst is the fact that the photoexcitation could be quantized to yield high energy charges (e.g., hot electrons), which makes it possible to access high energy intermediates that are often considered inaccessible by thermal or electrochemistry. When exploited, this feature may enable unusual reaction routes to yield unique products, especially multi-carbon ones.

Acknowledgements

Y.W and H.C. gratefully acknowledge the financial support from the National Natural Science Foundation of China (21673117, 21703104), Jiangsu Science and Technology Plan (SBK2017041514), Jiangsu Provincial Foundation for Specially-Appointed Professor, Nanjing Tech University (39837102, 39837131) and SICAM Fellowship from Jiangsu National Synergetic Innovation Center for Advanced Materials. D.H. and D.W. thank National Science Foundation (NSF) (CBET 1703662, 1703655) and American Chemical Society (ACS) (Petroleum Research Fund (PRF) 59820-ND5) for financial support.

References

[1] B. Obama, The irreversible momentum of clean energy, Science 355 (2017) 126–129.
[2] J.D. Figueroa, T. Fout, S. Plasynski, H. McIlvried, R.D. Srivastava, Advances in CO2 capture technology—the U.S. department of energy's carbon sequestration program, Int. J. Greenh. Gas Control. 2 (2008) 9–20.
[3] A. Goeppert, M. Czaun, J.-P. Jones, G.K. Surya Prakash, G.A. Olah, Recycling of carbon dioxide to methanol and derived products - closing the loop, Chem. Soc. Rev. 43 (2014) 7995–8048.
[4] A. Djaidja, S. Libs, A. Kiennemann, A. Barama, Characterization and activity in dry reforming of methane on NiMg/Al and Ni/MgO catalysts, Catal. Today 113 (2006) 194–200.
[5] J. Guo, H. Lou, H. Zhao, D. Chai, X. Zheng, Dry reforming of methane over nickel catalysts supported on magnesium aluminate spinels, Appl. Catal. A Gen. 273 (2004) 75–82.
[6] S. Tada, T. Shimizu, H. Kameyama, T. Haneda, R. Kikuchi, Ni/CeO_2 catalysts with high CO_2 methanation activity and high CH_4 selectivity at low temperatures, Int. J. Hydrogen Energy 37 (2012) 5527–5531.
[7] Y. Park, D. Shin, Y.N. Jang, A.-H.A. Park, CO_2 capture capacity and swelling measurements of liquid-like nanoparticle organic hybrid materials via attenuated total reflectance fourier transform infrared spectroscopy, J. Chem. Eng. Data 57 (2012) 40–45.
[8] T. Inoue, A. Fujishima, S. Konishi, K. Honda, Photoelectrocatalytic reduction of carbon dioxide in aqueous suspensions of semiconductor powders, Nature 277 (1979) 637.
[9] Y. Wang, J. Liu, Y. Wang, A.M. Al-Enizi, G. Zheng, Tuning of CO_2 reduction selectivity on metal electrocatalysts, Small 13 (2017), 1701809.
[10] R. Kortlever, J. Shen, K.J.P. Schouten, F. Calle-Vallejo, M.T.M. Koper, Catalysts and reaction pathways for the electrochemical reduction of carbon dioxide, J. Phys. Chem. Lett. 6 (2015) 4073–4082.
[11] Y. Li, S.H. Chan, Q. Sun, Heterogeneous catalytic conversion of CO_2: a comprehensive theoretical review, Nanoscale 7 (2015) 8663–8683.
[12] Q. Lu, F. Jiao, Electrochemical CO_2 reduction: electrocatalyst, reaction mechanism, and process engineering, Nano Energy 29 (2016) 439–456.
[13] D.D. Zhu, J.L. Liu, S.Z. Qiao, Recent advances in inorganic heterogeneous electrocatalysts for reduction of carbon dioxide, Adv. Mater. 28 (2016) 3423–3452.
[14] W. Zhang, Y. Hu, L. Ma, G. Zhu, Y. Wang, X. Xue, R. Chen, S. Yang, Z. Jin, Progress and perspective of electrocatalytic CO_2 reduction for renewable carbonaceous fuels and chemicals, Adv. Sci. 5 (2017), 1700275.
[15] B. Khezri, A.C. Fisher, M. Pumera, CO_2 reduction: the quest for electrocatalytic materials, J. Mater. Chem. A 5 (2017) 8230–8246.
[16] T. Zheng, K. Jiang, H. Wang, Recent advances in electrochemical CO_2-to-CO conversion on heterogeneous catalysts, Adv. Mater. (2018), 1802066.
[17] H. Xie, T. Wang, J. Liang, Q. Li, S. Sun, Cu-based nanocatalysts for electrochemical reduction of CO2, Nano Today 21 (2018) 41–54.
[18] D.H. Apaydin, S. Schlager, E. Portenkirchner, N.S. Sariciftci, Organic, Organometallic and bio organic catalysts for electrochemical reduction of CO_2, Chemphyschem 18 (2017) 3094–3116.
[19] L. Zhang, Z.-J. Zhao, J. Gong, Nanostructured materials for heterogeneous electrocatalytic CO_2 reduction and their related reaction mechanisms, Angew. Chemie Int. Ed. 56 (2017) 11326–11353.
[20] V.P. Indrakanti, J.D. Kubicki, H.H. Schobert, Photoinduced activation of CO_2 on Ti-based heterogeneous catalysts: current state, chemical physics-based insights and outlook, Energy Environ. Sci. 2 (2009) 745–758.
[21] B. Kumar, M. Llorente, J. Froehlich, T. Dang, A. Sathrum, C.P. Kubiak, Photochemical and photoelectrochemical reduction of CO_2, Annu. Rev. Phys. Chem. 63 (2012) 541–569.
[22] S.N. Habisreutinger, L. Schmidt-Mende, J.K. Stolarczyk, Photocatalytic reduction of CO_2 on TiO_2 and other semiconductors, Angew. Chemie Int. Ed. 52 (2013) 7372–7408.
[23] Y. Izumi, Recent advances in the photocatalytic conversion of carbon dioxide to fuels with water and/or hydrogen using solar energy and beyond, Coord. Chem. Rev. 257 (2013) 171–186.
[24] S. Navalón, A. Dhakshinamoorthy, M. Álvaro, H. Garcia, Photocatalytic CO_2 reduction using non-titanium metal oxides and sulfides, ChemSusChem 6 (2013) 562–577.
[25] S. Das, W.M.A. Wan Daud, A review on advances in photocatalysts towards CO_2 conversion, RSC Adv. 4 (2014) 20856–20893.
[26] W. Tu, Y. Zhou, Z. Zou, Photocatalytic conversion of CO_2 into renewable hydrocarbon fuels: state-of-the-Art accomplishment, challenges, and prospects, Adv. Mater. 26 (2014) 4607–4626.
[27] J.L. White, M.F. Baruch, J.E. Pander, Y. Hu, I.C. Fortmeyer, J.E. Park, T. Zhang, K. Liao, J. Gu, Y. Yan, T.W. Shaw, E. Abelev, A.B. Bocarsly, Light-driven heterogeneous reduction of carbon dioxide: photocatalysts and photoelectrodes, Chem. Rev. 115 (2015) 12888–12935.
[28] L. Yuan, Y.-J. Xu, Photocatalytic conversion of CO_2 into value-added and renewable fuels, Appl. Surf. Sci. 342 (2015) 154–167.
[29] X. Chang, T. Wang, J. Gong, CO2 photo-reduction: insights into CO_2 activation and reaction on surfaces of photocatalysts, Energy Environ. Sci. 9 (2016) 2177–2196.
[30] E. Karamian, S. Sharifnia, On the general mechanism of photocatalytic reduction of CO_2, J. Co2 Util. 16 (2016) 194–203.
[31] K. Li, B. Peng, T. Peng, Recent advances in heterogeneous photocatalytic CO_2 conversion to solar fuels, ACS Catal. 6 (2016) 7485–7527.
[32] G. Zhao, X. Huang, X. Wang, X. Wang, Progress in catalyst exploration for heterogeneous CO_2 reduction and utilization: a critical review, J. Mater. Chem. A 5 (2017) 21625–21649.
[33] P. Wang, S. Wang, H. Wang, Z. Wu, L. Wang, Recent progress on photo-electrocatalytic reduction of carbon dioxide, Part. Part. Syst. Charact. 35 (2018), 1700371.
[34] J. Twilton, C. Le, P. Zhang, M.H. Shaw, R.W. Evans, D.W.C. MacMillan, The merger of transition metal and photocatalysis, Nat. Rev. Chem. 1 (2017) 0052.
[35] M.H. Shaw, J. Twilton, D.W.C. MacMillan, Photoredox catalysis in organic chemistry, J. Org. Chem. 81 (2016) 6898–6926.
[36] A.S. Varela, M. Kroschel, T. Reier, P. Strasser, Controlling the selectivity of CO_2 electroreduction on copper: the effect of the electrolyte concentration and the importance of the local pH, Catal. Today 260 (2016) 8–13.
[37] A.S. Varela, M. Kroschel, N.D. Leonard, W. Ju, J. Steinberg, A. Bagger, J. Rossmeisl, P. Strasser, pH effects on the selectivity of the electrocatalytic CO_2 reduction on graphene-embedded Fe–N–C motifs: bridging concepts between molecular homogeneous and solid-state heterogeneous catalysis, ACS Energy Lett. 3 (2018) 812–817.
[38] M.R. Singh, Y. Kwon, Y. Lum, J.W. Ager, A.T. Bell, Hydrolysis of electrolyte cations enhances the electrochemical reduction of CO_2 over Ag and Cu, J. Am. Chem. Soc. 138 (2016) 13006–13012.
[39] M. Azuma, K. Hashimoto, M. Hiramoto, M. Watanabe, T. Sakata, Electrochemical reduction of carbon dioxide on various metal electrodes in low-temperature aqueous $KHCO_3$ media, J. Electrochem. Soc. 137 (1990) 1772–1778.

[40] X. Liu, J. Xiao, H. Peng, X. Hong, K. Chan, J.K. Nørskov, Understanding trends in electrochemical carbon dioxide reduction rates, Nat. Commun. 8 (2017) 15438.
[41] H. Ishida, A. Sakaba, Temperature dependence of photocatalytic CO_2 reduction by trans(Cl)–Ru(bpy)$(CO)_2Cl_2$: activation energy difference between CO and formate production, Faraday Discuss. 198 (2017) 263–277.
[42] Y.-J. Zhang, V. Sethuraman, R. Michalsky, A.A. Peterson, Competition between CO_2 reduction and H_2 evolution on transition-metal electrocatalysts, ACS Catal. 4 (2014) 3742–3748.
[43] M. Dunwell, Q. Lu, J.M. Heyes, J. Rosen, J.G. Chen, Y. Yan, F. Jiao, B. Xu, The central role of bicarbonate in the electrochemical reduction of carbon dioxide on gold, J. Am. Chem. Soc. 139 (2017) 3774–3783.
[44] S. Zhu, B. Jiang, W.-B. Cai, M. Shao, Direct observation on reaction intermediates and the role of bicarbonate anions in CO_2 electrochemical reduction reaction on Cu surfaces, J. Am. Chem. Soc. (2017).
[45] Y. Kuramochi, O. Ishitani, H. Ishida, Reaction mechanisms of catalytic photochemical CO_2 reduction using Re(I) and Ru(II) complexes, Coord. Chem. Rev. 373 (2018) 333–356.
[46] A. Wuttig, M. Yaguchi, K. Motobayashi, M. Osawa, Y. Surendranath, Inhibited proton transfer enhances Au-catalyzed CO_2-to-fuels selectivity, Proc. Natl. Acad. Sci. 113 (2016) E4585–E4593.
[47] W. Zhu, Y.-J. Zhang, H. Zhang, H. Lv, Q. Li, R. Michalsky, A.A. Peterson, S. Sun, Active and selective conversion of CO_2 to CO on ultrathin Au nanowires, J. Am. Chem. Soc. 136 (2014) 16132–16135.
[48] K.P. Kuhl, E.R. Cave, D.N. Abram, T.F. Jaramillo, New insights into the electrochemical reduction of carbon dioxide on metallic copper surfaces, Energy Environ. Sci. 5 (2012) 7050–7059.
[49] C.S. Diercks, Y. Liu, K.E. Cordova, O.M. Yaghi, The role of reticular chemistry in the design of CO_2 reduction catalysts, Nat. Mater. 17 (2018) 301–307.
[50] J.W. Maina, C. Pozo-Gonzalo, L. Kong, J. Schutz, M. Hill, L.F. Dumee, Metal organic framework based catalysts for CO_2 conversion, Mater. Horiz. 4 (2017) 345–361.
[51] C.-C. Wang, Y.-Q. Zhang, J. Li, P. Wang, Photocatalytic CO_2 reduction in metal–organic frameworks: a mini review, J. Mol. Struct. 1083 (2015) 127–136.
[52] C.D. Windle, R.N. Perutz, Advances in molecular photocatalytic and electrocatalytic CO_2 reduction, Coord. Chem. Rev. 256 (2012) 2562–2570.
[53] E.E. Benson, C.P. Kubiak, A.J. Sathrum, J.M. Smieja, Electrocatalytic and homogeneous approaches to conversion of CO_2 to liquid fuels, Chem. Soc. Rev. 38 (2009) 89–99.
[54] H. Takeda, C. Cometto, O. Ishitani, M. Robert, Electrons, photons, protons and earth-abundant metal complexes for molecular catalysis of CO_2 reduction, ACS Catal. 7 (2017) 70–88.
[55] J. Bonin, A. Maurin, M. Robert, Molecular catalysis of the electrochemical and photochemical reduction of CO_2 with Fe and Co metal based complexes. Recent advances, Coord. Chem. Rev. 334 (2017) 184–198.
[56] J. Hawecker, J.-M. Lehn, R. Ziessel, Efficient photochemical reduction of CO_2 to CO by visible light irradiation of systems containing Re(bipy)$(CO)_3$X or Ru(bipy)$_3^{2+}$–Co^{2+} combinations as homogeneous catalysts, J. Chem. Soc. Chem. Commun. (1983) 536–538.
[57] B.J. Fisher, R. Eisenberg, Electrocatalytic reduction of carbon dioxide by using macrocycles of nickel and cobalt, J. Am. Chem. Soc. 102 (1980) 7361–7363.
[58] C. Costentin, G. Passard, M. Robert, J.-M. Savéant, Ultraefficient homogeneous catalyst for the CO_2-to-CO electrochemical conversion, Proc. Natl. Acad. Sci. 111 (2014) 14990–14994.
[59] D.L. DuBois, A. Miedaner, R.C. Haltiwanger, Electrochemical reduction of carbon dioxide catalyzed by [Pd(triphosphine)(solvent)](BF4)$_2$ complexes: synthetic and mechanistic studies, J. Am. Chem. Soc. 113 (1991) 8753–8764.
[60] J. Schneider, H. Jia, J.T. Muckerman, E. Fujita, Thermodynamics and kinetics of CO_2, CO, and H^+ binding to the metal centre of CO_2 reduction catalysts, Chem. Soc. Rev. 41 (2012) 2036–2051.
[61] A.J. Morris, G.J. Meyer, E. Fujita, Molecular approaches to the photocatalytic reduction of carbon dioxide for solar fuels, Acc. Chem. Res. 42 (2009) 1983–1994.
[62] C. Cometto, L. Chen, P.-K. Lo, Z. Guo, K.-C. Lau, E. Anxolabéhère-Mallart, C. Fave, T.-C. Lau, M. Robert, Highly selective molecular catalysts for the CO_2-to-CO electrochemical conversion at very low overpotential. Contrasting Fe vs Co quaterpyridine complexes upon mechanistic studies, ACS Catal. 8 (2018) 3411–3417.
[63] L. Chen, Z. Guo, X.-G. Wei, C. Gallenkamp, J. Bonin, E. Anxolabéhère-Mallart, K.-C. Lau, T.-C. Lau, M. Robert, Molecular catalysis of the electrochemical and photochemical reduction of CO_2 with earth-abundant metal complexes. Selective production of CO vs HCOOH by switching of the metal center, J. Am. Chem. Soc. 137 (2015) 10918–10921.
[64] C. Costentin, M. Robert, J.-M. Savéant, A. Tatin, Efficient and selective molecular catalyst for the CO_2-to-CO electrochemical conversion in water, Proc. Natl. Acad. Sci. 112 (2015) 6882–6886.
[65] A. Glüer, S. Schneider, Iron catalyzed hydrogenation and electrochemical reduction of CO_2: the role of functional ligands, J. Organomet. Chem. 861 (2018) 159–173.
[66] S. Sung, D. Kumar, M. Gil-Sepulcre, M. Nippe, Electrocatalytic CO2 reduction by imidazolium-functionalized molecular catalysts, J. Am. Chem. Soc. 139 (2017) 13993–13996.
[67] K.A. Grice, Carbon dioxide reduction with homogenous early transition metal complexes: opportunities and challenges for developing CO_2 catalysis, Coord. Chem. Rev. 336 (2017) 78–95.
[68] J.M. Manriquez, D.R. McAlister, R.D. Sanner, J.E. Bercaw, Stoichiometric hydrogen reduction of carbon monoxide to methanol promoted by derivatives of bis(pentamethylcyclopentadienyl)zirconium, J. Am. Chem. Soc. 98 (1976) 6733–6735.
[69] J. Ni, Q. Zhou, D.K. Canseco, T.R. Calhoun, A.R. Graham, K.L. Carreras, C.N. Schultz, Transformation of carbon dioxide to methoxide by the complex $[(C_5H_5)Ti]_2(\mu\text{-}H)_2(\mu\text{-}C_{10}H_8)$, Inorganica Chim. Acta 309 (2000) 23–27.
[70] J. Agarwal, T.W. Shaw, H.F. Schaefer, A.B. Bocarsly, Design of a catalytic active site for electrochemical CO_2 reduction with Mn(I)-Tricarbonyl species, Inorg. Chem. 54 (2015) 5285–5294.
[71] Y.C. Lam, R.J. Nielsen, H.B. Gray, W.A. Goddard, A Mn bipyrimidine catalyst predicted to reduce CO_2 at lower overpotential, ACS Catal. 5 (2015) 2521–2528.
[72] M. Bourrez, F. Molton, S. Chardon-Noblat, A. Deronzier, [Mn(bipyridyl)$(CO)_3$Br]: an abundant metal carbonyl complex as efficient electrocatalyst for CO_2 reduction, Angew. Chemie 123 (2011) 10077–10080.
[73] S. Bontemps, L. Vendier, S. Sabo-Etienne, Ruthenium-catalyzed reduction of carbon dioxide to formaldehyde, J. Am. Chem. Soc. 136 (2014) 4419–4425.
[74] J. Shen, R. Kortlever, R. Kas, Y.Y. Birdja, O. Diaz-Morales, Y. Kwon, I. Ledezma-Yanez, K.J.P. Schouten, G. Mul, M.T.M. Koper, Electrocatalytic reduction of carbon dioxide to carbon monoxide and methane at an immobilized cobalt protoporphyrin, Nat. Commun. 6 (2015) 8177.
[75] S. Chakraborty, J. Zhang, J.A. Krause, H. Guan, An efficient nickel catalyst for the reduction of carbon dioxide with a borane, J. Am. Chem. Soc. 132 (2010) 8872–8873.
[76] H. Rao, L.C. Schmidt, J. Bonin, M. Robert, Visible-light-driven methane formation from CO2 with a molecular iron catalyst, Nature 548 (2017) 74.
[77] R.M. Bullock, A.K. Das, A.M. Appel, Surface immobilization of molecular electrocatalysts for energy conversion, Chem. Eur. J. 23 (2017) 7626–7641.
[78] Z. Weng, J. Jiang, Y. Wu, Z. Wu, X. Guo, K.L. Materna, W. Liu, V.S. Batista, G.W. Brudvig, H. Wang, Electrochemical CO_2 reduction to hydrocarbons on a heterogeneous molecular Cu catalyst in aqueous solution, J. Am. Chem. Soc. 138 (2016) 8076–8079.
[79] G. Seshadri, C. Lin, A.B. Bocarsly, A new homogeneous electrocatalyst for the reduction of carbon dioxide to methanol at low overpotential, J. Electroanal. Chem. 372 (1994) 145–150.
[80] E. Barton Cole, P.S. Lakkaraju, D.M. Rampulla, A.J. Morris, E. Abelev, A.B. Bocarsly, Using a one-electron shuttle for the multielectron reduction of CO2 to methanol: kinetic, mechanistic, and structural insights, J. Am. Chem. Soc. 132 (2010) 11539–11551.
[81] M.Z. Ertem, S.J. Konezny, C.M. Araujo, V.S. Batista, Functional role of pyridinium during aqueous electrochemical reduction of CO_2 on Pt(111), J. Phys. Chem. Lett. 4 (2013) 745–748.
[82] J.A. Keith, E.A. Carter, Theoretical insights into pyridinium-based photoelectrocatalytic reduction of CO_2, J. Am. Chem. Soc. 134 (2012) 7580–7583.
[83] J.A. Keith, E.A. Carter, Electrochemical reactivities of pyridinium in solution: consequences for CO2 reduction mechanisms, Chem. Sci. 4 (2013) 1490–1496.
[84] M. Lessio, E.A. Carter, What is the role of pyridinium in pyridine-catalyzed CO2 reduction on p-GaP photocathodes? J. Am. Chem. Soc. 137 (2015) 13248–13251.
[85] T.P. Senftle, M. Lessio, E.A. Carter, The role of surface-bound dihydropyridine analogues in pyridine-catalyzed CO_2 reduction over semiconductor photoelectrodes, ACS Cent. Sci. 3 (2017) 968–974.
[86] D.J. Boston, C. Xu, D.W. Armstrong, F.M. MacDonnell, Photochemical reduction of carbon dioxide to methanol and formate in a homogeneous system with pyridinium catalysts, J. Am. Chem. Soc. 135 (2013) 16252–16255.
[87] M. Dunwell, Y. Yan, B. Xu, In situ infrared spectroscopic investigations of pyridine-mediated CO_2 reduction on Pt electrocatalysts, ACS Catal. 7 (2017) 5410–5419.
[88] M. Can, F.A. Armstrong, S.W. Ragsdale, Structure, function, and mechanism of the nickel metalloenzymes, CO dehydrogenase, and Acetyl-CoA synthase, Chem. Rev. 114 (2014) 4149–4174.
[89] W. Shin, S.H. Lee, J.W. Shin, S.P. Lee, Y. Kim, Highly selective electrocatalytic conversion of CO_2 to CO at −0.57 V (NHE) by carbon monoxide dehydrogenase from Moorella thermoacetica, J. Am. Chem. Soc. 125 (2003) 14688–14689.
[90] A. Parkin, J. Seravalli, K.A. Vincent, S.W. Ragsdale, F.A. Armstrong, Rapid and efficient electrocatalytic CO_2/CO interconversions by carboxydothermus hydrogenoformans CO dehydrogenase I on an electrode, J. Am. Chem. Soc. 129 (2007) 10328–10329.
[91] Y. Amao, Photoredox systems with biocatalysts for CO2 utilization, Sustain. Energy Fuels 2 (2018) 1928–1950.
[92] Y. Amao, Formate dehydrogenase for CO_2 utilization and its application, J. Co2 Util. 26 (2018) 623–641.
[93] K. Schuchmann, V. Müller, Direct and reversible hydrogenation of CO_2 to formate by a bacterial carbon dioxide reductase, Science 342 (2013) 1382–1385.
[94] T. Reda, C.M. Plugge, N.J. Abram, J. Hirst, Reversible interconversion of carbon dioxide and formate by an electroactive enzyme, Proc. Natl. Acad. Sci. 105 (2008) 10654–10658.
[95] A. Bassegoda, C. Madden, D.W. Wakerley, E. Reisner, J. Hirst, Reversible interconversion of CO2 and formate by a molybdenum-containing formate dehydrogenase, J. Am. Chem. Soc. 136 (2014) 15473–15476.

[96] Z.-Y. Yang, V.R. Moure, D.R. Dean, L.C. Seefeldt, Carbon dioxide reduction to methane and coupling with acetylene to form propylene catalyzed by remodeled nitrogenase, Proc. Natl. Acad. Sci. 109 (2012) 19644–19648.
[97] S.K. Kuk, R.K. Singh, D.H. Nam, R. Singh, J.-K. Lee, C.B. Park, Photoelectrochemical reduction of carbon dioxide to methanol through a highly efficient enzyme cascade, Angew. Chemie Int. Ed. 56 (2017) 3827–3832.
[98] J.B. Varley, H.A. Hansen, N.L. Ammitzbøll, L.C. Grabow, A.A. Peterson, J. Rossmeisl, J.K. Nørskov, Ni–Fe–S Cubanes in CO_2 reduction electrocatalysis: A DFT study, ACS Catal. 3 (2013) 2640–2643.
[99] A. Roldan, N. Hollingsworth, A. Roffey, H.U. Islam, J.B.M. Goodall, C.R.A. Catlow, J.A. Darr, W. Bras, G. Sankar, K.B. Holt, G. Hogarth, N.H. de Leeuw, Bio-inspired CO_2 conversion by iron sulfide catalysts under sustainable conditions, Chem. Commun. 51 (2015) 7501–7504.
[100] S. Bagherzadeh, N.P. Mankad, Catalyst control of selectivity in CO_2 reduction using a tunable heterobimetallic effect, J. Am. Chem. Soc. 137 (2015) 10898–10901.
[101] E.A. Mohamed, Z.N. Zahran, Y. Naruta, Efficient electrocatalytic CO_2 reduction with a molecular cofacial iron porphyrin dimer, Chem. Commun. 51 (2015) 16900–16903.
[102] B.A. Rosen, I. Hod, Tunable molecular-scale materials for catalyzing the low-overpotential electrochemical conversion of CO_2, Adv. Mater. (2018), 1706238.
[103] Y. Chen, D. Wang, X. Deng, Z. Li, Metal-organic frameworks (MOFs) for photocatalytic CO_2 reduction, Catal. Sci. Technol. 7 (2017) 4893–4904.
[104] N. Kornienko, Y. Zhao, C.S. Kley, C. Zhu, D. Kim, S. Lin, C.J. Chang, O.M. Yaghi, P. Yang, Metal–organic frameworks for electrocatalytic reduction of carbon dioxide, J. Am. Chem. Soc. 137 (2015) 14129–14135.
[105] I. Hod, M.D. Sampson, P. Deria, C.P. Kubiak, O.K. Farha, J.T. Hupp, Fe-porphyrin-Based metal–Organic framework films as high-surface concentration, heterogeneous catalysts for electrochemical reduction of CO_2, ACS Catal. 5 (2015) 6302–6309.
[106] K. Takashi, F. Machiko, T. Masahiko, K. Katsuaki, H. Masakazu, T. Koji, K. Susumu, Photochemical reduction of low concentrations of CO_2 in a porous coordination polymer with a ruthenium(II)–CO complex, Angew. Chemie Int. Ed. 55 (2016) 2697–2700.
[107] G. Zhu, Y. Li, H. Zhu, H. Su, S.H. Chan, Q. Sun, Curvature-dependent selectivity of CO_2 electrocatalytic reduction on cobalt porphyrin nanotubes, ACS Catal. 6 (2016) 6294–6301.
[108] S. Lin, C.S. Diercks, Y.-B. Zhang, N. Kornienko, E.M. Nichols, Y. Zhao, A.R. Paris, D. Kim, P. Yang, O.M. Yaghi, C.J. Chang, Covalent organic frameworks comprising cobalt porphyrins for catalytic CO_2 reduction in water, Science 349 (2015) 1208–1213.
[109] G.-L. Chai, Z.-X. Guo, Highly effective sites and selectivity of nitrogen-doped graphene/CNT catalysts for CO_2 electrochemical reduction, Chem. Sci. 7 (2016) 1268–1275.
[110] B. Kumar, M. Asadi, D. Pisasale, S. Sinha-Ray, B.A. Rosen, R. Haasch, J. Abiade, A.L. Yarin, A. Salehi-Khojin, Renewable and metal-free carbon nanofibre catalysts for carbon dioxide reduction, Nat. Commun. 4 (2013) 2819.
[111] J. Wu, S. Ma, J. Sun, J.I. Gold, C. Tiwary, B. Kim, L. Zhu, N. Chopra, I.N. Odeh, R. Vajtai, A.Z. Yu, R. Luo, J. Lou, G. Ding, P.J.A. Kenis, P.M. Ajayan, A metal-free electrocatalyst for carbon dioxide reduction to multi-carbon hydrocarbons and oxygenates, Nat. Commun. 7 (2016) 13869.
[112] S. Back, J. Lim, N.-Y. Kim, Y.-H. Kim, Y. Jung, Single-atom catalysts for CO_2 electroreduction with significant activity and selectivity improvements, Chem. Sci. 8 (2017) 1090–1096.
[113] S. Back, Y. Jung, TiC- and TiN-supported single-atom catalysts for dramatic improvements in CO_2 electrochemical rtion to CH_4, ACS Energy Lett. 2 (2017) 969–975.
[114] H.B. Yang, S.-F. Hung, S. Liu, K. Yuan, S. Miao, L. Zhang, X. Huang, H.-Y. Wang, W. Cai, R. Chen, J. Gao, X. Yang, W. Chen, Y. Huang, H.M. Chen, C.M. Li, T. Zhang, B. Liu, Atomically dispersed Ni(i) as the active site for electrochemical CO_2 reduction, Nat. Energy 3 (2018) 140–147.
[115] K. Jiang, S. Siahrostami, T. Zheng, Y. Hu, S. Hwang, E. Stavitski, Y. Peng, J. Dynes, M. Gangisetty, D. Su, K. Attenkofer, H. Wang, Isolated Ni single atoms in graphene nanosheets for high-performance CO_2 reduction, Energy Environ. Sci. 11 (2018) 893–903.
[116] H. Yoshio, K. Katsuhei, S. Shin, Production of CO and CH_4 in electrochemical reduction of CO_2 at metal electrodes in Aqueous hydrogencarbonate solution, Chem. Lett. 14 (1985) 1695–1698.
[117] Y. Hori, Electrochemical CO2 reduction on metal electrodes, in: C.G. Vayenas, R.E. White, M.E. Gamboa-Aldeco (Eds.), Modern Aspects of Electrochemistry, Springer New York, New York, NY, 2008, pp. 89–189.
[118] E. Tayyebi, J. Hussain, Y. Abghoui, E. Skúlason, Trends of electrochemical CO_2 reduction reaction on transition metal oxide catalysts, J. Phys. Chem. C 122 (2018) 10078–10087.
[119] M. Asadi, K. Kim, C. Liu, A.V. Addepalli, P. Abbasi, P. Yasaei, P. Phillips, A. Behranginia, J.M. Cerrato, R. Haasch, P. Zapol, B. Kumar, R.F. Klie, J. Abiade, L.A. Curtiss, A. Salehi-Khojin, Nanostructured transition metal dichalcogenide electrocatalysts for CO_2 reduction in ionic liquid, Science 353 (2016) 467–470.
[120] J.F. He, N.J.J. Johnson, A.X. Huang, C.P. Berlinguette, Electrocatalytic alloys for CO_2 reduction, Chemsuschem 11 (2018) 48–57.
[121] Y. Ki Dong, L. Chan Woo, J. Jun Ho, H. Tak Rae, N. Ki Tae, Rise of nano effects in electrode during electrocatalytic CO_2 conversion, Nanotechnology 28 (2017), 352001.
[122] A.A. Peterson, F. Abild-Pedersen, F. Studt, J. Rossmeisl, J.K. Norskov, How copper catalyzes the electroreduction of carbon dioxide into hydrocarbon fuels, Energy Environ. Sci. 3 (2010) 1311–1315.
[123] K.J.P. Schouten, Y. Kwon, C.J.M. van der Ham, Z. Qin, M.T.M. Koper, A new mechanism for the selectivity to C1 and C2 species in the electrochemical reduction of carbon dioxide on copper electrodes, Chem. Sci. 2 (2011) 1902–1909.
[124] X. Nie, M.R. Esopi, M.J. Janik, A. Asthagiri, Selectivity of CO_2 reduction on copper electrodes: the role of the kinetics of elementary steps, Angew. Chemie Int. Ed. 52 (2013) 2459–2462.
[125] J.H. Montoya, A.A. Peterson, J.K. Nørskov, Insights into C–C coupling in CO_2 electroreduction on copper electrodes, ChemCatChem 5 (2013) 737–742.
[126] Y. Hori, R. Takahashi, Y. Yoshinami, A. Murata, Electrochemical reduction of CO at a copper electrode, J. Phys. Chem. B 101 (1997) 7075–7081.
[127] A.J. Garza, A.T. Bell, M. Head-Gordon, Mechanism of CO_2 reduction at copper surfaces: pathways to C2 products, ACS Catal. 8 (2018) 1490–1499.
[128] J. Qiao, Y. Liu, F. Hong, J. Zhang, A review of catalysts for the electroreduction of carbon dioxide to produce low-carbon fuels, Chem. Soc. Rev. 43 (2014) 631–675.
[129] K.P. Kuhl, T. Hatsukade, E.R. Cave, D.N. Abram, J. Kibsgaard, T.F. Jaramillo, Electrocatalytic conversion of carbon dioxide to methane and methanol on transition metal surfaces, J. Am. Chem. Soc. 136 (2014) 14107–14113.
[130] A.A. Peterson, J.K. Nørskov, Activity descriptors for CO_2 electroreduction to methane on transition-metal catalysts, J. Phys. Chem. Lett. 3 (2012) 251–258.
[131] S. Back, J.-H. Kim, Y.-T. Kim, Y. Jung, On the mechanism of high product selectivity for HCOOH using Pb in CO_2 electroreduction, J. Chem. Soc. Faraday Trans. 18 (2016) 9652–9657.
[132] D. Kim, J. Resasco, Y. Yu, A.M. Asiri, P. Yang, Synergistic reaction pathways for the geometric and electronic effects for electrochemical reduction of carbon dioxide using gold–copper bimetallic nanoparticles, Nat. Comm. 5 (2014) 4948.
[133] E.L. Clark, C. Hahn, T.F. Jaramillo, A.T. Bell, Electrochemical CO_2 reduction over compressively strained CuAg surface alloys with enhanced multi-carbon oxygenate selectivity, J. Am. Chem. Soc. (2017).
[134] R. Kortlever, I. Peters, S. Koper, M.T.M. Koper, Electrochemical CO_2 reduction to formic acid at Low overpotential and with high faradaic efficiency on carbon-supported bimetallic Pd–Pt nanoparticles, ACS Catal. 5 (2015) 3916–3923.
[135] B. Jiang, X.-G. Zhang, K. Jiang, D.-Y. Wu, W.-B. Cai, Boosting formate production in electrocatalytic CO_2 reduction over wide potential window on Pd surfaces, J. Am. Chem. Soc. 140 (2018) 2880–2889.
[136] N. Spataru, K. Tokuhiro, C. Terashima, T.N. Rao, A. Fujishima, Electrochemical reduction of carbon dioxide at ruthenium dioxide deposited on boron-doped diamond, J. Appl. Electrochem. 33 (2003) 1205–1210.
[137] A. Bandi, Electrochemical reduction of carbon dioxide on conductive metallic oxides, J. Electrochem. Soc. 137 (1990) 2157–2160.
[138] S. Zhang, P. Kang, T.J. Meyer, Nanostructured tin catalysts for selective electrochemical reduction of carbon dioxide to formate, J. Am. Chem. Soc. 136 (2014) 1734–1737.
[139] D. Gao, Y. Zhang, Z. Zhou, F. Cai, X. Zhao, W. Huang, Y. Li, J. Zhu, P. Liu, F. Yang, G. Wang, X. Bao, Enhancing CO_2 electroreduction with the metal–Oxide interface, J. Am. Chem. Soc. 139 (2017) 5652–5655.
[140] D. Ren, Y. Deng, A.D. Handoko, C.S. Chen, S. Malkhandi, B.S. Yeo, Selective electrochemical reduction of carbon dioxide to ethylene and ethanol on copper(I) oxide catalysts, ACS Catal. 5 (2015) 2814–2821.
[141] M. Ma, B.J. Trześniewski, J. Xie, W.A. Smith, Selective and efficient reduction of carbon dioxide to Carbon Monoxide on oxide-derived nanostructured silver electrocatalysts, Angew. Chemie Int. Ed. 55 (2016) 9748–9752.
[142] Y. Chen, C.W. Li, M.W. Kanan, Aqueous CO_2 reduction at very low overpotential on oxide-derived Au nanoparticles, J. Am. Chem. Soc. 134 (2012) 19969–19972.
[143] Y. Chen, M.W. Kanan, Tin oxide dependence of the CO_2 reduction efficiency on tin electrodes and enhanced activity for Tin/Tin oxide thin-film catalysts, J. Am. Chem. Soc. 134 (2012) 1986–1989.
[144] H. Mistry, A.S. Varela, C.S. Bonifacio, I. Zegkinoglou, I. Sinev, Y.-W. Choi, K. Kisslinger, E.A. Stach, J.C. Yang, P. Strasser, B.R. Cuenya, Highly selective plasma-activated copper catalysts for carbon dioxide reduction to ethylene, Nat. Commun. 7 (2016) 12123.
[145] S. Gao, Y. Lin, X. Jiao, Y. Sun, Q. Luo, W. Zhang, D. Li, J. Yang, Y. Xie, Partially oxidized atomic cobalt layers for carbon dioxide electroreduction to liquid fuel, Nature 529 (2016) 68.
[146] S. Gao, Z. Sun, W. Liu, X. Jiao, X. Zu, Q. Hu, Y. Sun, T. Yao, W. Zhang, S. Wei, Y. Xie, Atomic layer confined vacancies for atomic-level insights into carbon dioxide electroreduction, Nat. Commun. 8 (2017) 14503.
[147] J.E. Pander, M.F. Baruch, A.B. Bocarsly, Probing the mechanism of aqueous CO_2 reduction on post-transition-Metal electrodes using ATR-IR spectroelectrochemistry, ACS Catal. 6 (2016) 7824–7833.
[148] K. Hara, A. Tsuneto, A. Kudo, T. Sakata, Change in the product selectivity for the electrochemical CO2 reduction by adsorption of sulfide ion on metal electrodes, J. Electroanal. Chem. 434 (1997) 239–243.
[149] K. Chan, C. Tsai, H.A. Hansen, J.K. Nørskov, Molybdenum sulfides and selenides as possible electrocatalysts for CO_2 reduction, ChemCatChem 6 (2014) 1899–1905.
[150] M. Asadi, B. Kumar, A. Behranginia, B.A. Rosen, A. Baskin, N. Repnin, D. Pisasale, P. Phillips, W. Zhu, R. Haasch, R.F. Klie, P. Král, J. Abiade, A.

Salehi-Khojin, Robust carbon dioxide reduction on molybdenum disulphide edges, Nat. Commun. 5 (2014) 4470.
[151] Z. Cao, D. Kim, D. Hong, Y. Yu, J. Xu, S. Lin, X. Wen, E.M. Nichols, K. Jeong, J.A. Reimer, P. Yang, C.J. Chang, A molecular surface functionalization approach to tuning nanoparticle electrocatalysts for carbon dioxide reduction, J. Am. Chem. Soc. 138 (2016) 8120–8125.
[152] C. Zhi, S., D. J, X. Jun, G. Rui, G. Ming, M., N. E, T., S. P, L. Xingwu, W. Xiaodong, C. Christophe, J., C. C, Chelating N-heterocyclic carbene ligands enable tuning of electrocatalytic CO_2 reduction to formate and carbon monoxide: surface organometallic chemistry, Angew. Chemie Int. Ed. 57 (2018) 4981–4985.
[153] Q. Lu, J. Rosen, Y. Zhou, G.S. Hutchings, Y.C. Kimmel, J.G. Chen, F. Jiao, A selective and efficient electrocatalyst for carbon dioxide reduction, Nat. Commun. 5 (2014) 3242.
[154] J.T. Song, H. Ryoo, M. Cho, J. Kim, J.-G. Kim, S.-Y. Chung, J. Oh, Nanoporous Au thin films on Si photoelectrodes for selective and efficient photoelectrochemical CO_2 reduction, Adv. Energy Mater. 7 (2017), 1601103-n/a.
[155] W. Zhu, R. Michalsky, Ö. Metin, H. Lv, S. Guo, C.J. Wright, X. Sun, A.A. Peterson, S. Sun, Monodisperse Au nanoparticles for selective electrocatalytic reduction of CO_2 to CO, J. Am. Chem. Soc. 135 (2013) 16833–16836.
[156] H. Mistry, R. Reske, Z. Zeng, Z.-J. Zhao, J. Greeley, P. Strasser, B.R. Cuenya, Exceptional size-dependent activity enhancement in the electroreduction of CO_2 over Au nanoparticles, J. Am. Chem. Soc. 136 (2014) 16473–16476.
[157] C. Kim, H.S. Jeon, T. Eom, M.S. Jee, H. Kim, C.M. Friend, B.K. Min, Y.J. Hwang, Achieving selective and efficient electrocatalytic activity for CO_2 reduction using immobilized silver nanoparticles, J. Am. Chem. Soc. 137 (2015) 13844–13850.
[158] E.B. Nursanto, H.S. Jeon, C. Kim, M.S. Jee, J.H. Koh, Y.J. Hwang, B.K. Min, Gold catalyst reactivity for CO_2 electro-reduction: from Nano particle to layer, Catal. Today 260 (2016) 107–111.
[159] S. Back, M.S. Yeom, Y. Jung, Active sites of Au and Ag nanoparticle catalysts for CO_2 electroreduction to CO, ACS Catal. 5 (2015) 5089–5096.
[160] R. Reske, H. Mistry, F. Behafarid, B. Roldan Cuenya, P. Strasser, Particle size effects in the catalytic electroreduction of CO_2 on Cu nanoparticles, J. Am. Chem. Soc. 136 (2014) 6978–6986.
[161] K. Manthiram, Y. Surendranath, A.P. Alivisatos, Dendritic assembly of gold nanoparticles during fuel-forming electrocatalysis, J. Am. Chem. Soc. 136 (2014) 7237–7240.
[162] J.A. Trindell, J. Clausmeyer, R.M. Crooks, Size stability and H_2/CO selectivity for Au nanoparticles during electrocatalytic CO_2 reduction, J. Am. Chem. Soc. (2017).
[163] W. Luo, X. Nie, M.J. Janik, A. Asthagiri, Facet dependence of CO_2 reduction paths on Cu electrodes, ACS Catal. 6 (2016) 219–229.
[164] A. Loiudice, P. Lobaccaro, E.A. Kamali, T. Thao, B.H. Huang, J.W. Ager, R. Buonsanti, Tailoring copper nanocrystals towards C2 products in electrochemical CO_2 reduction, Angew. Chemie Int. Ed. 55 (2016) 5789–5792.
[165] H.-E. Lee, K.D. Yang, S.M. Yoon, H.-Y. Ahn, Y.Y. Lee, H. Chang, D.H. Jeong, Y.-S. Lee, M.Y. Kim, K.T. Nam, Concave rhombic dodecahedral au nanocatalyst with multiple high-index facets for CO_2 reduction, ACS Nano 9 (2015) 8384–8393.
[166] Z. Wang, G. Yang, Z. Zhang, M. Jin, Y. Yin, Selectivity on etching: creation of high-energy facets on copper nanocrystals for CO_2 electrochemical reduction, ACS Nano 10 (2016) 4559–4564.
[167] X. Feng, K. Jiang, S. Fan, M.W. Kanan, Grain-boundary-dependent CO_2 electroreduction activity, J. Am. Chem. Soc. 137 (2015) 4606–4609.
[168] K.-S. Kim, W.J. Kim, H.-K. Lim, E.K. Lee, H. Kim, Tuned chemical bonding ability of Au at grain boundaries for enhanced electrochemical CO_2 reduction, ACS Catal. 6 (2016) 4443–4448.
[169] D. Raciti, K.J. Livi, C. Wang, Highly dense Cu nanowires for low-overpotential CO_2 reduction, Nano Lett. 15 (2015) 6829–6835.
[170] L. Yanwei, J.W. Ager, Stability of residual oxides in oxide-derived copper catalysts for electrochemical CO_2 reduction investigated with ^{18}O labeling, Angew. Chemie Int. Ed. 57 (2018) 551–554.
[171] Y. Li, F. Cui, M.B. Ross, D. Kim, Y. Sun, P. Yang, Structure-sensitive CO_2 electroreduction to hydrocarbons on ultrathin 5-fold twinned copper nanowires, Nano Lett. 17 (2017) 1312–1317.
[172] A.S. Hall, Y. Yoon, A. Wuttig, Y. Surendranath, Mesostructure-induced selectivity in CO_2 reduction catalysis, J. Am. Chem. Soc. 137 (2015) 14834–14837.
[173] Y. Yoon, A.S. Hall, Y. Surendranath, Tuning of silver catalyst mesostructure promotes selective carbon dioxide conversion into fuels, Angew. Chemie Int. Ed. 55 (2016) 15282–15286.
[174] M. Ma, K. Djanashvili, W.A. Smith, Controllable hydrocarbon formation from the electrochemical reduction of CO_2 over Cu nanowire arrays, Angew. Chemie Int. Ed. 55 (2016) 6680–6684.
[175] A. Dutta, M. Rahaman, N.C. Luedi, M. Mohos, P. Broekmann, Morphology matters: tuning the product distribution of CO_2 electroreduction on oxide-derived Cu foam catalysts, ACS Catal. 6 (2016) 3804–3814.
[176] K.D. Yang, W.R. Ko, J.H. Lee, S.J. Kim, H. Lee, M.H. Lee, K.T. Nam, Morphology-directed selective production of ethylene or ethane from CO_2 on a Cu mesopore electrode, Angew. Chemie Int. Ed. 56 (2016) 796–800.
[177] M. Liu, Y. Pang, B. Zhang, P. De Luna, O. Voznyy, J. Xu, X. Zheng, C.T. Dinh, F. Fan, C. Cao, F.P.G. de Arquer, T.S. Safaei, A. Mepham, A. Klinkova, E. Kumacheva, T. Filleter, D. Sinton, S.O. Kelley, E.H. Sargent, Enhanced electrocatalytic CO_2 reduction via field-induced reagent concentration, Nature 537 (2016) 382.
[178] H. Jiang, Z. Hou, Y. Luo, Unraveling the mechanism for the sharp-tip enhanced electrocatalytic carbon dioxide reduction: the kinetics decide, Angew. Chemie Int. Ed. (2019), n/a-n/a.
[179] X. Huang, Q. Shen, J. Liu, N. Yang, G. Zhao, A CO_2 adsorption-enhanced semiconductor/metal-complex hybrid photoelectrocatalytic interface for efficient formate production, Energy Environ. Sci. 9 (2016) 3161–3171.
[180] H. Takeda, K. Ohashi, A. Sekine, O. Ishitani, Photocatalytic CO_2 reduction using Cu(I) photosensitizers with a Fe(II) Catalyst, J. Am. Chem. Soc. 138 (2016) 4354–4357.
[181] H. Fei, M.D. Sampson, Y. Lee, C.P. Kubiak, S.M. Cohen, Photocatalytic CO_2 reduction to formate using a Mn(I) molecular catalyst in a robust metal–organic framework, Inorg. Chem. 54 (2015) 6821–6828.
[182] S. Liu, Z. Zhao, Z. Wang, Photocatalytic reduction of carbon dioxide using sol-gel derived titania-supported CoPc catalysts, Photochem. Photobiol. Sci. 6 (2007) 695–700.
[183] K. Alenezi, S.K. Ibrahim, P. Li, C.J. Pickett, Solar fuels: photoelectrosynthesis of CO from CO_2 at p-Type Si using Fe porphyrin electrocatalysts, Chem. Eur. J. 19 (2013) 13522–13527.
[184] S. Sato, T. Arai, T. Morikawa, K. Uemura, T.M. Suzuki, H. Tanaka, T. Kajino, Selective CO_2 conversion to formate conjugated with H_2O oxidation utilizing semiconductor/complex hybrid photocatalysts, J. Am. Chem. Soc. 133 (2011) 15240–15243.
[185] R. Kuriki, K. Sekizawa, O. Ishitani, K. Maeda, Visible-light-driven CO_2 reduction with carbon nitride: enhancing the activity of ruthenium catalysts, Angew. Chemie Int. Ed. 54 (2015) 2406–2409.
[186] M.F. Kuehnel, K.L. Orchard, K.E. Dalle, E. Reisner, Selective photocatalytic CO_2 reduction in water through anchoring of a molecular Ni catalyst on CdS nanocrystals, J. Am. Chem. Soc. 139 (2017) 7217–7223.
[187] C.D. Windle, E. Pastor, A. Reynal, A.C. Whitwood, Y. Vaynzof, J.R. Durrant, R.N. Perutz, E. Reisner, Improving the photocatalytic reduction of CO_2 to CO through immobilisation of a molecular Re catalyst on TiO_2, Chem. Eur. J. 21 (2015) 3746–3754.
[188] M. Schreier, P. Gao, M.T. Mayer, J. Luo, T. Moehl, M.K. Nazeeruddin, S.D. Tilley, M. Gratzel, Efficient and selective carbon dioxide reduction on low cost protected Cu_2O photocathodes using a molecular catalyst, Energy Environ. Sci. 8 (2015) 855–861.
[189] M. Schreier, J. Luo, P. Gao, T. Moehl, M.T. Mayer, M. Grätzel, Covalent immobilization of a molecular catalyst on Cu2O photocathodes for CO_2 reduction, J. Am. Chem. Soc. 138 (2016) 1938–1946.
[190] C. Ci, J.J. Carbó, R. Neumann, Cd. Graaf, J.M. Poblet, Photoreduction mechanism of CO_2 to CO catalyzed by a rhenium(I)–polyoxometalate Hybrid compound, ACS Catal. 6 (2016) 6422–6428.
[191] Y.S. Chaudhary, T.W. Woolerton, C.S. Allen, J.H. Warner, E. Pierce, S.W. Ragsdale, F.A. Armstrong, Visible light-driven CO_2 reduction by enzyme coupled CdS nanocrystals, Chem. Commun. 48 (2012) 58–60.
[192] R. Hinogami, Y. Nakamura, S. Yae, Y. Nakato, Modification of semiconductor surface with ultrafine metal particles for efficient photoelectrochemical reduction of carbon dioxide, Appl. Surf. Sci. 121-122 (1997) 301–304.
[193] R. Hinogami, Y. Nakamura, S. Yae, Y. Nakato, An approach to ideal semiconductor electrodes for efficient photoelectrochemical reduction of carbon dioxide by modification with small metal particles, J. Phys. Chem. B 102 (1998) 974–980.
[194] G. Kumari, X. Zhang, D. Devasia, J. Heo, P.K. Jain, Watching visible light-driven CO_2 reduction on a plasmonic nanoparticle catalyst, ACS Nano 12 (2018) 8330–8340.
[195] Ş. Neaţu, J.A. Maciá-Agulló, P. Concepción, H. Garcia, Gold–copper nanoalloys supported on TiO2 as photocatalysts for CO_2 reduction by water, J. Am. Chem. Soc. 136 (2014) 15969–15976.
[196] J.-M. Lehn, R. Ziessel, Photochemical generation of carbon monoxide and hydrogen by reduction of carbon dioxide and water under visible light irradiation, Proc. Natl. Acad. Sci. 79 (1982) 701–704.
[197] J. Hawecker, J.M. Lehn, R. Ziessel, Photochemical and electrochemical reduction of carbon dioxide to carbon monoxide mediated by (2,2′-Bipyridine)tricarbonylchlororhenium(I) and related complexes as homogeneous catalysts, Helv. Chim. Acta 69 (1986) 1990–2012.
[198] V.S. Thoi, N. Kornienko, C.G. Margarit, P. Yang, C.J. Chang, Visible-light photoredox catalysis: selective reduction of carbon dioxide to carbon monoxide by a nickel N-Heterocyclic Carbene–isoquinoline complex, J. Am. Chem. Soc. 135 (2013) 14413–14424.
[199] P. Kang, C. Cheng, Z. Chen, C.K. Schauer, T.J. Meyer, M. Brookhart, Selective electrocatalytic reduction of CO_2 to formate by water-stable iridium dihydride pincer complexes, J. Am. Chem. Soc. 134 (2012) 5500–5503.
[200] R. Angamuthu, P. Byers, M. Lutz, A.L. Spek, E. Bouwman, Electrocatalytic CO_2 conversion to oxalate by a copper complex, Science 327 (2010) 313–315.
[201] Y. Kou, Y. Nabetani, D. Masui, T. Shimada, S. Takagi, H. Tachibana, H. Inoue, Direct detection of key reaction intermediates in photochemical CO_2 reduction sensitized by a rhenium bipyridine complex, J. Am. Chem. Soc. 136 (2014) 6021–6030.
[202] G. Sahara, R. Abe, M. Higashi, T. Morikawa, K. Maeda, Y. Ueda, O. Ishitani, Photoelectrochemical CO2 reduction using a Ru(ii)–Re(i) multinuclear metal complex on a p-type semiconducting NiO electrode, Chem. Commun. 51 (2015) 10722–10725.

[203] A. Nakada, K. Koike, T. Nakashima, T. Morimoto, O. Ishitani, Photocatalytic CO_2 reduction to formic acid using a Ru(II)–Re(I) supramolecular complex in an aqueous solution, Inorg. Chem. 54 (2015) 1800–1807.
[204] G. Sahara, O. Ishitani, Efficient photocatalysts for CO2 reduction, Inorg. Chem. 54 (2015) 5096–5104.
[205] Y. Ueda, H. Takeda, T. Yui, K. Koike, Y. Goto, S. Inagaki, O. Ishitani, A visible-light harvesting system for CO_2 reduction using a RuII–ReI photocatalyst adsorbed in Mesoporous Organosilica, ChemSusChem 8 (2015) 439–442.
[206] E. Kimura, S. Wada, M. Shionoya, T. Takahashi, Y. Litaka, A novel cyclam–nickel(II) complex appended with a tris-(2,2′-bipyridine) ruthenium(II) complex (cyclam = 1,4,8,11-tetra-azacyclotetradecane), J. Chem. Soc. Chem. Commun. (1990) 397–398.
[207] E. Kimura, S. Wada, M. Shionoya, Y. Okazaki, New series of multifunctionalized Nickel(II)-Cyclam (Cyclam = 1,4,8,11-Tetraazacyclotetradecane) complexes. Application to the photoreduction of carbon dioxide, Inorg. Chem. 33 (1994) 770–778.
[208] L. Liu, H. Zhao, J.M. Andino, Y. Li, Photocatalytic CO_2 reduction with H_2O on TiO_2 nanocrystals: comparison of Anatase, rutile, and brookite polymorphs and exploration of surface chemistry, ACS Catal. 2 (2012) 1817–1828.
[209] F. Saladin, I. Alxneit, Temperature dependence of the photochemical reduction of CO_2 in the presence of H_2O at the solid/gas interface of TiO_2, J. Chem. Soc. Faraday Trans. 93 (1997) 4159–4163.
[210] Y. Ku, W.-H. Lee, W.-Y. Wang, Photocatalytic reduction of carbonate in aqueous solution by UV/TiO_2 process, J. Mol. Catal. A Chem. 212 (2004) 191–196.
[211] S. Kaneco, H. Kurimoto, K. Ohta, T. Mizuno, A. Saji, Photocatalytic reduction of CO_2 using TiO_2 powders in liquid CO_2 medium, J. Photochem. Photobiol. A: Chem. 109 (1997) 59–63.
[212] M. Anpo, H. Yamashita, Y. Ichihashi, S. Ehara, Photocatalytic reduction of CO_2 with H_2O on various titanium oxide catalysts, J. Electroanal. Chem. 396 (1995) 21–26.
[213] K. Bhattacharyya, A. Danon, B.K. Vijayan, K.A. Gray, P.C. Stair, E. Weitz, Role of the surface lewis acid and base sites in the adsorption of CO_2 on titania nanotubes and platinized titania nanotubes: an in situ FT-IR study, J. Phys. Chem. C 117 (2013) 12661–12678.
[214] M. Xing, Y. Zhou, C. Dong, L. Cai, L. Zeng, B. Shen, L. Pan, C. Dong, Y. Chai, J. Zhang, Y. Yin, Modulation of the reduction potential of TiO_{2-x} by fluorination for efficient and selective CH_4 generation from CO_2 photoreduction, Nano Lett. 18 (2018) 3384–3390.
[215] L. Liu, F. Gao, H. Zhao, Y. Li, Tailoring Cu valence and oxygen vacancy in Cu/TiO2 catalysts for enhanced CO_2 photoreduction efficiency, Appl. Catal. B 134-135 (2013) 349–358.
[216] J. Yu, J. Low, W. Xiao, P. Zhou, M. Jaroniec, Enhanced photocatalytic CO_2-Reduction activity of anatase TiO_2 by coexposed {001} and {101} facets, J. Am. Chem. Soc. 136 (2014) 8839–8842.
[217] G.K. Ramesha, J.F. Brennecke, P.V. Kamat, Origin of catalytic effect in the reduction of CO2 at nanostructured TiO2 films, ACS Catal. 4 (2014) 3249–3254.
[218] K. Hirota, D.A. Tryk, T. Yamamoto, K. Hashimoto, M. Okawa, A. Fujishima, Photoelectrochemical reduction of CO_2 in a high-pressure CO_2 + methanol medium at p-Type semiconductor electrodes, J. Phys. Chem. B 102 (1998) 9834–9843.
[219] H. Li, Y. Lei, Y. Huang, Y. Fang, Y. Xu, L. Zhu, X. Li, Photocatalytic reduction of carbon dioxide to methanol by Cu_2O/SiC nanocrystallite under visible light irradiation, J. Nat. Gas Chem. 20 (2011) 145–150.
[220] M. Halmann, Photoelectrochemical reduction of aqueous carbon dioxide on p-type gallium phosphide in liquid junction solar cells, Nature 275 (1978) 115–116.
[221] L. Wan, X. Wang, S. Yan, H. Yu, Z. Li, Z. Zou, ZnO plates synthesized from the ammonium zinc nitrate hydroxide precursor, CrystEngComm 14 (2012) 154–159.
[222] Y.P. Xie, G. Liu, L. Yin, H.-M. Cheng, Crystal facet-dependent photocatalytic oxidation and reduction reactivity of monoclinic WO_3 for solar energy conversion, J. Mater. Chem. 22 (2012) 6746–6751.
[223] A.H. Yahaya, M.A. Gondal, A. Hameed, Selective laser enhanced photocatalytic conversion of CO_2 into methanol, Chem. Phys. Lett. 400 (2004) 206–212.
[224] H.-a. Park, J.H. Choi, K.M. Choi, D.K. Lee, J.K. Kang, Highly porous gallium oxide with a high CO_2 affinity for the photocatalytic conversion of carbon dioxide into methane, J. Mater. Chem. 22 (2012) 5304–5307.
[225] S.C. Yan, S.X. Ouyang, J. Gao, M. Yang, J.Y. Feng, X.X. Fan, L.J. Wan, Z.S. Li, J.H. Ye, Y. Zhou, Z.G. Zou, A room-temperature reactive-template route to mesoporous $ZnGa_2O_4$ with improved photocatalytic activity in reduction of CO_2, Angew. Chemie Int. Ed. 49 (2010) 6400–6404.
[226] Y. Liu, B. Huang, Y. Dai, X. Zhang, X. Qin, M. Jiang, M.-H. Whangbo, Selective ethanol formation from photocatalytic reduction of carbon dioxide in water with $BiVO_4$ photocatalyst, Catal. Commun. 11 (2009) 210–213.
[227] Y. Zhou, Z. Tian, Z. Zhao, Q. Liu, J. Kou, X. Chen, J. Gao, S. Yan, Z. Zou, High-yield synthesis of ultrathin and uniform Bi_2WO_6 square nanoplates benefitting from photocatalytic reduction of CO_2 into renewable hydrocarbon fuel under visible light, ACS Appl. Mater. Interfaces 3 (2011) 3594–3601.
[228] L. Zhang, W. Wang, D. Jiang, E. Gao, S. Sun, Photoreduction of CO_2 on BiOCl nanoplates with the assistance of photoinduced oxygen vacancies, Nano Res. 8 (2015) 821–831.
[229] X. Li, J. Chen, H. Li, J. Li, Y. Xu, Y. Liu, J. Zhou, Photoreduction of CO_2 to methanol over Bi_2S_3/CdS photocatalyst under visible light irradiation, J. Nat. Gas Chem. 20 (2011) 413–417.
[230] B.-J. Liu, T. Torimoto, H. Yoneyama, Photocatalytic reduction of CO_2 using surface-modified CdS photocatalysts in organic solvents, J. Photochem. Photobiol. A: Chem. 113 (1998) 93–97.
[231] S. Das, S. Biswas, T. Balaraju, S. Barman, R. Pochamoni, S. Roy, Photochemical reduction of carbon dioxide coupled with water oxidation using various soft-oxometalate (SOM) based catalytic systems, J. Mater. Chem. A 4 (2016) 8875–8887.
[232] W. Hou, W.H. Hung, P. Pavaskar, A. Goeppert, M. Aykol, S.B. Cronin, Photocatalytic conversion of CO_2 to hydrocarbon fuels via plasmon-enhanced absorption and metallic interband transitions, ACS Catal. 1 (2011) 929–936.
[233] S. Yu, A.J. Wilson, J. Heo, P.K. Jain, Plasmonic control of multi-electron transfer and C–C coupling in visible-light-Driven CO2 reduction on Au nanoparticles, Nano Lett. 18 (2018) 2189–2194.
[234] S. Yu, A.J. Wilson, G. Kumari, X. Zhang, P.K. Jain, Opportunities and challenges of Solar-Energy-Driven Carbon Dioxide to fuel conversion with plasmonic catalysts, ACS Energy Lett. 2 (2017) 2058–2070.